

Linköping university | Department of Management and Engineering
Division of Applied Thermodynamics and Fluid Mechanics
Master Thesis 30 HP | Mechanical Engineering - Applied Mechanics
Spring 2019 | LIU-IEI-TEK-A-19/03420—SE

Investigation of Timber Vehicle Aerodynamics - using CFD

A study of the aerodynamic influence of timber, drag reduction devices, and CFD method automation. As part of the ETTaero2 project, an effort to lower fuel consumption

Marcus Gustavsson

Simon Johansson

June 24, 2019

Academic Supervisor: Petter Ekman

Examiner: Matts Karlsson

Abstract

Lowering the environmental impact from transportation is one of the most important challenges that the automotive industry face today. Vehicle manufacturers make big efforts to improve engines, explore alternative fuels and completely different drivetrains, in order to not let these efforts be wasted it is paramount that the aerodynamics is also considered. A sector that has not gotten as much attention as regular goods freight is the forestry industry, which in Sweden transports 6 billion ton-km yearly. Timber vehicles such as the ones used in Sweden consume on average 0.025 liter diesel per ton-km, of which approximately 30 % can be attributed to drag at 80 km h^{-1} , the speed that a timber vehicle spends most of its time. Timber transport vehicles are specialized and purpose build vehicles that not only perform worse in terms of drag than regular box shaped trucks but they are unloaded when traveling to the pickup destination with limited possibility to load something else. An automated process for ground vehicle aerodynamics was further developed to reduce the amount of user interaction. The automated process allows for more throughput and faster turnaround of the simulations. A study of different timber configurations examining drag and flow features showed that log length and stack diversity are important factors of the timber's effect on total vehicle drag. Using the findings from the timber study a timber stack model was made and the specifics of timber vehicle aerodynamics were investigated. With these findings and literature aerodynamic concepts to reduce drag were evaluated and combined to a final aero kit. This aero kit showed a wind averaged drag reduction of 171 and 169 drag counts for a loaded and unloaded vehicle respectively, representing an estimated fuel saving of 5-10 %.

Keywords: CFD, Timber vehicle, Aerodynamics, Heavy truck aerodynamics, Heavy transport, Automation, Drag reduction, Fuel savings

Acknowledgements

We would like to thank our Academic supervisor Petter Ekman for the interesting discussions and enthusiastic involvement in this master thesis. Thank you for sharing so much of the knowledge you have gathered during your years in academia. Our examiner Matts Karlsson has given guidance and important insights during our many meetings. Thanks to the rest of employees at the division Applied Thermodynamics and Fluid Mechanic at Linköpings University for the warm welcome and discussions. National Supercomputer Center in Linköping have provided us with computing resources many master thesis applicants can only dream of; the staff of which have also been an invaluable source of help and information, especially during the automation process where Frank Bramkamp gave his much appreciated support. Hans Weslien at Biometria helped us to find information regarding the statistics of timber giving the results in this work even more ground to stand on. Thanks to Scania for both providing a truck model and taking the time to share their knowledge through meetings and visits. Finally, we would like to express our gratitude to Skogforsk and Henrik Von Hofsten for the support of the project and the industry insight.

Marcus Gustavsson and Simon Johansson Linköping, June 2019

Contents

Nomenclature	vii
1 Introduction	1
1.1 Background	1
1.2 Problem Statement	2
1.3 Purpose	2
1.4 Objectives	3
1.5 Delimitations	3
1.6 Limitations	3
2 Theory	5
2.1 Fundamentals of Fluid Dynamics	5
2.1.1 Reynolds Number	5
2.1.2 Turbulence	5
2.1.3 Near Wall Region	6
2.1.4 Governing Equations	8
2.1.5 Solving the Governing Equations	8
2.2 Fundamentals of Aerodynamics	10
2.2.1 Forces	10
2.2.2 Truck Aerodynamics	11
2.2.3 Timber vehicle Specifics	12
3 Method	15
3.1 Geometry	16
3.1.1 Vehicle Configurations	17
3.1.2 Domain	18
3.2 Boundary Conditions	19
3.2.1 Porous media	20
3.3 Solver	22
3.4 Meshing	24
3.4.1 Inflation Study	28
3.4.2 Mesh Density	29
3.5 Method Problems	31
3.6 Post-Processing	34
3.7 Automation	35
3.8 Timber Study	36
3.8.1 Surface Roughness	37
3.8.2 Log size	37
3.8.3 Stack Shuffle	38

3.9	Concepts: Drag Reduction	38
4	Results and Discussion	41
4.1	Timber Study	42
4.1.1	Surface Roughness	42
4.1.2	Log size	44
4.1.3	Shuffle	49
4.1.4	Baseline Stack	51
4.1.5	Specific Aerodynamics of Timber On Vehicles	51
4.2	Loading Configurations	52
4.3	Baseline Vehicle	55
4.4	Drag Reduction Concepts	64
4.4.1	Skirts	64
4.4.2	Bulkhead Shield	71
4.4.3	Gap Spoiler and Boat Tail	74
4.4.4	Gap Seal	78
4.5	Final aero kit	80
4.6	Future concepts discussion	86
5	General Discussion	89
6	Conclusion	91
7	Outlook	93
8	Perspectives	95
	Bibliography	99
A	Realizable k-epsilon model	A1
B	Inflation Study	A3
C	Method Problem data	A5
D	Results Baseline Vehicle	A7

Nomenclature

Abbreviations and Acronyms

DNS	Direct Numerical Simulation
k- ε	k- ε turbulence model
EVR	Eddy Viscosity Ratio
CFD	Computational Fluid Dynamics
LiU	Linköping University
RANS	Reynolds Averaged Navier Stokes
CAD	Computer Aided Design
NSC	National Supercomputer Center
SAE	Society of Automotive Engineers
FVM	Finite Volume Method
FEM	Finite Element Method
LES	Large Eddy Simulation
BOI	Body of Influence

Mathematical definitions

β	Yaw angle	°
\mathbf{u}	Velocity Vector Test	m s^{-1}
δ_{ij}	Kronecker's delta	—
κ	Von Karman's constant	—
μ	Dynamic viscosity	Pa s
μ_t	Eddy viscosity	Pa s
ν	Kinematic viscosity	$\text{m}^2 \text{s}^{-1}$
$\bar{\Phi}$	Mean of Arbitrary variable	—
Φ	Arbitrary variable	—
Φ'	Fluctuating part of Arbitrary variable	—
ρ	Density	kg m^{-3}

Nomenclature

τ_w	Wall Shear Stress	Pa
ε	Dissipation	$\text{J kg}^{-1} \text{s}^{-1}$
A	Area of vehicle	m^2
B	The additive constant	—
C_D	Drag coefficient	—
C_i	Force coefficient $i = x, y, z$	—
C_L	Lift coefficient	—
C_S	Side force coefficient	—
F	Force	N
H	Height of vehicle	m
I_i	Inertial resistance	m^{-1}
k	Turbulent Kinetic Energy	J kg^{-1}
L	Characteristic length	m
p	Pressure	Pa
Re	Reynolds number	—
Re_{crit}	Critical Reynolds number	—
t	Time	s
u	Velocity in x-direction	m s^{-1}
u^*	Frictional velocity	m s^{-1}
u^+	Nondimensional velocity	—
U_∞	Mean bulk flow velocity	m s^{-1}
U_{wall}	Wall velocity	m s^{-1}
u_n	Velocity in index notation $n = 1, 2, 3$	m s^{-1}
U_Y	Side wind of velocity inlet	m s^{-1}
v	Velocity in y-direction	m s^{-1}
V_i	viscous resistance	m^{-2}
W	Width of vehicle	m
w	Velocity in z-direction	m s^{-1}
x_n	Coordinate in index notation $n = 1, 2, 3$	m
y^+	Nondimensional wall distance	—
x	Longitudinal coordinate	m

y	Transverse coordinate	m
z	Height coordinate	m

Other Symbols

$\frac{1}{\alpha}$	Viscous resistance coefficient
C	Inertial loss term matrix
C_2	Inertial resistance coefficient
D	Viscous loss term matrix
S_i	Porous media source term

1 Introduction

This master thesis presents the work done at Linköpings University (LiU) as a part of the research project ETTaero2. The ETTaero2 project was introduced in 2015 and is aiming to lower aerodynamic drag on timber vehicles [1]. This has been done using Computational Fluid Dynamics (CFD), where the aerodynamics of timber vehicles and different drag reducing concepts have been evaluated.

This thesis implements aerodynamic devices on a more realistic timber vehicle model than examined before in the project [2, 3]. A selection of the concepts evaluated in the earlier studies have been evaluated on the new model. Further, some new concepts that have not been evaluated before are introduced. Concepts were evaluated together with industry partners Scania and Skogforsk to ensure the usability.

Further, the thesis has also dealt with further development of the CFD methodology for ground vehicle aerodynamics developed and used at LiU. This method consist of automation procedures for CFD, which eliminates the need for user interaction for meshing, solving and post-processing.

1.1 Background

Every year in Sweden there are a lot of vehicles hauling timber, in 2015 there were about 2000 timber vehicles hauling around 6 billion ton-km (metric ton kilo metre). While doing so the average fuel consumption was about 0.025 liters of diesel per ton-km, this is around 30-50 % more than a regular tractor-trailer configuration [4]. Further, for a fully loaded timber vehicle the aerodynamic drag is responsible for 20-30 % of the fuel consumption [4].

“En Trave Till” (ETT) (One more stack) is a research project where the goal is to lower the emissions in the timber transport industry. The research focuses on adding more cargo weight on one vehicle and in this way lower total emissions. This is done by reducing the number of vehicles and the emissions per ton of wood.

As a part of this project the aerodynamics of these vehicles have been investigated in the ETTaero projects. Since these heavy vehicles will be preferred during longer hauls of timber the aerodynamics are a major factor in the fuel consumption. The timber vehicles are travelling long distances both loaded and unloaded since they are purpose built to transport timber. For this reason they differ alot from regular vehicles that have an exterior box shape whether fully loaded or empty, and it has been shown that the aerodynamic performance for timber vehicles is significantly worse [4].

The main research of the aerodynamics is done at LiU. Earlier wind tunnel experiments have been done on a simplified model, however, most of the research has been done using CFD. CFD simulations has been done on the same simplified timber vehicle model using both RANS [2, 3] and scale resolving methods [4]. During the earlier investigations the timber stack was found to have a major impact on the drag of the timber vehicle [2]. Depending how the timber stack was modelled different amount of separation occurred on the leeward side of the vehicle for some yaw angles. Multiple different concepts have been evaluated in an effort to find devices that can reduce the drag of timber vehicles, some of which shows great potential. In the methodology used in the previous studies some sort of user input is required in many steps of the procedure [2, 3]. This means that the turnaround time for a case from mesh to results is very dependent on the user being available.

Different from many other vehicle types the timber vehicle is not built by one single party or even two, the tractor vehicle, trailer, banks, stakes, etc. are manufactured by different entities and in most cases assembled by another. Also meaning that one vehicle might be very different from another. This means that no single party inherently has full overview and insight to the whole vehicle, much less the aerodynamics of it. Recently a new road classification has made it possible to utilize bigger and heavier vehicles, which inherently have a better fuel consumption per ton-km [5]. In the future these vehicles together with even bigger configurations will replace those of today to a great extent.

1.2 Problem Statement

The problem consists of employing CFD simulations to develop usable concepts and solutions that reduce aerodynamic drag of a timber vehicle model representative of a real timber vehicle as used or to be used in Sweden. This is done in a methodized manner in line with the current work flow and CFD procedure for ground vehicle aerodynamics used at LiU. The automation of the CFD procedure is expanded and improved. The project is carried out as a master thesis work at LiU.

1.3 Purpose

The purpose of this master thesis is to continue upon the work done earlier within ETTaero2 done at LiU, specifically the earlier master theses that have been carried out at LiU [2, 3]. This is done in order to advance the knowledge of what improvements can be found in terms of drag reduction on a more realistic timber vehicle model than previously used. This constitute the next step towards implementation of drag reduction devices on real timber vehicles in order to lower fuel consumption.

1.4 Objectives

In order to produce a CFD model and method that can achieve the overall goal of reducing the aerodynamic drag of future timber vehicles the following objectives were identified.

- Assemble, and prepare the complete timber vehicle CAD model which consists of a realistic truck tractor unit, trailer, bulkhead, bunks and stakes; supplied by Scania, MT Ekjö, Vemservice, and Exte respectively. The resulting model is be suitable for the current work flow.
- A baseline CFD model of the realistic timber vehicle configuration is be established and verified.
- Investigate and compare differences in the flow to that of the previous simplified model.
- Timber stack modelling sensitivity study. Investigating the impact of shape, volume, length, roughness, and stack diversity on the result.
- Selected drag reducing concepts found in the previous studies [2, 3] are implemented, evaluated, and possibly improved in the realistic timber vehicle model.
- Improving upon the CFD procedure in general, with focus on automation and post processing.

1.5 Delimitations

Softwares that are used: BETA CAE Systems ANSA Pre-processor [6], ANSYS Fluent CFD software [7], Kitware ParaView Post-processor [8], and MathWorks MATLAB [9], which are the tools employed in the CFD procedure for ground vehicle aerodynamics used at LiU. Many of the timber vehicles in Sweden have a crane used for loading timber in the forest. In this work the crane is not considered as the vehicle in focus is so-called group vehicles which does not have a crane and usually travel longer distances between larger operations. Also, this thesis only conduct its investigation using steady state RANS simulations.

1.6 Limitations

Computational resources were be available both in the from of a handful workstation computers as well as supercomputer resources on the Sigma cluster at National Supercomputer Centre at Linköping university (NSC) [10]. Allocation of CPU time was limited at NSC.

2 Theory

In this chapter the reader will be introduced to the fundamentals of the main topics that are used in this master thesis. It covers the the basics of fluid dynamics and aerodynamics. Some specifics regarding timber trucks are also presented.

2.1 Fundamentals of Fluid Dynamics

In fluid dynamics the behaviour of fluids are studied, in this section the reader will get an introduction to the fundamentals of this field of engineering. To begin with, flow of a fluid can either be turbulent, laminar, or in transition between these; real engineering problems are almost exclusively turbulent. Laminar flow is aligned and predictable while turbulent flow is fully chaotic with alot of mixing. In general laminar flow is easier to predict while turbulent flows are one of the few fields of mechanical science currently not solved analytically.

In the following chapter most of the equations contain a velocity component or vector. The velocity vector, denoted with bold text as \mathbf{u} . This vector contains the velocity components for x-, y- and z-direction denoted as u , v and w .

2.1.1 Reynolds Number

In fluid dynamics the Reynolds number (Re) is used to compare the ratio between the inertial and viscous forces in a flow. The Reynolds number, Re , is calculated as

$$Re = \frac{\rho U_{\infty} L}{\mu} \quad (1)$$

where ρ is the density of the fluid, μ the dynamic viscosity, U_{∞} the freestream velocity and L is the characteristic length. The characteristic length can be the chord length of a wing, length of a surface, or as commonly used in heavy vehicle aerodynamics the height or width of the vehicle. This ratio, the Reynolds number, gives an indication of if the flow is laminar or turbulent.

2.1.2 Turbulence

Earlier the concept of turbulence was touched on, here the concept will be given further consideration. To understand turbulence a good start is to understand the

simpler laminar flow. Laminar flow will flow in a structured manner and tend to flow in streamlines and not mix too much.

Turbulent flow is hard to define and still there exists no single doctrine on the subject. It can be described in words as that turbulence exist of eddies, chaos and diffusion. Turbulent flow exist of alot of eddies in different sizes. In turn an eddie is a region of flow with high vorticity. This means that eddies do not fully describe the concept of turbulence since a laminar flow can still have high vorticity. When also bringing in the chaos of turbulence the description becomes more complete. The chaos is in the movement, creation and destruction of said eddies. Furthermore, the flow will diffuse, which is basically mixing. This is a result from that the flow no longer moves in the structured way.

The eddies in the flow have different sizes varying from the largest turbulent feature down to the smallest scales, Kolmogorov microscales, where the turbulence is dampened out by the viscous forces and turned in to heat. The sizes of these eddies are called the turbulent length scale. Different problems consists of different largest length scales but always tumble down to the smallest scales. Also different scales are present in different flow problems, the largest scales that can be observed on earth would be the diameter of a hurricane. The smallest scales also depend on the flow problem at hand but in the example of a hurricane the scales will be in the magnitude of millimetres or less. For better understanding, in classical mechanics one often talks about kinetic energy on the macro and micro scales i.e., kinetic energy of a moving body and heat. In turbulence each length scale represent a new level of kinetic energy, the energy contained in a set size of eddies tends to cascade with the length scale.

2.1.3 Near Wall Region

When a fluid flows close to a wall the fluid in contact with this wall will due to viscous forces have the same velocity as said wall, U_{wall} . Since the fluid has a velocity in the bulk flow there need to exist a region between the wall and the bulk flow where the velocity changes from U_{wall} to U_{∞} . This region is called the boundary layer and is defined as the region close to the wall where the velocity of the fluid is below 99% of the bulk flow velocity i.e., $U \leq 0.99U_{\infty}$.

The boundary layer formed over a plate will start as a laminar boundary layer that develops to a turbulent boundary layer further downstream on the plate. Between these the transition region exists. In engineering applications the laminar boundary layer is very small part of the near wall region and the turbulent boundary layer is dominant.

When solving problems using CFD the law of the wall is an important concept that describes the boundary layer. The law describes the velocity profile of a fully developed turbulent boundary layer at a certain distance from the wall. Before the law of the wall is true there exists other regions where this logarithmic expression does not hold. Two non-dimensional variables are defined, u^+ and y^+ , to describe

the velocity profile close to a wall. These are defined as

$$u^+ = \frac{U}{u^*} \quad (2)$$

$$y^+ = \frac{u^* y}{\nu} \quad (3)$$

where U is the local velocity, u^* is the frictional velocity this is further defined using the wall shear stress τ_w . y is the distance from the wall and ν the kinematic viscosity. The variables u^* and τ_w are defined as

$$u^* = \sqrt{\frac{\tau_w}{\rho}} \quad (4)$$

$$\tau_w = \mu \left(\frac{\partial u}{\partial y} \right)_{y=0} \quad (5)$$

where the indexing of the velocity gradient means that the wall shear stress is only evaluated at the wall. In the calculations τ_w is the wall shear stress, ρ the density, μ the dynamic viscosity and $(\frac{\partial u}{\partial y})$ is the velocity gradient. The variables u^+ and y^+ are non-dimensional expressions of the velocity and distance from the wall respectively.

With these two dimensionless variables the boundary layer can be divided into different areas depending on the distance from the wall. The region closest to the wall, where $y^+ < 5$, is called the viscous sublayer. Here the velocity change is linear and is approximately $u^+ = y^+$. The flow is also laminar this close to the wall. Above this a region between $5 < y^+ < 30$ called the buffer layer exists. In this region no analytic equation holds, but above this region the law of the wall is true. This region is called the log-law region and the log-law is defined as

$$u^+ = \frac{1}{\kappa} \ln y^+ + B \quad (6)$$

where $\kappa \approx 0.4$ is the Von Karman's constant and the additive constant $B \approx 5.5$. y^+ is the earlier defined non-dimensional wall distance. Both of these are defined by experiments and are true for a smooth wall. The log-law is true around the region of $30 < y^+ < 500$ depending on the Reynolds number.

Depending on what model or method the CFD user chooses to use different approaches to modelling the near wall region will be used. It becomes important that the user knows the prerequisites for the model used and that the first cell from the wall has a height small enough. The concept of cells is introduced in section 2.1.5.

It is important to capture the boundary layer because of the high viscous forces that produce friction drag, further discussed in section 2.2.1. Also the production of turbulence has an impact on flow features. For example the boundary layer is important for predicting separations around curved surfaces. This is also further described in 2.2.2.

2.1.4 Governing Equations

The governing equations that are the most common for describing fluid flow are the Navier-Stokes equations, the momentum equation in x-direction is defined as

$$\frac{\partial(u)}{\partial t} + \text{div}(u\mathbf{u}) = -\frac{1}{\rho} \frac{\partial p}{\partial x} + \text{div}(\nu \text{grad}(u)) \quad (7)$$

where t is time, p is the pressure, and ν is the kinematic viscosity. Velocity in x-direction is u and the velocity vector is shown as \mathbf{u} . Similarly equations for y-, and z-direction also exist.

As in all physics it is impossible to create and destroy mass, therefore the flow also needs to obey the continuity equation defined as

$$\frac{\partial \rho}{\partial t} + \nabla(\rho\mathbf{u}) \quad (8)$$

where ρ is the fluid density, t is time and the vector \mathbf{u} is the velocity vector.

2.1.5 Solving the Governing Equations

The governing equations for fluid flow are a set of non linear partial differential equations. There are very few general analytic solution for this set of equations. However, there are numerical methods that allow the flow field to be estimated. Two numerical techniques that can be used to solve the Navier Stokes equations are the finite volume method (FVM) and finite element method (FEM). Also, worth mentioning is that there exist other equations than the Navier Stokes ones that can be used to solve fluid flow problems. For example the Boltzmann equation can be used to simulate a finite set of particles with collision models. In this thesis FVM is used to solve the flow field. In FVM the domain that the flow field is to be solved in is divided in many smaller regions called cells. The cells forms a grid of many smaller volumes, the cells, where the flow field variables can be evaluated.

There are different methods to handle the turbulence in a simulation, common methods are Reynolds Averaged Navier Stokes (RANS) methods, Large Eddy Simulation (LES) and Direct Numerical Simulation (DNS). The main difference between these methods are how much of the energy spectrum that are either resolved or modelled. A RANS method models all of the turbulence while a DNS solver resolves all of the turbulence. In between the two is the LES method that resolves some of the turbulence and models the rest. When more of the turbulence is resolved more computing power is needed due to increased demands on the grid refinement. With the available computing power of today and problem sizes most of the industry uses RANS methods for CFD simulations.

The RANS equations are derived using a simple but very clever way of composing a properties change during time. This is called Reynolds decomposition and basically divide the property into a fluctuating and mean part,

$$\Phi = \bar{\Phi} + \Phi' \quad (9)$$

here Φ represents an arbitrary variable that is divided into its mean part $\bar{\Phi}$ and fluctuating part Φ' . This is also illustrated by graphics in figure 1. Using this clever

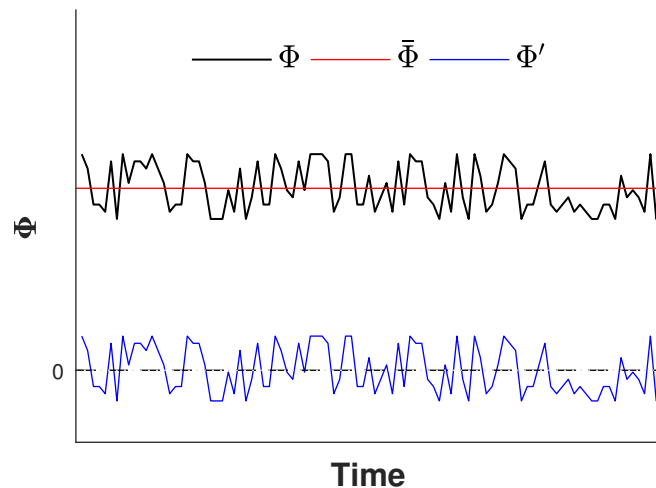


Figure 1: Reynolds decomposition applied on an arbitrary property Φ . The variable is decomposed in to the mean part, $\bar{\Phi}$ and the fluctuating part, Φ' .

decomposition on the governing equations result in the RANS equations. The RANS equation form momentum in x-direction become

$$\bar{u} \operatorname{div}(\bar{\mathbf{u}}) = -\frac{1}{\rho} \frac{\partial \bar{p}}{\partial x} + \operatorname{div}(\nu \operatorname{grad}(\bar{\mathbf{u}})) - \overline{\operatorname{div}(\mathbf{u}'\mathbf{u}')} \quad (10)$$

and can be compared with (7). In this equation both the mean velocity in x-direction \bar{u} and mean velocity vector $\bar{\mathbf{u}}$ can be found together with the mean pressure \bar{p} . The fluctuating part of the velocities is also present as u' and \mathbf{u}' . Both the density ρ and kinematic viscosity ν is part of the equation. It can be seen that some of the terms do disappear during this operation but also a new term appears. This last term, $-\overline{\operatorname{div}(\mathbf{u}'\mathbf{u}')}$ is called the Reynolds stresses and the problem with finding a way of solving this term is called the closure problem.

To solve the closure problem different techniques can be used, these do also impact the computational time but also the accuracy of the results. The most common way of solving the problem is to use an eddy viscosity model that introduces a theoretical viscosity, μ_t to model the Reynolds stresses. All eddy viscosity models are based on the Boussinesq hypothesis that assumes that the Reynolds stresses are proportional to mean rates of deformation

$$-\overline{u'_i u'_j} = \mu_t \left(\frac{\partial \bar{u}_i}{\partial x_j} + \frac{\partial \bar{u}_j}{\partial x_i} \right) - \frac{2}{3} k \delta_{ij} \quad (11)$$

this gives a relation between eddy viscosity and the Reynolds stresses [11]. The Boussinesq hypothesis is expressed in index form and uses the Kronecker delta δ_{ij} which is equal to 1 when $i = j$ but equals 0 when $i \neq j$. The turbulent kinetic energy, k is also a part of the equation. The mean and fluctuating velocities is also given in index form as \bar{u}_i and u'_i respectively.

One of the most common eddy viscosity models is the k- ε model that uses two new partial differential equations to model the turbulence. In short the k- ε model uses one transport equation for the turbulent kinetic energy and one for the dissipation, ε together with a model for the turbulent viscosity, μ_t . There exist different kinds of k- ε models that model the eddy viscosity in different ways and have some extra terms in the dissipation equation. A more in depth description of the realizable k- ε model is provided in appendix A. When using the realizable k- ε model the solver might use a wall function based on the law of the wall.

A small side note that will become important later is how the solver collect values to when computing a flow variable at a certain cell. This is called discretization, there exist different schemes that have different properties and different complexity, one of these properties is the order of accuracy.

2.2 Fundamentals of Aerodynamics

This section will give a brief introduction to the field of aerodynamics. This field is the application of fluid dynamics on object where the interest lays in how the object interacts with the flow and vise versa.

2.2.1 Forces

When an object moves through a fluid the fluid will exert a force on the travelling object. This force comes from two main factors, namely pressure and friction. The pressure force is simply the reaction force due to the object moving air around itself. The friction force comes from the shearing forces between fluid and object.

In the automotive industry the most important force on a object is the drag force. This is the aerodynamic forces preventing the object from moving forward. There does also exist forces that act in the transverse direction of the object. This force is not as important as the drag force but can be important in the development of trucks due to their large side area. The force in the vertical direction is called lift force if acting up and down force when acting down. This force is not important in truck aerodynamics either since the weight of a truck is so much more than any realistic wing could lift in the speeds reached by a truck. In cars the lift force could

become a problem if a particular bad design was chosen reducing the grip and possibly introducing unnecessary instabilities.

In the industry there exist a lot of different vehicles from motorcycles to heavy trucks. Since these vehicles are so different in size the forces acting on them will be not only dependant on the design but also on the size of the vehicle. This is also true when comparing trucks to trucks and so on. For a fair comparison in between vehicles a non dimensional value called the force coefficient is used. This can be applied in all three directions of the vehicle and a generic equation is shown in (12). Most often the force coefficient is renamed to the force that is relevant for the investigation; i.e. in this particular coordinate system C_x is the same as C_D (Coefficient of drag), C_z is called C_L (Coefficient of lift) and C_y is C_S (Coefficient of side force).

$$C_i = \frac{F_i}{\frac{1}{2}\rho AU_\infty} \quad (12)$$

Where $i = x, y, z$, ρ is density, F_i the force in either x, y, z , A the characteristic area and U_∞ is the freestream velocity. These quantities of forces are in the report often referred to in terms of “counts”, $\frac{1}{1000}$ of C_i , e.g., $C_D \times 1000 = \text{drag in counts}$.

2.2.2 Truck Aerodynamics

The flow around an object will depend a lot on the geometry of said object. Sudden changes in geometry are often bad for the efficiency of aerodynamic devices. In this section the most important flow features that can develop due to interactions with an object will be discussed.

Separation is a phenomenon where the boundary layer detaches from the geometry. This occurs when an adverse pressure gradient occurs from a geometry change. This is more prone to occur when the geometry change is fast and abrupt. A separation will be accompanied by a wake formed behind the separation with a low pressure region. This region of low pressure behind the object is bad for the aerodynamic efficiency since the low pressure “pulls” the object backwards. A low pressure zone could likewise pull something forward if it is in front of an object. In road vehicles there is most often a low pressure zone behind the vehicle, often called wake, reducing the wake size can lead to significantly lower drag. One way of doing this is by delaying separation or eliminating it if possible by adapting the geometry and using other ways of controlling the flow.

Wind average drag is a method used to evaluate a vehicles aerodynamic performance with the different yaw angles it will be subjected to in real wind conditions, making it a more representative measure of the real world performance. For ground vehicle aerodynamics the standard method to use is the SAE J5212 [12] which will also be used in this work.

In general the drag accounts for about 25-50 % fuel consumption for heavy goods transport vehicles, depending on shape, weight, and road conditions [13]. Specifically for timber trucks in Sweden drag is responsible for around 30 % of the fuel consumption when loaded and traveling at 80 km h^{-1} which they do most of the time [4].

2.2.3 Timber vehicle Specifics

A timber vehicle transports the timber without any covers, this means that the timber is in direct interaction with the aerodynamics of the vehicle. This is a huge difference to regular swap body trucks where the flow interacts with flat surfaces. In this report many of these irregular parts will be mentioned and the flow interacting with them is the key to understanding the increased drag that can be found on a timber vehicle.

A timber vehicle in Sweden is most commonly consisting of a truck-trailer combination [5]. In this work the whole timber truck consisting of both truck and trailer will be called the vehicle and the truck and trailer will be treated separately when needed. Other important regions of the vehicle is the cab in the front of the vehicle and the chassis of both the truck and trailer.

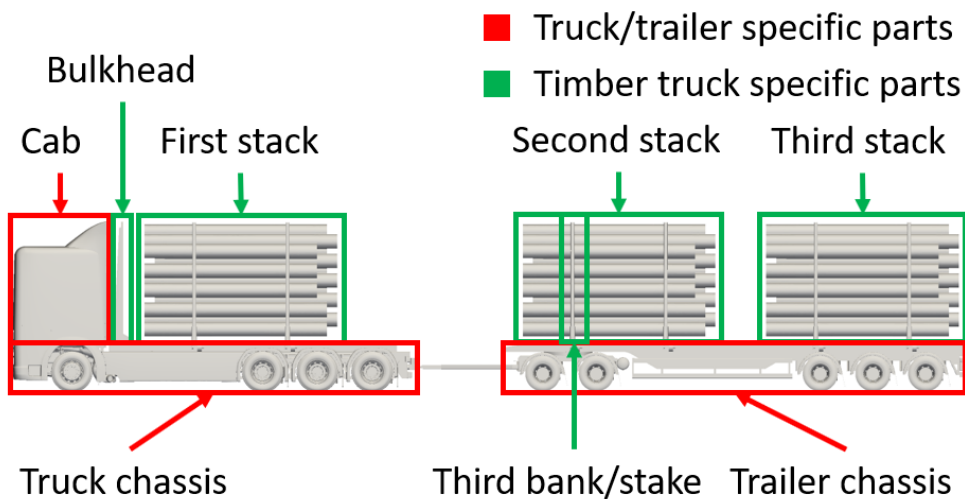


Figure 2: Illustration of the important regions of the timber truck. The naming scheme that will be used through out the work is presented and illustrated. Note that not all of the stack and banks are annotated but the counting starts after the bulkhead and move to the rear of the vehicle.

The timber is loaded on the vehicle on so called bank and stakes. The banks are basically a beam that is connected to the vehicle chassis, on these banks the stakes are mounted to keep the timber from sliding off in the transverse direction. To securely fasten the timber on the vehicle straps are commonly used and the timber is strapped down to the vehicle. To do this there is some times winches mounted on

the banks to tighten these straps. On the vehicle there is a total of three pairs of stacks and banks that allows for there different stacks to be loaded. The first stack is located on the truck and stack two and three on the trailer. Specific for timber trucks is also the bulkhead that is located behind the cab. This is a plate that in the case of a crash or hard braking will protect the driver in the cab from timber penetrating the cab.

Another thing that is specific to a timber tuck is the way the loading and unloading proceeds. When the timber truck is loaded this is commonly done by a small crane that loads one or a few logs at a time depending on the size. The crane can be mounted on the truck itself or on a special loading truck. During unloading it is common to use large timber forklifts which can grab the whole stack in one single lifting operation. This is done from the side so the timber truck needs to be open on the sides between the banks and stakes where the truck needs to place the lifting equipment.

3 Method

As this work was a continuation of the previous studies done within ETTaero2, large parts of the methodology build upon on the results and methods established [2, 3, 14]. The basis was the CFD procedure for ground vehicle aerodynamics used at LiU; a semi-automated processes where pre-processing is done in ANSA [6], scripted volume meshing and solving in Fluent [7], and scripted post-processing in ParaView [8] and MATLAB [9]. These parts were already used in a workflow where they are independently automated by scripting.

During this work the CFD methodology used at LiU was further developed, originally this methodology required the user interaction in all the steps from a geometry to post-processed results. This process was mostly automated and in the end minimal inputs from the user were required. The steps of the new CFD procedure in terms of software and function are shown in figure 3. In the first step the user needs

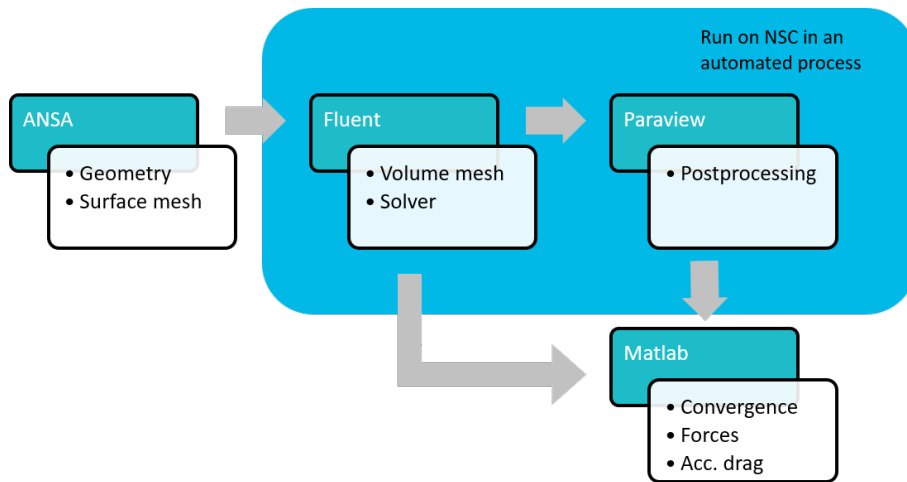


Figure 3: Schematics of CFD procedure, the user only has to prepare the geometry in ANSA and produce data plots in Matlab. In between these steps the process is automated and run on the NSC cluster Sigma [10].

to supply a CAD model of the geometry, most often this geometry needs to be prepared for use in CFD, meaning that it has to be watertight and unnecessary features are removed. The user also has to generate a surface mesh after which the user sends the the model into the automated procedure. Following steps were preformed on the NSC computing resources [10]. Fluent Meshing will read the surface mesh and output a volume mesh with the mesh statistics and quality limits for the user to assess. When the meshing is done a dependent job for solving in Fluent is started, from which the necessary data is exported. A third job is started on the cluster to run Paraview using a Python script. ParaView produces figures that show results

of surface field data and bulk flow data. It also export data to be used in Matlab to produce accumulated drag plots. Finally the user checks convergence and produce the plots of accumulated drag using Matlab.

The purpose of the method was to evaluate aerodynamic concepts on the timber vehicle. Turnaround time of a complete case run for one yaw angle was about 11-14 hours in total, 5-7 hours meshing, 4-5 hours solving, and 2 hours post-processing. If more yaw angles are to be run the solving and post processing time is multiplied by the number of angles to be investigated. Following sections go more into depth of how each part of the method works and how they were developed.

3.1 Geometry

The level of detail of the current timber truck model was more realistic than in the previous studies [2, 3]. Some major differences are chassis and wheels which in the previous model was very simple and based on a previously used wind tunnel model [15], many peripherals were added such as bumpers, air tanks, tie-down winches, a detailed grill, cooler, and engine compartment which allow for flow through it. Figure 4 show the different models and figure 5 depicts the difference in model detail.

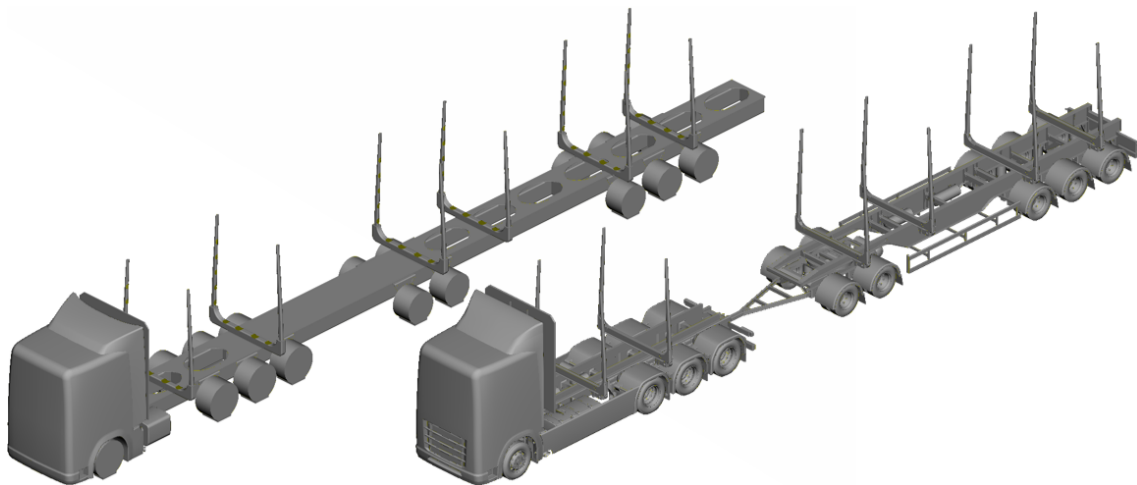


Figure 4: Left: previous model, Right: current model. The difference in realistic detail is large, notable is the chassis and wheels which in the previous model was very simple. Further, the current model add details in the form of peripherals parts as bumpers, air tanks, tie-down winches, etc. which are not present in the previous model.

The vehicle geometry for this master thesis was collected from multiple sources. Scania provided the bare truck, i.e., the truck excluding the timber banks and stakes that are mounted to the truck. Timber banks and stakes are from the manufacturer ExTe. The trailer is rebuilt from a wood chip trailer provided by MT Eksjö. And the bulkhead geometry was provided by Vemservice.

The raw model geometry has to be prepared for volume meshing, this was done

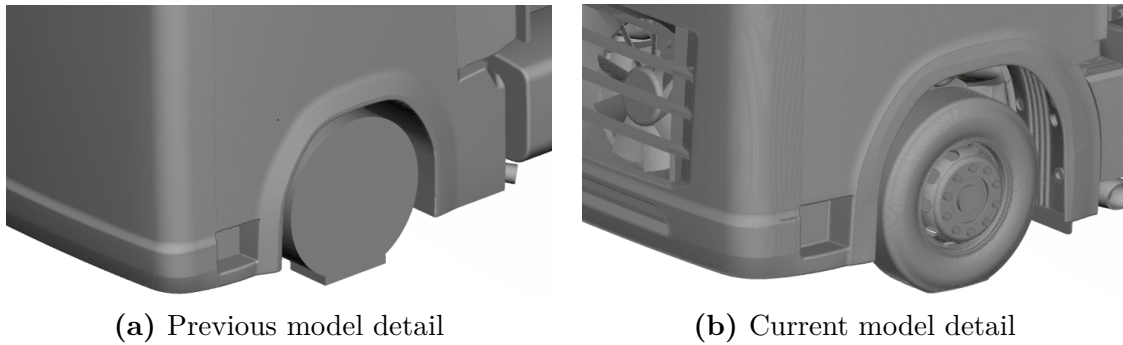


Figure 5: Model detail comparison; the current model have a detailed grill, cooler, and engine compartment which allow for flow through it.

in ANSA [6]. First the geometry reconstructed such that all edges of the surface model have one mating edge thus making it watertight which is required for the volume meshing. Next step is to assign so-called PID's to the surfaces, a strict naming convention was used for the PID's. The naming referred to part/region of the geometry and which boundary type, mesh sizing, and prism layers setting were to be used in the generation of the volume mesh and solver setup. Then the surface mesh can be created.

3.1.1 Vehicle Configurations

The different timber vehicle configurations in this work are gathered from a report made by Skogforsk explaining the different vehicle configurations [5]. As earlier mentioned the work is focused on the group vehicle type, meaning it does not have a crane mounted on the truck. Three different configurations are commonly used today in Sweden, they are 64, 70, and 74 ton variants of a truck trailer vehicle. The 64 ton version is built up using a 1-2 axle truck and a 2-2 dolly-trailer, or in total 1-2-2-2 as seen in figure 6a. In Sweden this is and has been for a long time the by far most common vehicle configuration used in the industry today [5].

During the year 2018 a new road classification was established called BK4, which allows for heavier vehicles, up to 74 ton, on BK4 roads [5]. By adding one more wheel axle on both the truck and trailer in a 1-3-2-3 configuration as shown in figure 6c, this vehicle is allowed to load significantly more without increasing axle load. In the future most timber vehicles will be of this type when older vehicles are replaced as more and more roads earns the BK4 classification. However, the 74 ton vehicle effectively needs the truck to be higher as a higher bulkhead is required for safety reasons. As the original cab was equipped with a top wind deflector suitable for a 64 ton vehicle the geometry of the deflector was manipulated for the 74 ton truck.

The new road class also made the introduction of the 70 ton configuration possible, where only the trailer is different from the 64 ton type. By adding a third axle on the rear of the trailer, making this a 1-2-2-3 configuration, as shown in figure 6b. The extra weight is distributed so that the load per axle is within legal limits, hence making it possible to load higher stacks on the trailer. This configuration becomes

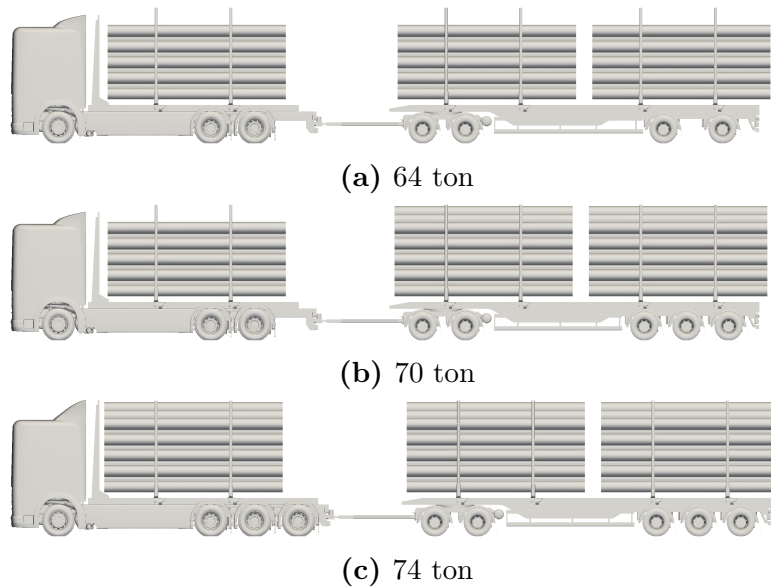


Figure 6: Today’s most common timber vehicle configurations in Sweden. Often a crane is seen mounted on timber trucks, this is not included in this study as it focus on crane-less “group vehicles”. The difference between the 64 ton vehicle and the newer 70 and 74 ton types are the additional wheel axles allowing for loading higher stacks of timber.

more and more common on the roads as the possibility to haul more timber is beneficial but also, the ability to have larger margins when loading 64 ton on smaller roads is beneficial. Compared to the 74 ton vehicle the 70 ton is a simpler and less expensive way to take advantage of the new regulations as only the trailer needs to be changed or modified while an existing truck can be used [5].

The vehicle total dimensions are limited by the European Modular System; maximum length L is 25.25 m, width W 2.6 m, and height H is 4.5 m; due to the nature of loading timber maximum length is rarely reached [5]. All configurations and concepts evaluated in this report followed these standards.

3.1.2 Domain

The computational domain, as shown in figure 7, consisted of a rectangular box, 11.5 vehicle lengths longitudinally (x), 55 vehicle widths transversely (y), and 13.5 vehicle heights vertically (z). The timber truck was placed transversely in the middle, and longitudinal position was such that the distance to the inlet was 3.5 truck lengths and 7 truck lengths downstream to the outlet. Compared to the the previous study the domain size was increased [3], the solid blockage from the vehicle was 0.15 %. The domain was compliant with the SAE J2966 standard [16]. The vehicle was modeled at real life scale. Reference vehicle dimensions are length $L = 24.5$ m, width $W = 2.6$ m, and height $H = 4$ m; it follows that the reference area A is 10.4 m^2 . Real vehicle dimensions may vary somewhat between models, but in the context of domain size and requirements this was deemed insignificant.

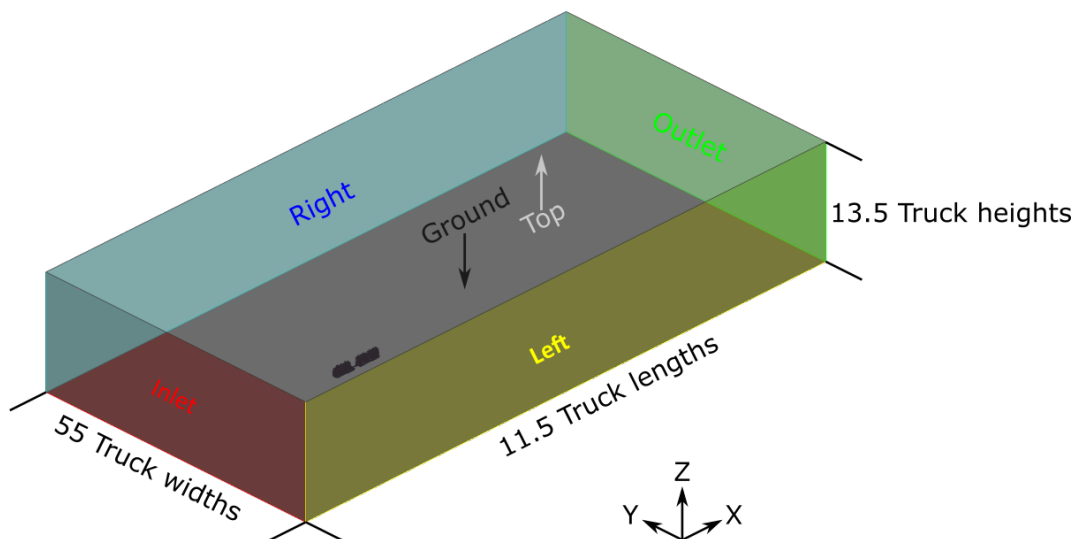


Figure 7: Computational domain and boundaries, vehicle placed 3.5 vehicle lengths downstream of the inlet and 7 truck lengths upstream of the outlet. Reference vehicle dimensions are truck length 24.5 m, truck height is 4 m, truck width is 2.6 m, 0.15 % blockage.

3.2 Boundary Conditions

Physical properties that were used in the fluid model for air was density $\rho = 1.225 \text{ kg m}^{-3}$ and dynamic viscosity $\mu = 1.7894 \times 10^{-5} \text{ kg m}^{-1} \text{ s}^{-1}$. The reference velocity was the longitudinal freestream velocity $U_{x\infty} = 22.2222 \text{ m s}^{-1} \approx 80 \text{ km h}^{-1}$, also used as the vehicle velocity. This represents road-like conditions where the vehicle speed is independent of the side wind, i.e. the velocity x -component on velocity inlet boundary conditions was always $U_{x\infty}$. Using a full scale model at a realistic velocity implies a relatively high Reynolds number, applying a lower Reynolds number would be less expensive computationally as a coarser mesh can be used. However, for heavy transport ground vehicles it has been demonstrated that for the results to be representative at all the width-based Reynolds number has to be a minimum of 2 million [17]. Using the Reynolds number that correspond to full scale realistic case improves accuracy of the drag prediction as it highly depends on the Reynolds number [17]. The width based Reynolds number Re_w was in this study 4 million, using $U_{x\infty}$ as characteristic velocity.

Side wind or yaw was introduced by imposing a velocity y -component, $U_{y\infty}$, on all on velocity inlets. A detailed Summary of the boundary conditions is shown in table 1. The type of boundary conditions of Inlet, Left, and Right are dependent on the yaw condition. In the case of 0° yaw Inlet was set to a velocity inlet with the velocity $U_{x\infty} =$ only in the x -direction, Right and Left used a symmetry condition. For a yawed case both Inlet and Left utilized a velocity inlet boundary condition where

the velocity x -component was $U_{x\infty}$ and the added y -component defined as

$$U_{y\infty} = U_{x\infty} \tan \beta \quad (13)$$

where β is the yaw angle around the z -axis relative to the x -axis. The main yaw angle for the study was 5° , this is based on previous studies [2, 3, 14] and also recommendations from Scania. For the ground a moving wall boundary condition was used; a no-slip wall with a prescribed velocity of $U_{x\infty}$ in the x -direction was used. Top of the domain used a symmetry condition. Wheel rotation was emulated by applying a moving wall velocity with no-slip condition on tires, rims, and break disks; an angular velocity ω was applied to each row of wheels using its axis as a reference such that the outer diameter of the tire had the same velocity as the moving ground.

Table 1: Summary of boundary conditions, some boundary conditions are dependent on whether any yaw condition is specified or not.

Boundary	Condition	
	$\beta = 0^\circ$	$\beta \neq 0^\circ$
Yaw		
Inlet	$(U_{x\infty}, 0, 0)$	$(U_{x\infty}, U_{y\infty}, 0)$
Right	Symmetry	Constant 0 Pa
Left	Symmetry	$(U_{x\infty}, U_{y\infty}, 0)$
Outlet	Constant 0 Pa	
Top	Symmetry	
Ground	Moving no-slip wall $(U_{x\infty}, 0, 0)$	
Wheels	Rotating no slip wall ω	
Walls	No slip wall	

3.2.1 Porous media

In the truck there is a cooling system located under the driver compartment. The cooling system use radiators to transfer excess heat from the systems that need cooling to the passing air. The resistance caused by the radiators when air flows through them causes a pressure drop, which in turn results in a significant contribution to drag, about 40 counts of drag. Also, air passing through the radiators is forced to only move in one direction by its vanes. No heat transfer was considered for this study.

This was modelled in the CFD solver using the porous media functionality, in order to assign different cell properties each radiator was modelled as a separated cell zone. The cell zone is then later set to be a so called porous media zone. In this zone the solver will then add a extra momentum source term to the momentum equations that represent the porosity of the media. All of the information presented in this section is gathered from Ansys Fluent user guide [18]. The source term S_i is defined as

$$S_i = \left(\sum_{j=1}^3 D_{ij} \mu v_j + \sum_{j=1}^3 C_{ij} \frac{1}{2} \rho |v| v_j \right) \quad (14)$$

and uses two prescribed matrices, the viscous loss matrix D and inertial loss matrix C that have to be specified for the zone. Other quantities in the equation are the dynamic viscosity, μ , v_j the velocity in direction j and $|v|$ the velocity magnitude. In Fluent these are defined by the user who need to specify the viscous resistance coefficients $\frac{1}{\alpha}$ to fill D and the inertial resistance coefficient C_2 to fill C . The user does just have to specify values for these coefficient in each direction.

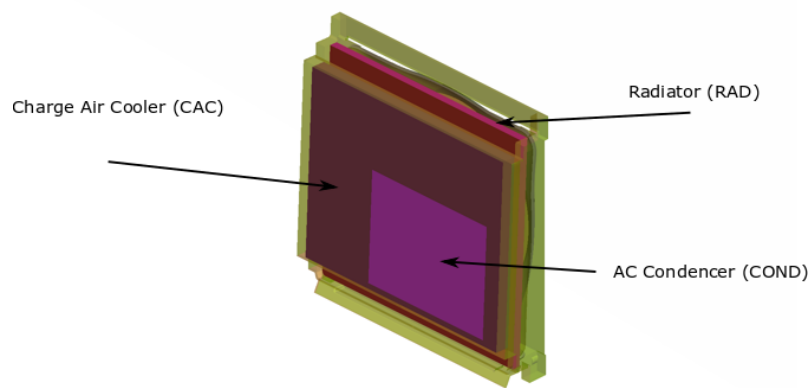


Figure 8: Layout of the different radiators in the cooling package.

In the truck that Scania have provided there are three radiators that needs to be accounted for. The position of these in the cooler package are shown in figure 8. Also given by Scania are experimental data for the pressure drop over the radiators. The data are given on the form as shown in equation (15) and values for I_i , the inertial resistance and V_i , the viscous resistance and thickness of the radiators provided.

$$\frac{1}{\rho} \frac{\partial p}{\partial x} = I_i u^2 + V_i u \quad (15)$$

This equation contains the the pressure p , density ρ and velocity u . Using equation (15) and the values provided it is possible to derive that the following relations are true

$$\frac{1}{\alpha} = \frac{V_i \rho}{\mu} \quad (16)$$

$$C_2 = 2I_i \rho \quad (17)$$

Using equation (16) and the provided data from Scania the values shown in table 2 were calculated. The coefficients are to be defined for each direction in the cell

Table 2: Settings for porous zones as used in Fluent.

Zone name	Viscous resistance (m^{-2})	Inertial resistance (m^{-1})
Radiator	3.0122×10^7	140
CAC	1.6430×10^7	160
COND	2.9437×10^7	210

zone. From recommendation in the Fluent user guide the values were multiplied by 10^3 in the y and z directions in order to emulate the aligning effect from the vanes in the cooler

Important to notice is that the radiators are tilted by 2.5° around the y -axis, therefore, the local coordinate systems for each of the zones was tilted. This was solved in Fluent as the user need to specify a local coordinate system for the porous media. The drag force F_{cooler} of the cooler parts was calculated from the drop in total pressure p_{tot} multiplied by its area A_{cooler} in the x-direction as

$$F_{\text{cooler}} = (A_{\text{cooler,out}}p_{\text{tot,out}} - A_{\text{cooler,in}}p_{\text{tot,in}}) \cos(2.5^\circ) \quad (18)$$

3.3 Solver

All simulations were steady state and carried out in Fluent [7] using the pressure based solver with the realizable $k - \epsilon$ RANS turbulence model paired with Enhanced Wall Treatment. This setup has previously shown good capability to predict drag on heavy ground vehicles [3, 19, 20], and follows the setup used in the previous studies [2, 3, 14]. The solver discretization is summarized in table 3, these are the same settings as used in the previous studies except for 2nd-order k and ϵ [2, 3]. It was discovered that the difference between 1st- and 2nd-order discretization of k and ϵ had a great impact on total drag, further explained in section 3.5. The entirety of the solver setup was automated using scripts in Fluent.

Table 3: Summary of final solver discretization schemes.

Quantity	Discretization
p - v coupling	Coupled
Gradient	Least Squares Cell-Based
Pressure	Standard
Momentum	2 nd -order Upwind
k, ϵ	2 nd -order Upwind

When using the coupled solver it is required to specify the flow Courant number which together with explicit relaxation factors for momentum and pressure are used to control the solution convergence rate and stability. These setting were adjusted to improve convergence, as displayed in table 4. Doing so had a major impact on the computational cost as the convergence rate and stability increased. Convergence was reached in 2500 - 3000 iterations and the result had much less fluctuations.

Table 4: Comparison of solver relaxations, the “Old” settings are those used in the previous studies [2, 3] and “New” are the final settings that were used in the procedure developed in this study.

Old			New (Final)		
No. iterations	CFL	Relaxation	No. iterations	CFL	Relaxation
20	20	0.35	20	20	0.35
100	200	0.7	400	500	0.5
150	75	0.5	300	200	0.45
3500(to end)	20	0.35	300	100	0.4
			500(to end)	30	0.35

As mentioned previously the discretization of turbulent quantities, 1st- or 2nd-order, has a significant influence on estimation of drag, it also had a positive impact on solution convergence. In contrary to the common issue where it is harder to achieve converge for 2nd-order schemes than for 1st-order it instead improved convergence greatly for the problem at hand; total number of iterations were cut from ≈ 3500 to ≈ 1500 , figure 9a shows the convergence of the baseline vehicle. Altogether, the final solver setup showed very good performance and convergence, the computational cost was about 4000 - 4500 core hours. The cost was even comparable to that of the previous simpler model, 150 million cells, with the old solver strategy which cost around 3000 - 3500 core hours on Sigma [10].

Total drag was calculated as an average of the last 500 iterations for robustness in the event of oscillations in the solution. For each case the forces were examined to deem convergence, plots like figure 9a were used.

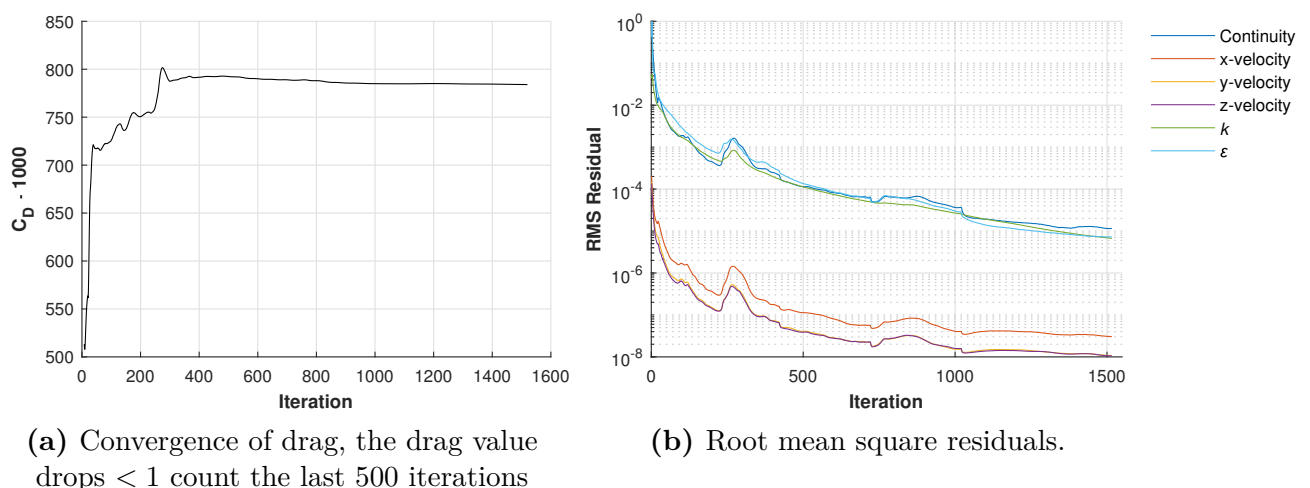


Figure 9: Solver convergence history, drag coefficient and Root mean square residuals during simulation run for loaded baseline vehicle at 5°.

Residuals of the governing equations were also monitored, although there were never any issues with them. The typical behaviour of the residuals can be seen in figure 9b, where the root mean square residual quantities for the baseline vehicle are shown.

3.4 Meshing

The meshing procedure was in principle the same with regard to type of mesh and meshing method as established in the previous studies [2, 3], however, with some differences which are described later in this section. The meshing was a part of the fully automated method through the scripts in Fluent. A watertight triangular surface mesh of the all surfaces was generated in ANSA, with a quality requirement of a maximum element skewness of 0.5, the same as previously used [3].

This is done by first assigning spacing to the edges of the model surfaces which corresponds to the desired surface mesh size, when doing so the “Refine Trailing Edge Ratio” option was used to improve quality. This option automatically refine the nodal spacing on thin edges where otherwise elements would have been skewed. When the spacing had been done the surface mesh could be generated. These two steps were repeated for each level of mesh size from fine to coarse to achieve the desired surface mesh. Surface mesh sizings were divided into 4 levels, coarse, medium, fine, and extra-fine, figure 10 show the distribution of the final surface mesh and sizing details in table 5.

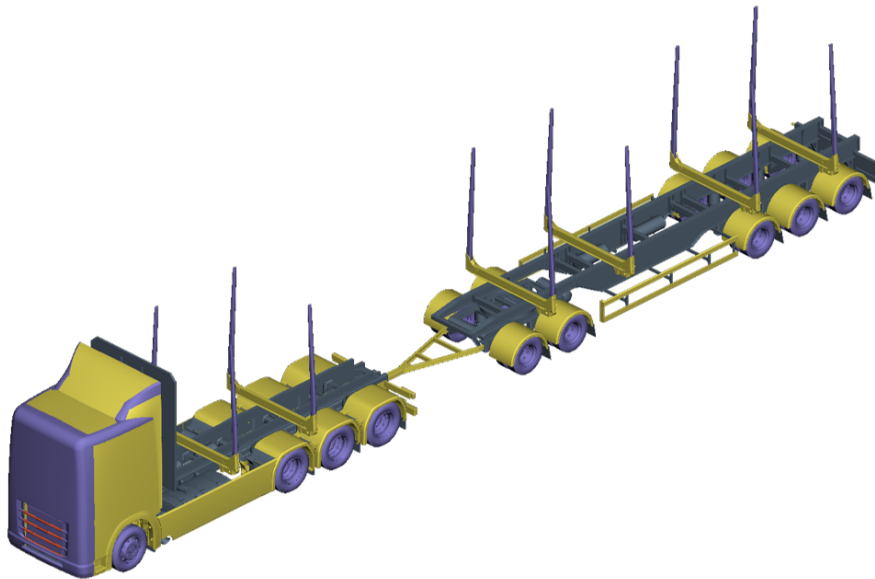


Figure 10: The 74 ton unloaded baseline truck. The different colours show the applied surface sizing, orange Extra-fine, purple Fine, yellow Medium, and grey Coarse.

After the initial surface mesh had been generated the model was checked for quality and surface proximity issues which then were fixed. Quality measure of element skewness was allowed to be ≤ 0.5 . Proximity issues is when neighbouring surfaces are so close to each other so that it the produced volume mesh most certainly will be of poor quality in that area.

Fluent Meshing was used for the generation of the volume mesh with the meshing method octree hexcore as found most suitable [2, 3, 14]. In short, hexcore mesh is a hybrid mesh type that consists of tetrahedron cells and mainly Cartesian cells

Table 5: Surface mesh sizing, (mm). The surfaces of the model were divided into different categories to control the distribution of mesh density.

Sizing	Min	Max
Extra-fine	1	2
Fine	2	4
Medium	4	8
Coarse	8	16
Ground	32	2048
Boundaries	2048	2048

in the bulk of the domain. From the triangular surface mesh there are layers of triangular prism cells that interface with the tetrahedron cells connecting with the Cartesian cells. The layers of triangular prism cells are so-called inflation layers. The main advantage of the hexcore method is that it maintains the versatility of a pure tetrahedron mesh but reduces the number of cells dramatically [21]. An example of the volume mesh is show in figure 11.

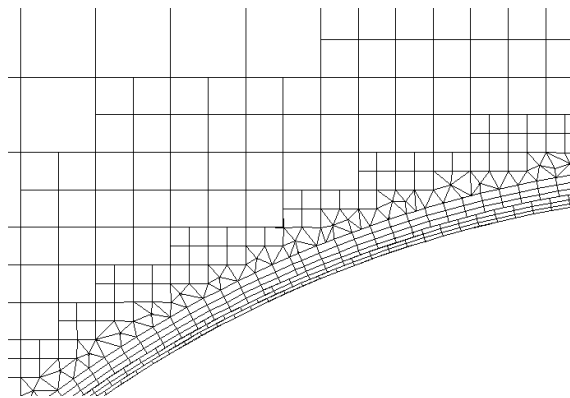


Figure 11: Volume mesh, cells transitioning from Cartesian to tetrahedron to wedge prism, located at the top radius of the truck cabin.

Octree is a way to fill the domain with Cartesian cells, an important aspect of this is how these cells are sized. The surface mesh prescribes its size to the most adjacent Cartesian cells while sizing in the bulk cells are controlled by global settings and a so-called Body of Influence (BOI) scoped sizing [21]. In this case BOI's were used to locally refine the mesh around the truck at 5 levels, figure 12 shows the final BOI setup. The surface mesh of the ground was also sized in accordance to these BOI's.

All three loaded truck configurations used the same set of BOI's while they were adjusted for the unloaded trucks. The unloaded trucks have a similar *BOI 5* that also cover the cab but instead of enclosing the whole loading volume just enclose the stakes angled in a way to catch the wake with and without yaw angles.

As mentioned earlier in this section the mesh was built up of different types of mesh topologies, one of them inflation layers. The main feature of the inflation layers is the high resolution of the mesh in the direction normal to the wall in order to capture the boundary layer effects near the wall surfaces. Another benefit of this

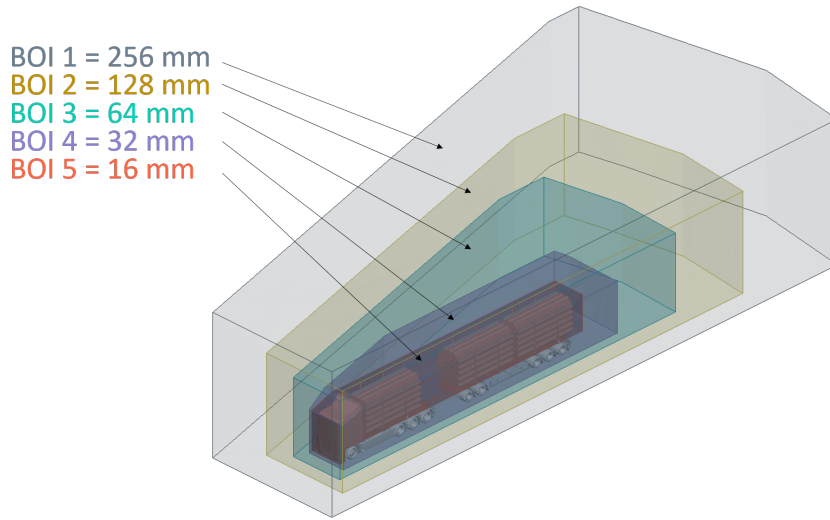


Figure 12: Bodies of Influence used for the loaded timber truck, the surface mesh of the ground was also sized in accordance to these sized.

is that the flow near the wall which is aligned with the wall is allowed to pass through the cell closer to perpendicular to the cell sides, which is better due to less numerical diffusion, often called false diffusion [11]. Wall surfaces with inflation layers was divided into four groups P1-P3 and ground, as per table 6 and figure 13. P1 had 6 layers and used the last aspect ratio method [18] for good control of y^+ in critical areas. P2 and P3 uses the first aspect ratio method [18] as it ensures good transition between inflation layers and bulk volume mesh; P2 used 6 layers and P3 used 3 layers.

Table 6: Inflation layers settings were different depending of the location on the model. This was done both to have more control of the y^+ value in certain important locations and to have fewer layers at other locations.

Name	No. layers	Settings
P1	6	Last aspect ratio = 0.4, first layer height = 0.75 mm
P2	6	First aspect ratio = 6, growth rate = 1.2
P3	3	First aspect ratio = 6, growth rate = 1.2
Ground	6	First aspect ratio = 8, growth rate = 1.2

P3 was used in areas not directly exposed to the freestream, mainly parts of the chassis, to reduce the number of cells. 6 inflation layers were applied to the ground using first aspect ratio. The ground mainly consist of relatively large elements thus the cost of maintaining 6 layers is not significant compared with switching to 3 layers, this also makes for a better transition to the tires of the vehicle.

However, it is important to note that the first cell height y^+ value in this study was not small enough to reside in the viscous sublayer or buffer layer for most of the model surface. Instead, the method relies on a wall function to evaluate the

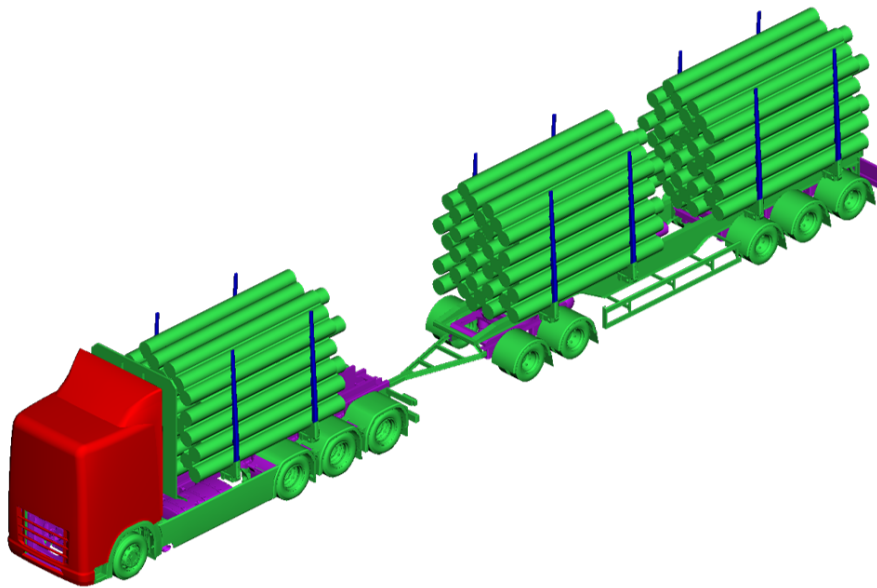


Figure 13: The 74 ton unloaded baseline truck. The different colours show the inflation settings according to table 6, red and blue p1, green p2, and purple p3.

region below the first cell which resides in the log-law region of the boundary layer, $30 < y^+ < 300$. Enhanced Wall Treatment function (EWT) was used together with the Realizable $k - \varepsilon$ turbulence model as it has shown good capabilities to predict realistic estimations of drag on ground vehicles in the past [2, 3, 14, 19, 20]. When wall functions are used it is recommended to maintain a $y^+ > 30$ because wall shear stress will deteriorate, therefore, it is recommended to utilize an so-called y^+ -insensitive wall function such as EWT [18]. As all y^+ -insensitive wall functions aim to overcome this issue, EWT uses a blend of wall function for coarser mesh and the standard two- layer model for finer mesh to achieve this [22]. This makes it less important to achieve a certain value for y^+ , it is more important that the inflation covers the boundary layer sufficiently [18]. The distribution of y^+ on the loaded baseline timber vehicle model is shown in figure 14.

Initially meshes were checked manually to ensure good transition between inflation prism cells and bulk Cartesian cells until the robustness of the method was deemed sufficient. Quality measures in Fluent Meshing that were considered for the volume mesh was ICEMCFD-quality and orthoskew, the former was prioritized and used for automated quality improvement by the “auto-node-move” function. For ICEMCFD-quality a < 0.95 was allowed; ICEMCFD-quality is a measurement of multiple quality measures depending on cell type. For Cartesian cells the determinant, max “orthogls” which is the maximum deviation of internal angles from 90° , and max “warppls” calculated as maximum face warp of the cell. For tetrahedron cells it is calculated as the skewness, and prism cells use warp and determinant [21].

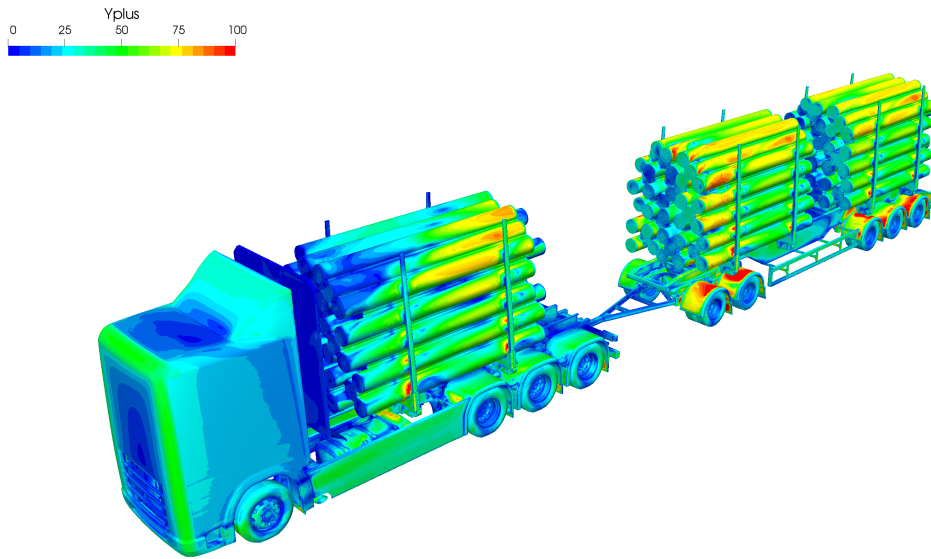


Figure 14: Distribution of y^+ on the geometry during on the loaded baseline model at 5° yaw.

3.4.1 Inflation Study

The level of detail of the current more realistic timber truck model required a finer surface mesh than in the previous studies to be able to capture the geometry accurately. However, the requirement for a finer surface mesh constitutes a problem with regard to the size of the volume mesh. Using 10 - 16 layers inflation layers as previously [2, 3] would result in a high number of cells and increased simulation time, therefore, the number of inflation layers was reduced to 3 - 6.

By conducting a study comparing this new inflation strategy to the previous one it was verified that it was a suitable approach as there was no significant difference in the result. From figure 15, which compares the total drag between the two meshes for different yaw conditions, it was deemed that the total drag was captured sufficiently good with a maximum difference of approximately 1 %. Using the previous vehicle model in a loaded configuration the new finer surface mesh together with fewer inflation layers, a maximum of 6 was compared to the old mesh settings with a maximum of 16 inflation layers [2, 3]. This was done for yaw angles of 0° - 15° , using the same solver settings as in the previous studies [2, 3], these simulations were run for an excessive amount of iterations to also evaluate convergence. Convergence was obtained after about 4000 - 5000 iterations, drag coefficient was calculated as an average of the last 1000 iterations. 0° yaw was left out here because of the solution suffered from a very high amplitude oscillatory behaviour, however, the trends showed good agreement. A tabulated comparison is found in appendix B.

As important as the total drag is correct the distribution of drag also needs to be correct; there can be many local errors that are not discovered if only integrated quantities are evaluated. Therefore, the accumulation of drag along the vehicle was compared, see figure B.2 in appendix, where the two methods also showed very good

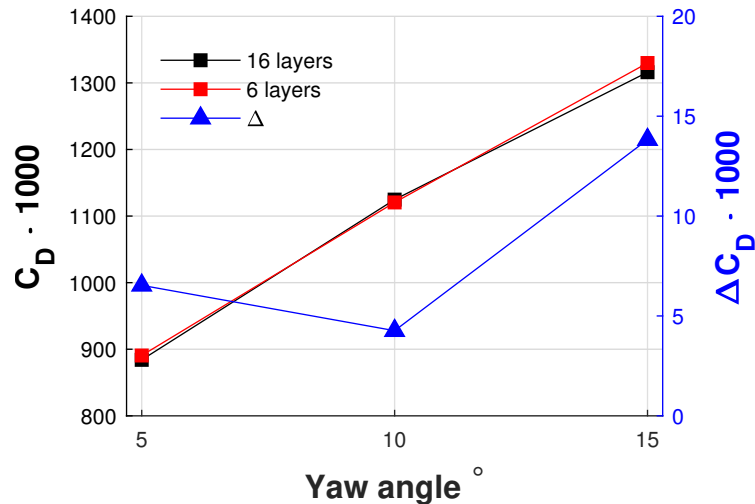


Figure 15: Comparison of total drag coefficient between the two meshes for three different yaw angles. Maximum relative difference was 14 counts for 15° of yaw or approximately 1 %.

agreement in terms of drag distribution.

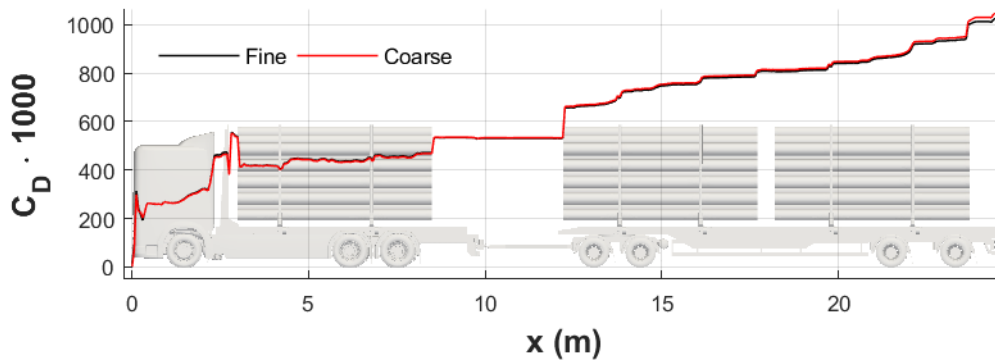
3.4.2 Mesh Density

Even though the new meshing strategy resulted in satisfactory results the number of cells was still very high, > 550 million cells for the detailed current model of a fully loaded truck. In the end it was possible to reduce the number of cells to 430 and 375 million cells for the loaded and unloaded vehicle respectively, which helped to reduce computational cost; convergence was reached in approximately 3500 iterations instead of 5000 - 6000 iterations. This was accomplished by adjusting the sizing and definition of the BOI's, i.e., sizing in the bulk mesh was adjusted, the surface mesh did not change.

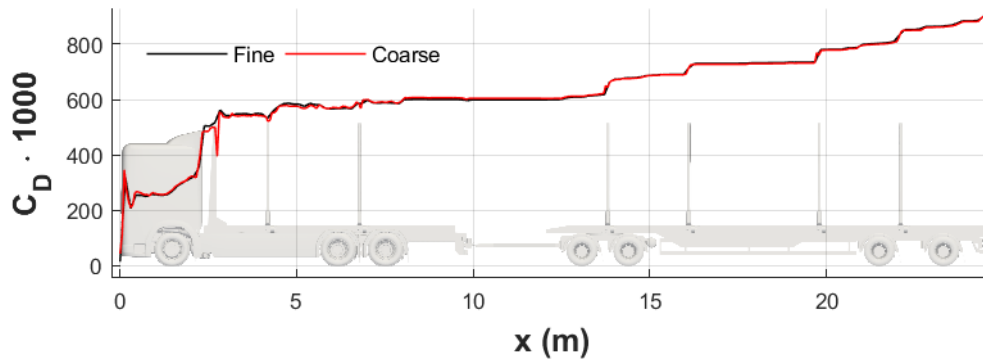
Figure 16a and 16b show the comparison between the coarse and fine mesh in the form of accumulated drag along the vehicle. The distribution of drag did not change significantly between meshes, and the difference in total drag was less than 2 %.

The geometry definition of BOI's 1-4 were directly carried over from the previous studies [2, 3]. Sizing prescribed by the BOI's were as follows: BOI 4 16 mm, BOI 3 32 mm, BOI 2 64 mm, and BOI 1 128 mm, which was finer than in the previous studies. This produced the 550 million cell mesh, here called “fine”. To reduce the number of cells the sizings were simply increased by a factor of 2, and instead a smaller BOI named BOI 5 was introduced. BOI 5 just covers the front of the truck and loading area along the entire vehicle and the sizing prescribed by it was 16 mm. This became the final set of BOIS, and the mesh it produced had 400 million cells and is here called “coarse”.

Note that the model used in the mesh density study was somewhat different from the final models in terms of wheel configuration. However, this was not expected



(a) Loaded state



(b) Unloaded state

Figure 16: Mesh comparison, accumulated drag at 5° yaw, distribution shows very good agreement for both loaded and unloaded conditions. Note on the unloaded vehicle that the results differ just downstream of the bulkhead, this was due to a somewhat lower sample density for the fine case missing the local minimum point.

to affect the result of what mesh density was appropriate. Also, the results were produced using 1st-order discretization of the turbulent quantities. As will be further explained in section 3.5 this had a big effect on the total drag, not so much the trends or distribution of drag just the magnitude; there was simply not time to redo them.

3.5 Method Problems

The method developed in earlier work have used the 1st order discretization on turbulent quantities [2, 3]. There is also literature that shows that this setup gives good correlation to wind tunnel data [19]. In both this study and the previous this have produced a result where there is a large leeward side separation from the A-pillar at 5° yaw, as seen in figure 17a. In the previous studies this wake was present for most of cases but was found to disappear for some concepts and stack configurations [2, 3]. The explanation for this behaviour was traced back to a flow feature behind the bulkhead that promoted this separation, which seemed reasonable and physically plausible.

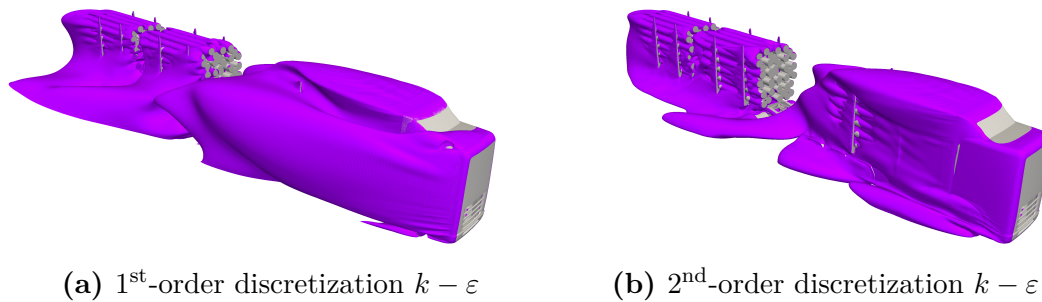


Figure 17: Total pressure = 0 Pa contour at 5° yaw. It was found that changing the discretization to 2nd-order for the turbulent quantities removed the large separation from the leeward A-pillar.

During the earlier model development this separation was always present at 5° yaw, even when testing the same stack configurations that earlier work saw large differences on. Finally in the early concept phase the area behind the bulkhead was closed of and the separation was expected to reduce in size, this was not the case and thus this phenomenon was further investigated. After discussions with Scania, according to whom this separation is not expected to occur at 5° yaw for a regular swap body truck, the method was tested with a swap body in place of the timber and timber specific parts which showed that the separation was still present.

When this was found different boundary conditions and other discretization were tested. The moving ground previously only specified in the close proximity to the truck was expanded to cover the entire ground as it seemed to have some impact on the wake close to the ground. The discretizations that was 1st order was increased to 2nd order. In the end it was found that the turbulent quantities was changing the separation and 2nd-order discretization made the flow stay attached as seen in figure 17b.

This separation had a huge impact on the total vehicle drag, alone it was responsible for 300 drag counts. This meant that some simulations had to be re-run during the end of the work. As all of the work was based on simulations done using 1st order of accuracy on the turbulent quantities it was investigated if these could be used in some way. As the accumulated drag over the vehicle was investigated it was found that the trends of the drag did not change and that the difference in drag was mainly isolated to the separation. This is shown in figure 18, the characteristics and the relative magnitude of the drag distribution was nearly identical, however, the general slope of the 1st-order result is somewhat steeper. For this reason the method development from earlier in this work was kept and motivated with simulations that was done with 1st order discretization for turbulent quantities.



Figure 18: Accumulated drag distribution for the full vehicle at 5° yaw using 1st and 2nd order schemes for turbulent quantities. The difference was found to be in the separation and when the lines are superimposed there is no significant difference between them.

The reason behind this behaviour when changing the discretization was investigated. Profiles of the eddy viscosity ratio (EVR) was investigated around the A-pillar. The distribution of these lines are shown in figure 19. The EVR is defined as the ratio between eddy viscosity and dynamic viscosity. As the simulations was too expensive to re-run and the solution data was deleted this was the closest variable to k and ϵ data was present for. As shown in equation 28 the eddy viscosity is closely related to the turbulent kinetic energy.

In figure 20 the EVR profiles for the defined lines are shown. At line 1 before the separation it can be seen that the 1st order simulation predicts a higher EVR. Line 2 is very close to the point of separation and a jump in the profile can be seen in the first mm's from the wall. The 3rd and 4th line do show that the flow keeps attached when using 2nd order schemes and separates with the 1st order. Note the different scales on EVR used for the different lines. The velocity profiles at the same lines, found in appendix figure C.3, show that the velocity was under predicted at all lines using the 1st order scheme.

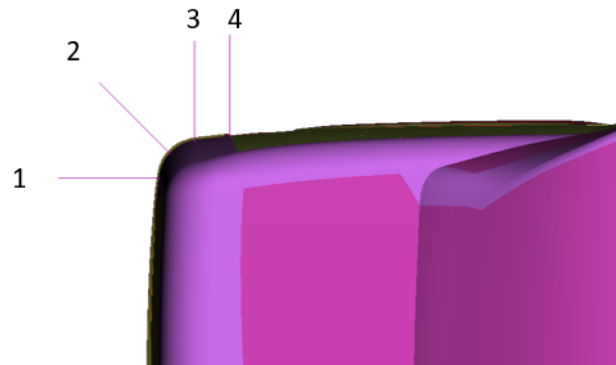


Figure 19: Viewed from above, the leeward side of the cab radius with the lines used to create velocity and EVR profiles. The lines were placed 2030 mm above the ground plane and extending 0.5 m normal from the cab wall.

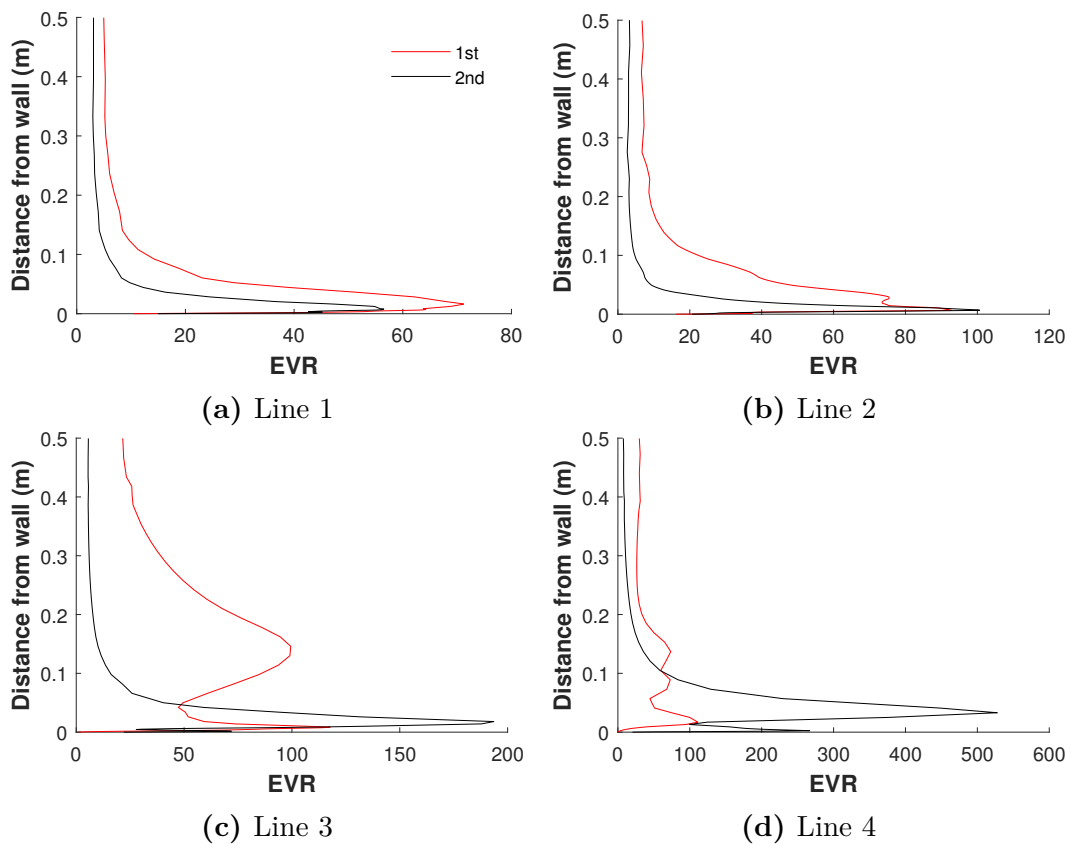


Figure 20: EVR profiles at different lines normal to the cab. The first order discretization can be seen to over predict k until the separation.

3.6 Post-Processing

Multiple forms of data were exported from the solver both during and after the simulation for post-processing. Most of the post-processing was done in ParaView [8], such as coloured surface data and iso-contours as a part of the fully automated process. Matlab [9] was used to produce line plots and scalar data, this was done in a semi-automated fashion where a script was run manually in the local result's directory where it also saved its output. Forces were defined as monitors and written continuously for each iteration in `.out` format, residuals are outputted in the Fluent terminal, the Slurm [23] environment on Sigma [10] saves the application output automatically as a `.out` file. These files are used to evaluate convergence, and also monitor the simulation during its run, this is done in Matlab via a script that is simply run from the solver output directory. This produces plots of force coefficients and residuals, e.g., figure 9a and 9b; scalar values for force coefficients calculated here as an average of the last 500 iterations.

For post-processing in ParaView select variables were exported post solving in EnSight-Gold format, a more compact format than full solver data files were only selected variables are saved. Post-processing in ParaView was entirely scripted in Python, which for a set of prescribed views would export imagery of quantities of interest. In form of surface data this was y^+ , static pressure coefficient C_p , skin friction coefficient C_f , as the latter two is what constitutes the forces on the vehicle. Definition of these coefficients are

$$C_p = \frac{p - p_\infty}{\frac{1}{2}\rho U_{x\infty}^2} \quad (19)$$

$$C_f = \frac{\tau_w}{\frac{1}{2}\rho U_{x\infty}^2} \quad (20)$$

where p is static pressure at the evaluated point, p_∞ is static pressure in the freestream, ρ is air density, $U_{x\infty}$ is reference freestream velocity, and τ_w is wall shear stress.

Total pressure coefficient $C_{p_{tot}}$ is defined as

$$C_{p_{tot}} = \frac{p_{tot} - p_\infty}{\frac{1}{2}\rho U_{x\infty}^2} \quad (21)$$

$$p_{tot} = p + \frac{1}{2}\rho U_{x\infty}^2 \quad (22)$$

where p and p_{tot} are static and total pressure respectively at the evaluated point, p_∞ is static pressure in the freestream, ρ is air density, $U_{x\infty}$ is reference freestream velocity. Total pressure coefficient was used as this is a good way to depict wake and flow structures; high total pressure equates to highly energized flow such as free stream whereas low values are within wakes and separations. Iso-contours at different levels of $C_{p_{tot}}$, mainly zero, was used to show wake structures, example see figure 17. Slices through the domain of $C_{p_{tot}}$ was also produced in x, y, z , this shows the distribution of flow energization which is a great tool to identify aerodynamically

problematic areas and what potential improvements there might be. Further, images of the geometry without any data was also exported, any named modifications in the model was colored red for presentation purposes as is seen in the results chapter when evaluating concepts.

Finally, to create the figures of drag accumulation along the vehicle both ParaView and Matlab were used. In ParaView the force on the vehicle was calculated, first for a small portion of the vehicle starting from the front, for each sample the length of the sample portion was elongated, in a total of 500 steps. This was saved in .CSV format, which could then be read via a script in Matlab that produce the accumulated drag plots seen throughout the report.

3.7 Automation

As stated in previous work [2, 3, 14] the meshing, solving, and post-processing were individually scripted, in this work this was taken a step further where these parts of the workflow were automated. This resulted in that the user is only required to prepare a watertight surface meshed model in ANSA, assign some settings such as case-name, configuration, yaw angle, etc. and in the end evaluate convergence using Matlab in a semi-automated fashion. The workflow of this procedure is shown in figure 21.

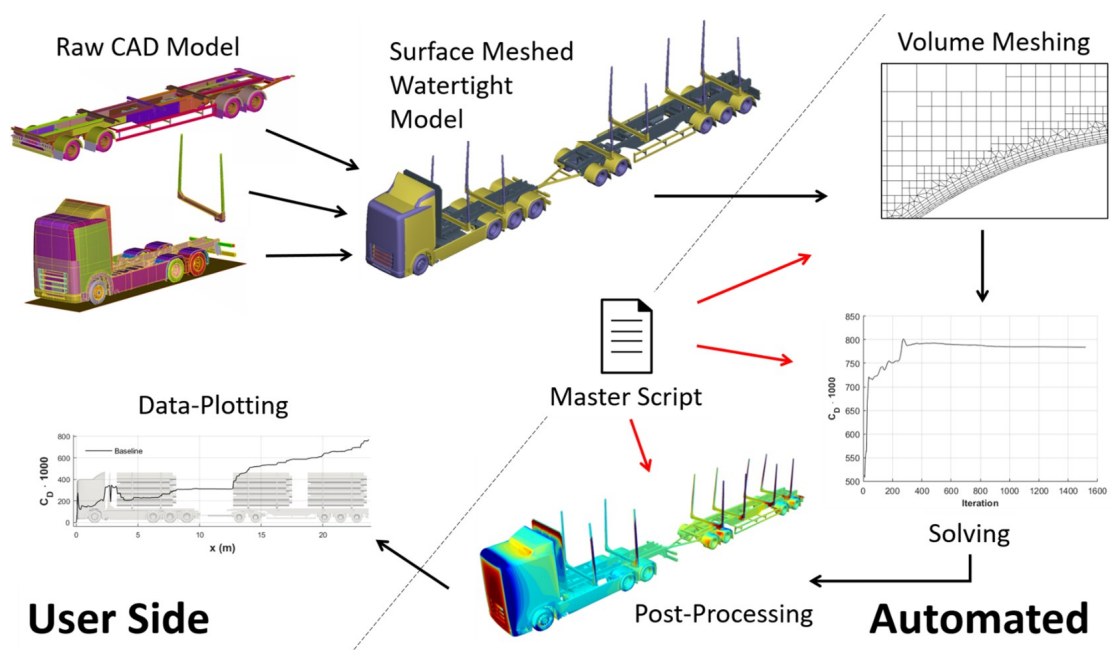


Figure 21: Workflow in the automated CFD procedure, the user only has to prepare a watertight surface meshed model and define settings in the Master script while volume meshing, solving, and post-processing are automated on the Sigma cluster [10]. The semi-automated convergence monitoring was done during or after solving, data-plotting after solving was also semi-automated step.

Continuing with some details of the automated procedure. Running the meshing, solving, and post-processing using scripts makes it possible to submit batch jobs in a non-graphic environment on Sigma [10], by using bash-scripting all of this was tied together in completely automated procedure. A bash-script, designated “Master script”, contained settings defining the case, created the case folder structure, defined cluster allocation requests, fetched the scripts for meshing, solving, and post-processing, and started a chain of dependent batch jobs for the whole case. Together, a Master script and a surface mesh is all that is needed to run a case. The end result was a method that produced drag accumulation data and close to 1000 images, figure 22 gives an idea of the scale, all from two files. Total turnaround time was about 11-14 hours, solving on 960 cores, time of a complete case run for one yaw angle, adding a another yaw angle added 4-5 hours. Out of the total wall clock time, 11-14 hours, only 0.5-1 hour was spent by the user depending on the complexity of the concept geometry.



Figure 22: Image output from the automated method, geometry with modifications marked in red, surface quantities such as pressure coefficient, skin friction, etc., and total pressure iso-contours and cut-planes.

3.8 Timber Study

As the timber is exposed to the freestream when loaded on the vehicle one major part of this work was to investigate the effects this has on the whole vehicle’s aerodynamics. Every log of timber looks different to each other in length, diameter and roughness. This section will present the method of the investigation that was made to get a better understanding how the timber effects the aerodynamics of a timber truck.

Biometria is the organization for timber measurement and reporting in Sweden; in email correspondence with Hans Weslien, (Hans.Weslien@biometria.se) March 2019, measurements of typical timber were obtained. A normal timber stack has a volume fill of 70 %, i.e., 30 % air, timber length is very rarely outside a span of 3 - 5.5 m, the diameter is 120 - 350 mm which within the logs are tapered to some degree. Protrusion of separate logs, called shuffle in this report, is something that can be an issue, mainly on badly delimbed timber. The timber stack can in some cases have a substantial slope longitudinally.

To compare the different effects each change has, a control stack was made. This stack was based on the data given by Biometria using the maximum dimensions of length and diameter, 5.5 meter and 0.35 meter respectively. No tapering of the logs was considered and the log walls were smooth. The control stack was placed on the 74 ton vehicle and was earlier shown in figure 6c. This will in the future be referred to the control.

3.8.1 Surface Roughness

To get a surface roughness on the logs the free to use modelling software Blender was used. By exporting STL geometry of the logs from ANSA the geometry could be imported to Blender. In blender there exist functions to connect the movement of nodes, by defining this connection as random and using a sphere of influence \gg than the stack all nodes in the stack could be moved in a controlled random fashion. The movement was defined in one node and the investigated movements was 10 and 20 mm. The movement was also combined with a size on the exported STL elements, here sizes of 32 mm was used.

3.8.2 Log size

The timber that is transported can be of different length, this depend on the timber sort or other reasons for cutting the timber in smaller logs. The stack data that was earlier presented states that on average timber can vary between 3 - 5.5 m in length. Both these extreme cases was tested, also the mean value of these was tested to gain an extra data point. For all simulations the stacks was kept centred on the two banks.

Timber size does also vary in diameter depending on type and age of the logs. During earlier work done at LiU this was found to induce a separation on the leeward side of the cab [2]. The method when making these did change from that of the control stack. Instead of filling a area with logs the outline of the stack was modelled first and then holes was filled inside the stack instead. This reduced the time required to make the stacks considerably. Both of the methods have drawbacks when the logs or holes are to be placed. When the area to fill is just to small the log or hole is left out at that position. This is clearly illustrated in figure 23. The different stacks do have different face area, the $\varnothing = 0.35$ m and $\varnothing = 0.15$ m have the same area.

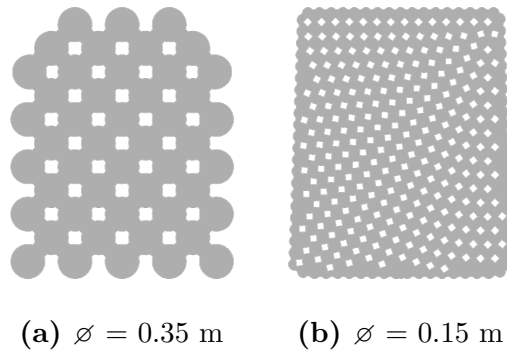


Figure 23: Front faces of the stacks using different diameter. Here the effects from how the stacks was modelled can be seen. In 23a there was an empty space at the two top edges and in the other two there was some areas where the holes was not able to place close to the boundaries.

3.8.3 Stack Shuffle

In nature all logs look different, this does also include length. An argument for that the newer modern methods of deforestation will result in equal lengths for most of the logs there will always be some logs that becomes shorter or slightly longer. This together with the loading of a timber truck by crane will result in some type of shuffle of the logs in a stack. The shuffle of the stacks was done in ANSA by changing the end sections of the stack. The different stacks tested are shown in figure 24 together with the control stack.

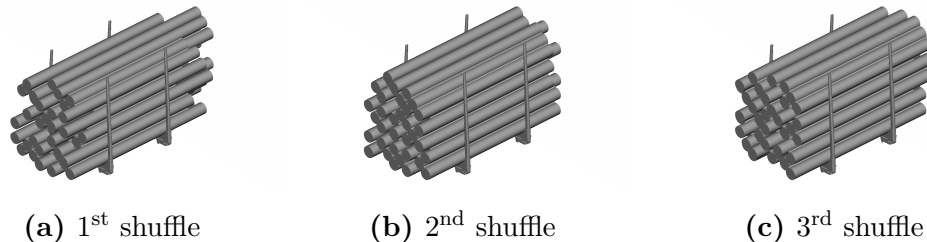


Figure 24: Investigated shuffled timber stacks: 1st shuffle consisted of 3 - 5.5 m timber, shuffled in steps of 0.25 m, max offset 1.25 m. 2nd shuffle, all logs 5 m, shuffle in steps of 0.25 m, max offset 0.5 m. 3rd shuffle was 2nd shuffle mirrored in x .

3.9 Concepts: Drag Reduction

For a long time engineers have experimented with different methods of lowering the drag on a vehicle. For a truck there exist some go to solutions such as a boat-tails, skirts and cab extenders [24]. On the road today deflectors can be seen on the most of the trucks cabs and some trucks do use skirts too. The aerodynamic devices investigated in this work was selected from the earlier work by Fernández [3] and

Colombi [3] together with some new concepts inspired by work mainly done in the USA where longer gaps are more common on regular truck, see gap seal in [25].

All of the concepts were made in ANSA and merged with the model. This work focused on the loaded vehicle, but a final concept was evaluated both loaded and unloaded for different yaw conditions. Only passive aerodynamic devices were considered. When concepts were designed one objective besides drag reduction was to interfere as little as possible with the loading area.

Based on the findings in the timber study a new stack was constructed as what was thought to be a more representative model than the idealized control stack. This “Baseline” vehicle was the benchmark for the concepts to be compared with.

4 Results and Discussion

This chapter presents the results from the different part of this work, namely the timber study, baseline model, drag reduction concepts, final aero kit, and loading configurations. There is also a section with discussion regarding concepts that was not tested in this work but could be interesting to investigate in the future. 5° yaw is the main working angle in the timber study and concept development as it previously has been shown to be most representative [2, 3, 14], which is also confirmed in the results found in this report.

When the drag data are presented in this chapter the difference between cases will vary from very small to very large. In a CFD method there will always be some errors, therefore it is important to reflect over how small differences to look at. When evaluating the results small differences should be treated more carefully.

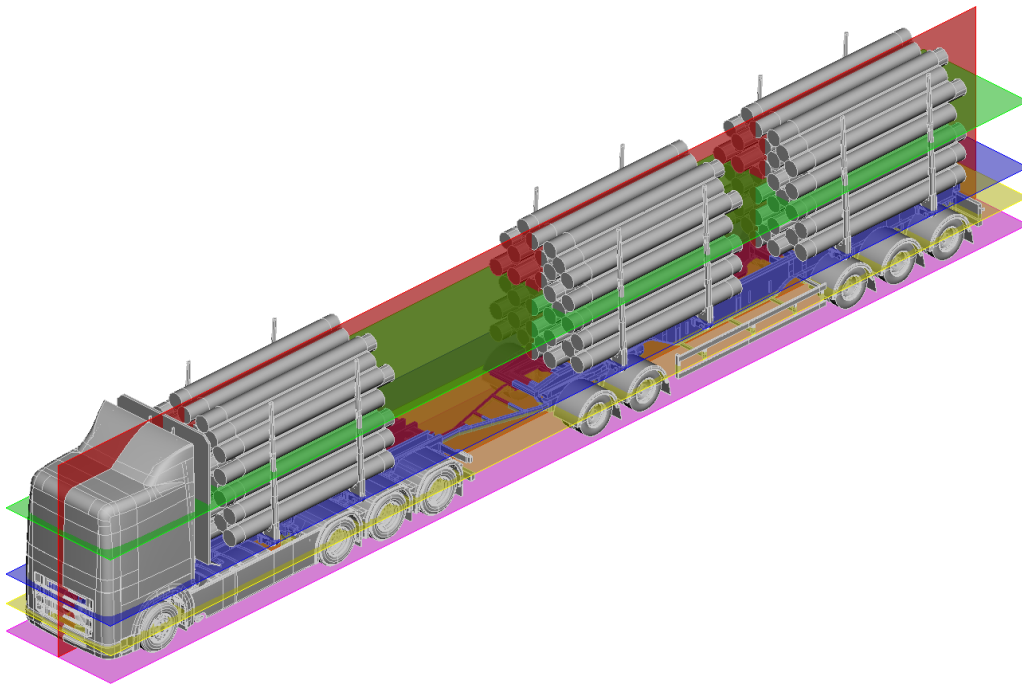


Figure 25: Positioning of standard cut-planes. Planes in the z -direction: pink is just above the ground at 0.05 m, yellow is in height with the chassis at 0.6 m, blue is at 1.25 m through the banks, and green approximately the middle of the stacks at 2.6 m. The red plane, normal in y , is placed in the middle of the vehicle. This color coding is used to distinguish standard cut-planes by a colored frame.

When investigating the flow field around the truck cut planes showing pressure distribution around the truck will frequently be used. For easier orientation a set of standard cut planes have been chosen, these are shown in figure 25. When a cut

plane is shown it is framed by the colour and described which of these planes that are shown for the reader. If a cut plane that is not part of the standard set it will not be framed and the figure caption describe the placement. The planes with a normal in z-direction are placed at a height of ≈ 0.05 m, 0.6 m, 1.25 m and 2.6 m. The red plane is placed in the vehicle transverse $y = 0$ plane.

4.1 Timber Study

The results from the timber study is presented and important features are highlighted to be used as arguments when making the baseline model. The investigated features is log roughness, log length, log diameter and shuffle. The results from these investigations are used to build a baseline stack later used in future studies.

4.1.1 Surface Roughness

Effect from surface roughness on logs is shown in table 7 and compared with the result from the smooth control stack. The drag increase with roughness, this increase is almost linear for the data points collected in this study. There is no clear feature found in the results that gives an answer to why the roughness increase the drag. The cause of the drag increase is instead motivated by the increased area and the minor increase of smaller features around the logs.

Table 7: The effect of timber surface roughness on total vehicle drag.

Roughness	$1000 \cdot C_D$	$\Delta 1000 \cdot C_D$	$\Delta\%$
None	750	\leftarrow Reference	
10 mm	758	+8	+1.15 %
20 mm	764	+14	+1.9 %

Accumulated drag over the vehicle was investigated and shown in figure 26. The accumulated drag have very good agreement between the different surface roughness and no particular area of the vehicle show large deviations. This implies that the drag increase found for the full vehicle is accumulated all over the vehicle and no particular region is alone responsible. The 10 mm case can be seen to have some differences at the start of the trailer. This is due to a small error when the geometry was prepared and this stack was placed a couple of millimeter to far forward. This small difference is not deemed to have any effect on the total vehicle drag and nothing in the results give any reason to suspect anything else.

When the surface was modified one of the expected quantities to change is the skin friction coefficient, C_f . This is shown in figure 27 between the smooth control and 20 mm roughness. There is no difference between the two figures that can be seen which is in agreement of what was seen in the accumulated drag.

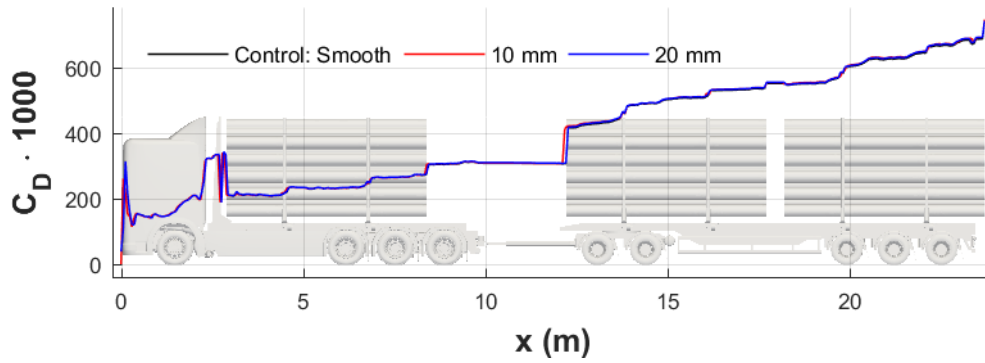


Figure 26: Accumulated drag over the vehicle comparing different surface roughness at 5° yaw. In the figure no large differences between the different cases can be seen. The 10 mm case is shortly before smooth and 20 mm is due to a small miss in the geometry preparation where the stacks was placed a couple of millimetres to far forward.

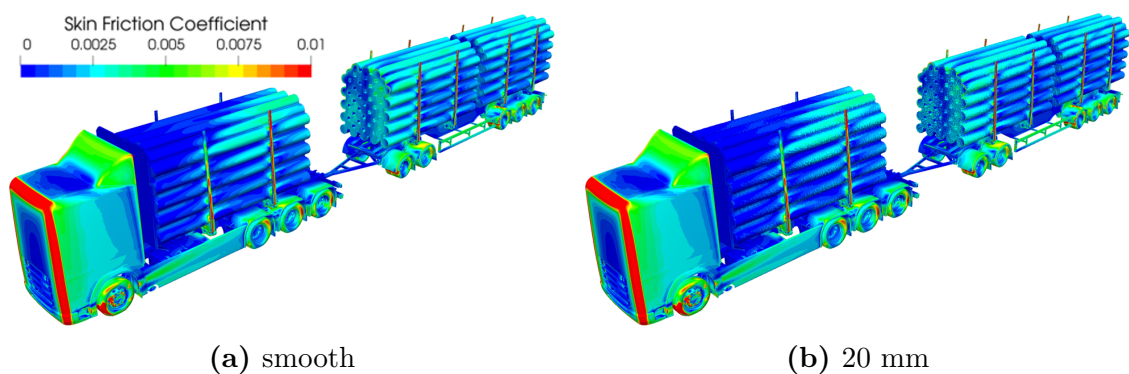


Figure 27: The smooth control and 20 mm coloured by C_f , results obtained with 5° yaw. No differences can be noted between the two runs in terms of skin friction.

The implementation of roughness on logs did not have a significant impact on the total vehicle drag. When the results were investigated no clear distinct differences could be found between the different cases. The increase of drag is probably a result from more area that are in contact with the fluid and some minor separations around the highest peak of roughness.

From these results there does not seem to be any large effect from the timber roughness. There exist different methods of investigating and modeling the timber roughness that was not done in this work due to as many reasons. Using CFD a finer mesh with combined with a method that resolves some turbulence for example LES could be used to see if the RANS model used here is simply a too strict of approximation. This was not done in this work due to the limited resources and set scope of the study. In Fluent there exist methods of controlling the surface roughness numerically in the solver. This method can not be used together with the enhanced wall treatment in combination with a $k-\varepsilon$ turbulence model that was used in this work [18]. These two proposed methods of modeling the surface roughness could be investigated with a more thorough investigation of what roughness that actually exist on a timber log.

4.1.2 Log size

Log length was shown to have a large impact on the total vehicle drag as shown in table 8. The results of logs with length of 4.25 m and 3.00 m is compared with the 5.50 m control log size. A considerable drag increase is seen when the timber length is reduced.

Table 8: The effect from timber length on total vehicle drag at 5° yaw. An large increase of drag can be noted when the log length is reduced.

Log length	$1000 \cdot C_D$	$\Delta 1000 \cdot C_D$	$\Delta\%$
5.50 m	750	← Reference	
4.25 m	779	+29	+3.9 %
3.00 m	812	+62	+8.3 %

The accumulated drag shown in figure 28 shows where the differences in drag can be found. Over the truck the accumulated drag is very close all the way up to the end of the first stack. It can be seen that the shortest 3.00 m logs produce some more drag at the truck. In the figure background is the control vehicle, this is why the steps in these curves come at different positions. After the first stack the accumulated drag starts to differ but stay reasonable close to each other until the second stack. From this point and to the end the curves look different because they have different distances between features. Note that the longer control stacks keeps the accumulation of drag more steady and less steep than the shorter stacks do. The gap position between the second and third stack can be seen in all of the curves. It is the trailer that most of the drag accumulation differences can be found when the log length is changed. It is important to note that the aerodynamics of

a vehicle is very complex and that features downstream have an effect on upstream components. This means that shorter logs could create features on the truck that decrease the efficiency of the trailer.

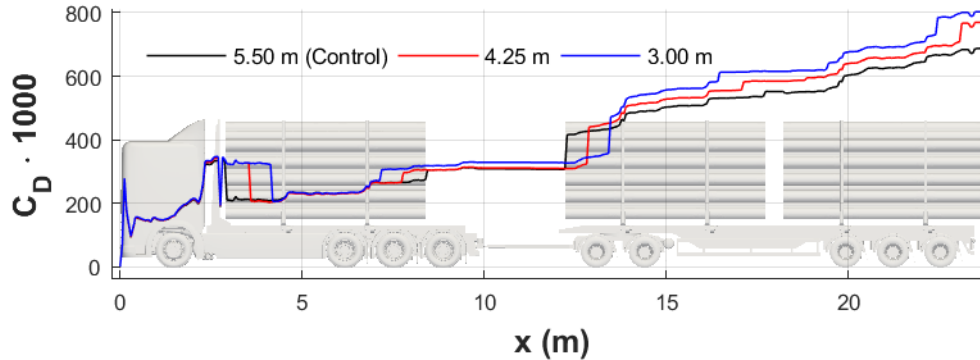


Figure 28: Accumulated drag over the truck comparing different length stacks at 5° yaw. The drag accumulation over the vehicle is the very close until the end of the first stack and very similar until the start of the second stack. On the truck the shortest 3.00 m logs do produce some more drag. Over the trailer shorter logs does accumulates more drag. Note that the background vehicle is the control, this is why the accumulated drag for the sorter logs have sudden jumps at different places.

The increase at the start of the second stack as seen in figure 28 leads the thoughts to pressure drag on the front face of this stack. The impact can be seen in the pressure on the vehicle surfaces as shown in figure 29, which show the coefficient of pressure around the trailer viewed from an iso view from the windward side. It was found that the pressure did get higher on the front face of the second stack. But there is also large increases of pressure on the wheel covers when shorter logs are loaded. This is due to the longer logs on the truck makes the truck wake start further down the vehicle making the region between truck and trailer contain less high energy flow. At the start of the triple axle in the end of the trailer the pressure

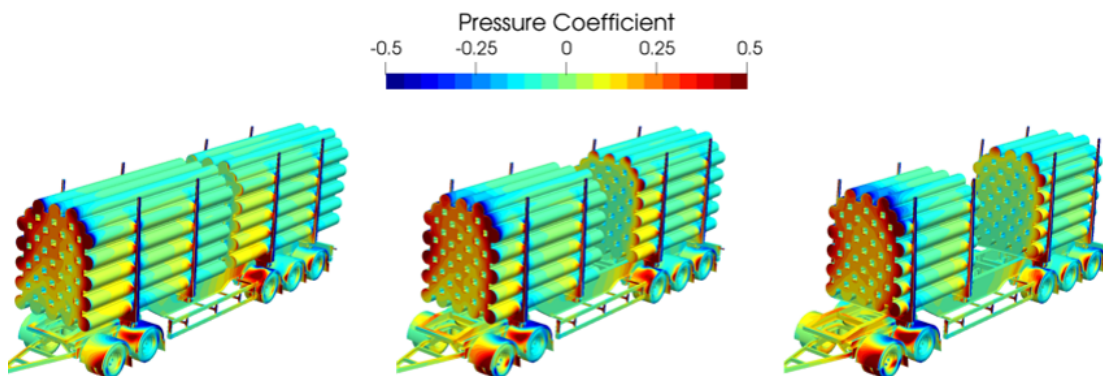


Figure 29: Coefficient of pressure on the surface of the trailer for different lengths of stacks for 5° yaw. The pressure on the front face of the second and third stack increase when the log length is reduced. Pressure distribution on the wheel cover also change when the log length is changed.

is higher on the wheel cover when longer logs are loaded. This have the same reason

as mentioned above with less high energy flow between the first and second stacks. This leads to a different flow path around the dolly that in the end increase the amount of high energy flow entering before the triple axle. There is differences on the third stack front face too, as shorter logs are used more pressure on this surface can be found. This is simply due to the flow having more time to enter between the stacks.

This is shown in figure 30 where cut planes showing the total pressure coefficient at a height of 2.6 m for the 5.5 m and 3.0 m cases are shown. Other differences that can be noted is the larger separation around the trailer where the flow is more effected by stakes. This results in a larger wake behind the vehicle.

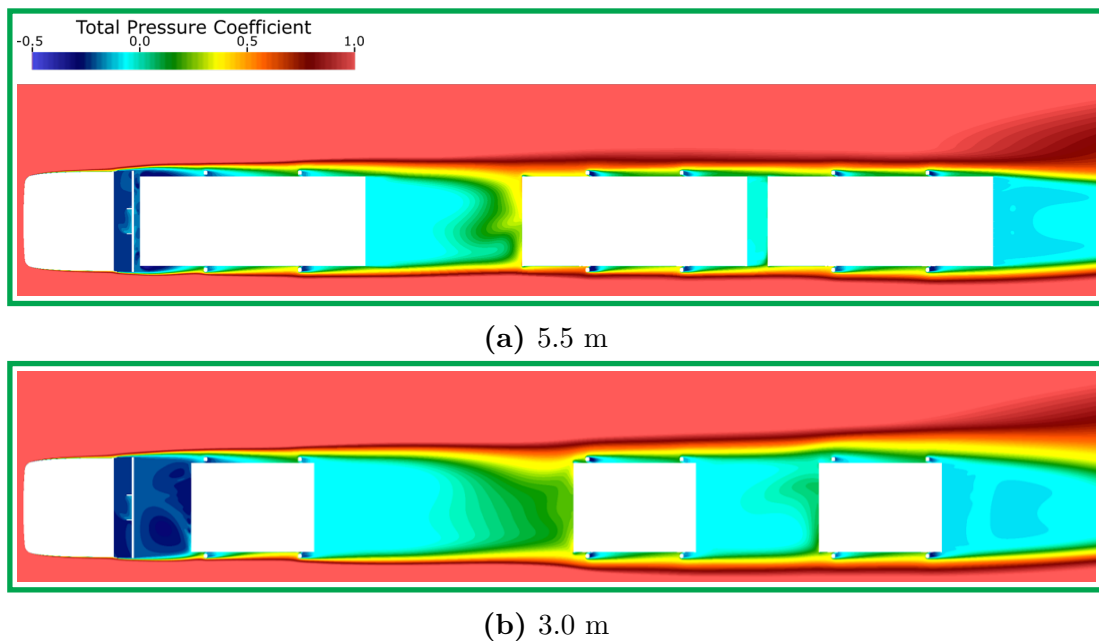


Figure 30: A cut plane coloured by $C_{p,tot}$ at a height of 2.6 m where the vehicle is at 5° yaw. The cases compared is the a) 5.5 m and b) 3.0 m. A larger region of high pressure can be found between truck and trailer. Flow around the trailer for 3.0 m is more disturbed by the stakes and leads to a larger wake.

The results in this study are in agreement with the results from [26] where a timber length study was done on an American tractor semi-trailer configuration was done.

The other log size parameter that was investigated was the log diameter. It was found as shown in table 9 that a smaller diameter increased the drag on the vehicle. It was also found that if the holes between the logs were closed there was a gain in performance. This closed stack could be achieved by closing off the holes of the stack by for example a tarpaulin.

The accumulated drag for these cases that is shown in figure 31 shows that the difference in drag is mainly located at the second stack front face. After the front face of the second stack the difference between 0.35 m and 0.15 m is 17 counts. As the total vehicle drag differs by 40 counts this means that around half of the difference comes from the front face and the rest throughout the trailer. The no

Table 9: Drag for different diameter and flow through cases at 5° yaw.

Log diameter	$1000 \cdot C_D$	$\Delta 1000 \cdot C_D$	$\Delta\%$
0.35 m	750	← Reference	
0.15 m	790	+40	+5.3 %
No flow	736	-14	-1.9 %

flow case shows good agreement to the 0.35 m control stack even at the second stack impact but later differs along the trailer.

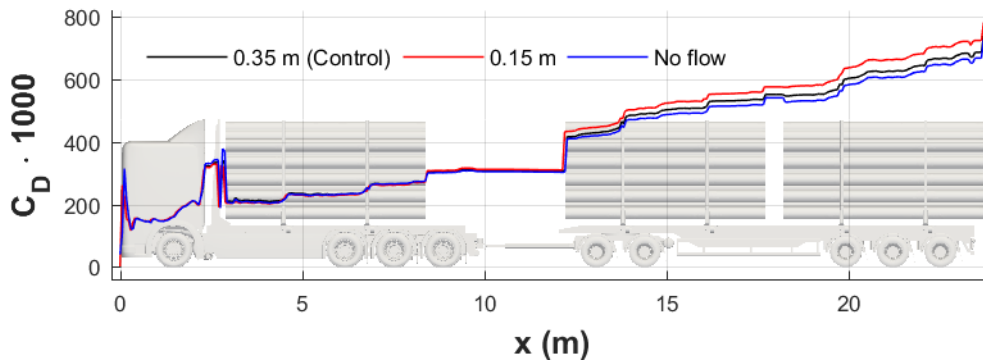


Figure 31: Accumulated drag over the truck comparing different diameter logs and no flow at 5° yaw. The accumulated drag is in good agreement between the different geometries until the start of the trailer. Here the logs with a diameter of 0.15 m have a larger increase of drag. Further down the trailer this difference between the control and 0.15 m diameter case keeps growing. The no flow case does show less drag accumulation along the trailer compared to 0.35 m case.

Increase of drag around the front face of stack two is due to the logs being smaller allowing for tighter packing moving more surface in to regions of higher pressure. The stakes does also have larger regions of higher pressure due to the reduction of flow that can pass between stack and stake when smaller logs are loaded. This is illustrated by the pressure coefficient on the surface shown in figure 32. Between the two cases frontal area on stacks is the same.

Gain along the trailer is due to an increased surface area that is subjected to flow, this increase viscous drag along the vehicle. Note that this area refereed here is not the frontal area of stacks but rather the surface around the logs. There is some difference in the skin friction coefficient along the trailer as seen in figure 33. The smaller diameter logs have more skin friction at the top of the logs than the large diameter logs have. Also the mantle area increases when a smaller diameter is used. Further, there is no significant difference between the the no flow and 0.35 m diameter case implying that the drag difference comes from the reduction of surface area inside the stacks.

One source of error in this investigation is the different methods that was used to make the stacks. With the smaller diameters this resulted in less holes through the stack close to the edges. As almost half of the drag increase of the 0.15 m diameter

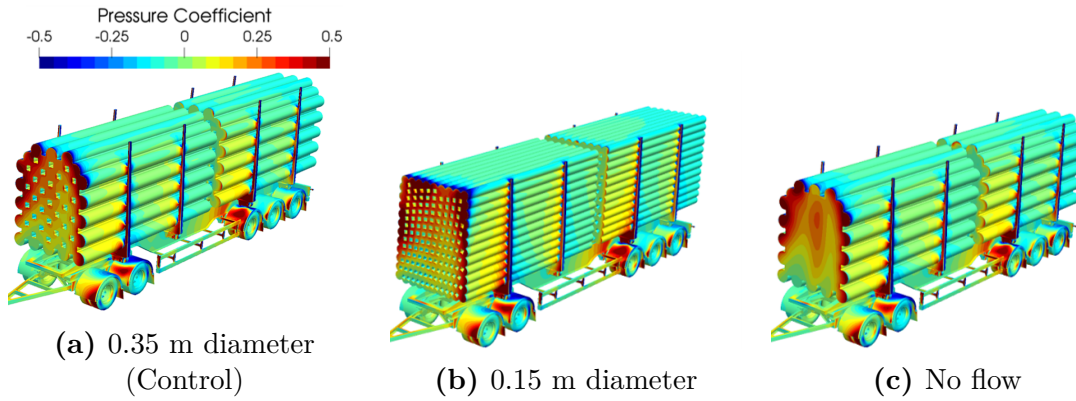


Figure 32: Coefficient of pressure on the trailer for 0.35 m, 0.15 m logs and no flow at 5° yaw. As the smaller logs makes it possible to load more logs higher and further out the area where high energy flow can impact is larger. The pressure drag on stakes does also increase for the 0.15 m case.

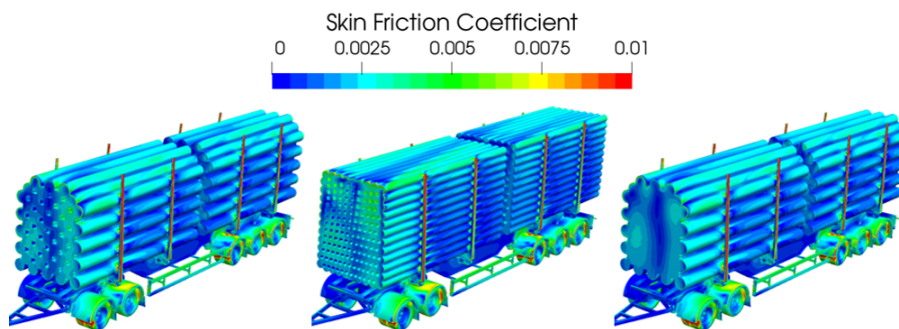


Figure 33: Skin friction coefficient shown on the surface of the trailer at 5° yaw for different diameters of logs. From left to right 0.35 m, 0.15 m and no flow. There is no significant difference between the 0.35 m logs and no flow. For the 0.15 m logs a region of higher friction was found on the top.

logs came from the flow impact at this region the geometry certainly does not make this better. However, the reasoning that a smaller diameter log will allow for loading closer to the stakes at the top still holds and a difference would probably always be present but probably not as large as seen in this study.

The 0.15 m logs did not work well in the method that was used for this thesis. When the earlier defined settingre-run used the solver did have problems with reversed flow at an outlet and a to high EVR. Thire-run solved for this particular case with a different under relaxation strategy where the relaxation was reduced and the solution got to run more iterations. This will not have an effect on the results but does have an impact on the time it takes to get an converged solution.

There was a positive effect from closing of the stacks, 14 drag counts lower. The implementation of this would be hard as it would take alot of time if the drivers had to cover the stacks with for example a tarpaulin. When a soft cover as a tarpaulin is used this cover would also flutter when the truck starts driving producing drag to if not tightly strapped down.

4.1.3 Shuffle

The shuffled stacks did all have a similar effect on the total vehicle drag as seen in table 10. All of the tested concepts did increase the drag with an average increase of 26 counts.

Table 10: The effect from shuffled timber on total vehicle drag at 5° yaw. The effect that can be seen is a constant increase of drag when the logs are shuffled. The average increase is 26 drag counts.

Shuffle	$1000 \cdot C_D$	$\Delta 1000 \cdot C_D$	$\Delta\%$
No Shuffle	750	← Reference	
Shuffle 1	784	+34	+4.5 %
Shuffle 2	772	+22	+2.9 %
Shuffle 3	773	+23	+3.1 %

The accumulated drag shown in figure 34 shows that the drag gain is spread over more smaller steps at stack faces. The drag on the truck is in very good correlation and starts to differ at the trailer. At this point the accumulation curves starts to diverge.

This can be explained by the small flow structures that arises around the individual logs. This is illustrated in figure 35 where a cut plane one metre in to the second stack is shown for no shuffle and shuffle 2. There exist difference in the pressure map around the stack at this point. The shuffled stack produces areas where the pressure is much lower than seen in the no shuffle case. These low pressure zones removes more energy from the flow thus increasing the total vehicle drag.

Shuffling the timber had a notable effect on the total vehicle drag and the surrounding flow field. This effect is timber vehicle specific and is important to remember

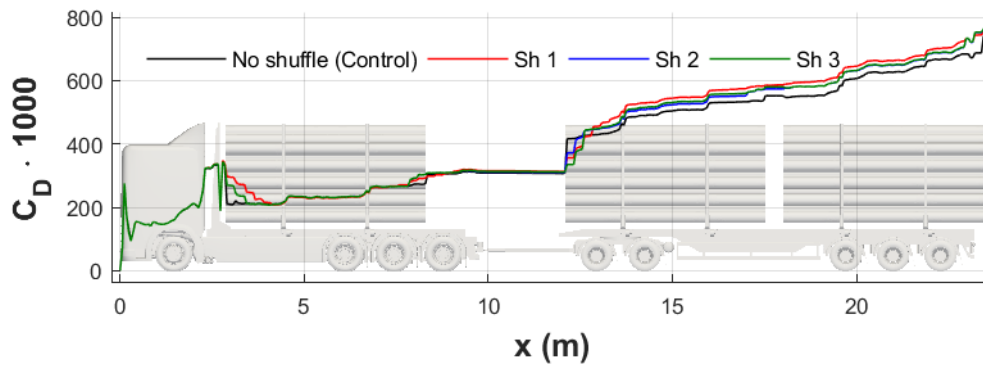


Figure 34: Accumulated drag over the truck comparing different stack shuffles at 5° yaw, “Sh” is short for shuffle. The drag accumulation shows differences as soon as the first stack is reached. At the stack starts the accumulated drag is gained over more but smaller steps. These steps does in the end sum to the same drag all the way until the start of the trailer. Here the drag accumulates over in different ways once again. Most of the difference in total drag can be found on the trailer.

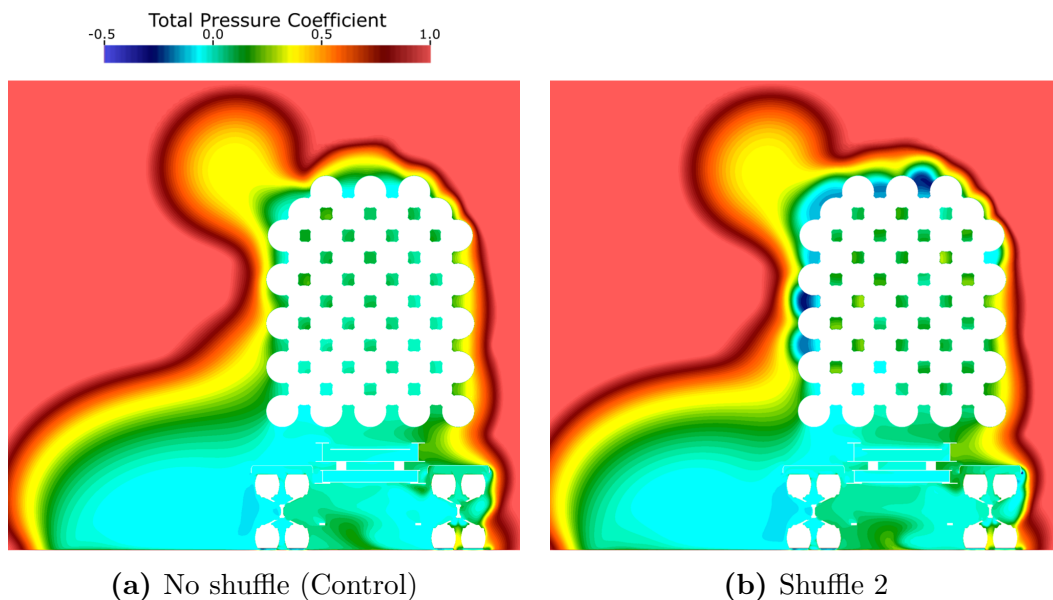


Figure 35: $C_{p_{tot}}$ in a cut plane located 1 m in to the second stack with a normal in x-direction for no shuffle and shuffle 2 at 5° yaw. When the logs is shuffled low pressure zones appear around the stack.

when concepts for lower aerodynamic drag is designed.

4.1.4 Baseline Stack

From the results presented in the section above a stack to be used in a baseline model was created. The combination that was chosen consists of logs that do not have any surface roughness. They have a diameter of 0.35 m and a length of 4.25 m. Finally, the logs are shuffled in the stack in a similar way of shuffle 2 and 3 shown before. The baseline stack that will be used in further investigations is shown in figure 36.

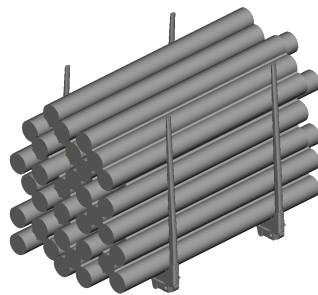


Figure 36: The baseline stack that is to be used for aerodynamic concept design. The logs have a length of 4.25 m, diameter of 0.35 m and are shuffled in the stack as in shuffle 2 and 3. No surface roughness is used on the baseline stack.

This stack was deemed to represent an average stack that is being transported on the roads. Roughness of did show an impact on the drag but no significant changes with regard to flow features were found with it. This geometrical modification did also come with worse mesh quality and larger amount of cells in the mesh. This is why surface roughness was not included in the baseline stack. Changing log length showed the largest effect on total vehicle drag and is therefore included in the baseline model. A length of 4.25 m was chosen since it did show features that the longer logs did not have. The length is also in the middle of the span that was given to us from Biometria. Log diameter was not changed since there was not major flow features that changed due to different diameters. The effect should not effect any aerodynamic concepts that are designed for the vehicle in the following part of the work. Shuffling of the logs was included since it is how a timber stack often look on the roads and some effects in the flow field was found during the investigation.

4.1.5 Specific Aerodynamics of Timber On Vehicles

In the section above different types of timber have been evaluated and some final remarks on these results can be done. When the types of timber was tested the difference in drag was always found to occur on the trailer. This shows that the truck part of the vehicle is rather insensitive to what type of logs that are hauled.

This is due to the large wake behind the cab enclosing most of the load on the truck. This in combination with the fact that the cab is well designed by the truck company aerodynamicist the focus for any work where the timber vehicle should be on the trailer.

One finding is also that no stack is like the other one, this becomes a problem when designing aerodynamic concepts as all logs and stacks look different. When a swap body vehicle is investigated the geometry effecting the airflow are the same for all cargo. This is an extra hassle that needs to be worked around when working with a timber vehicle.

4.2 Loading Configurations

The different timber truck variants mentioned in the method chapter was investigated. This was done to see if any one of them have some benefits when it comes to aerodynamic drag. The result from this investigation is shown in table 11. Note that the vehicles investigated here are using the control stack used in the timber study. The drag was found to increase with the weight of the vehicle. The 64 ton vehicle have considerable lower drag than the 70 and 74 configurations.

Table 11: Drag for different loading weight configurations at 5° yaw. The 74 and 70 ton are close when it comes to aerodynamic drag. The 64 ton vehicle have considerable lower drag.

Configuration	$1000 \cdot C_D$	$\Delta 1000 \cdot C_D$	$\Delta\%$
74 ton	750	← Reference	
70 ton	740	-10	-1.3 %
64 ton	694	-56	-7.5 %

When the accumulated drag, shown in figure 37, was investigated it was found that the 64 ton and 70 ton vehicles shows good agreement in drag until the trailer. The same is true for 70 and 74 ton vehicles on the trailer. Note that the background is a 74 ton vehicle, this explains why the drag from the trailer starts earlier on the 64 and 70 ton vehicles. This is related to the flow impacting the vehicle at different places for different configurations. As the 74 ton vehicle is higher this flow impact occur on the truck while it gets added at the second stack for the 70 ton vehicle that uses the higher trailer as the 74 ton vehicle.

Another difference between the loading configurations was a high pressure zone between the truck and trailer for the 70 ton vehicle. This is shown in figure 38 where a cut plane showing total pressure coefficient located 0.05 m above the ground. In figure 38b the high pressure zone can be seen between the truck and trailer, at the same location the 64 and 74 ton vehicle in figure 38c and 38a shows a smaller zone. This higher pressure zone is formed due to the increased trailer height compared to the truck for the 70 ton vehicle.

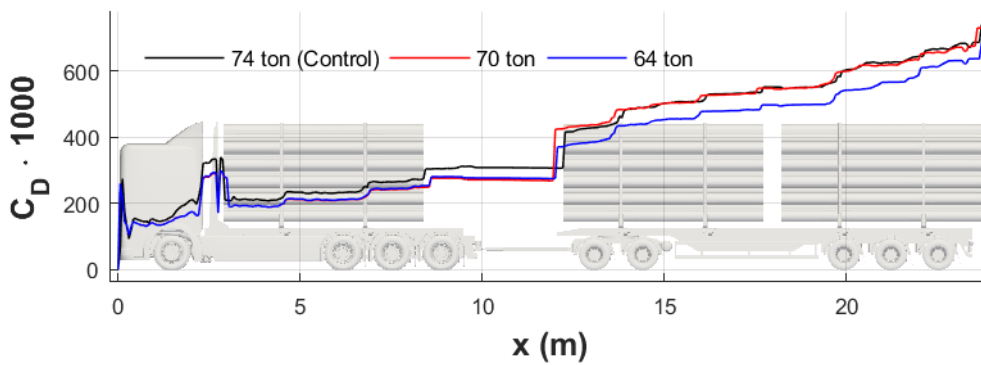


Figure 37: Accumulated drag for the different loading configurations at 5° yaw. Note the agreement between the 64 and 70 ton vehicles on the truck and on the trailer agreement between 70 and 74 ton. There is a sudden increase of drag at the sixth bank and stake for the 64 ton vehicle not present in for 70 and 74 ton. The vehicle shown in the background is a 74 ton vehicle, this is why the drag from the trailer comes earlier on the 64 and 70 ton vehicles.

The increase of drag around the sixth bank for the 64 ton vehicle was investigated. It was found that this high pressure zone is a result from the wheel placement combined with the banks placement. In the heavier trailer variant that was used on 70 and 74 ton vehicles the first wheel and fifth bank align in x-direction and simply blocks the high energy flow entering from the side to pass over the wheel cover and enter this region.

As the different vehicles uses different axle combinations the impact of adding a wheel was investigated. In table 12 it is shown that there is no considerable difference between the different axle configurations. The 1-2-2-3 combination shows a better

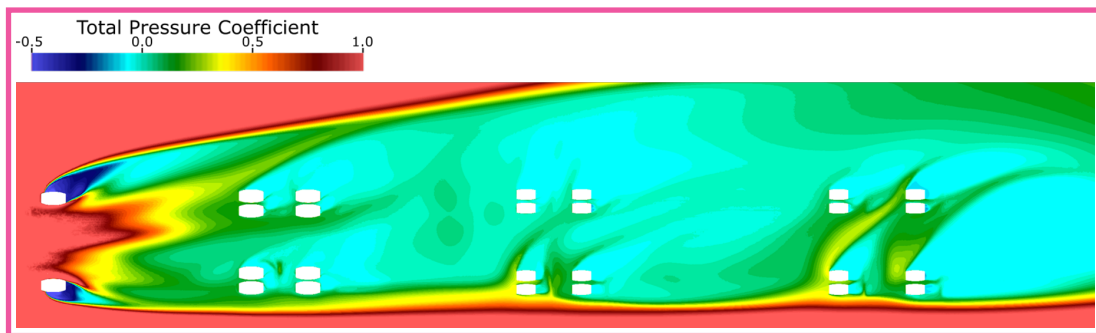
Table 12: The part of drag that comes from the wheels for different wheel configurations. The results were obtained with loaded vehicles at 5° yaw.

Configuration	$1000 \cdot C_D$
1-3-2-3	56
1-2-2-3	42
1-2-2-2	49

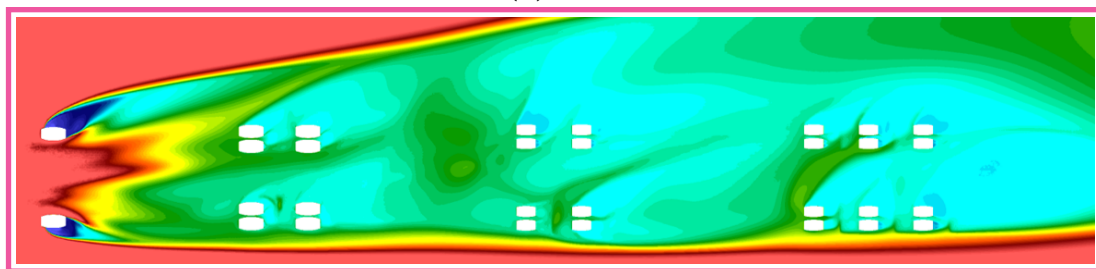
performance than 1-2-2-2 combination. The reason for this is the higher pressure zone between truck and trailer that changes the amount of inflow of high energy air. This could also be seen in figure 38.

The result from the different loading configurations shows that there is no great aerodynamic benefit to running a 70 ton vehicle using the configuration shown in this work. The higher trailer will in the end result in almost the same frontal area making the total vehicle drag very similar. If the 70 ton vehicle could be made using a lower trailer and kept as low as the 64 ton vehicle this type of configuration would be beneficial.

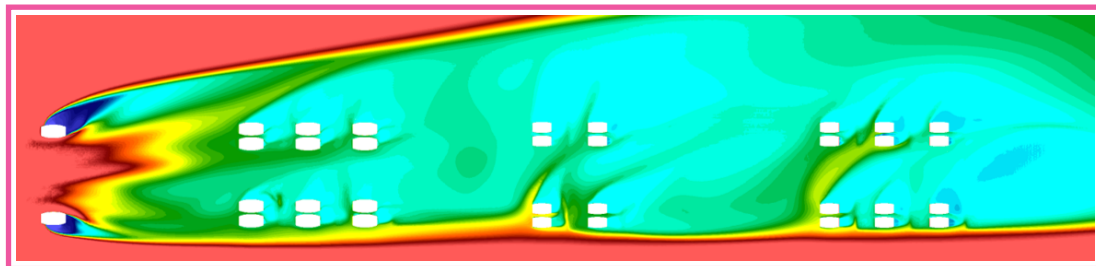
In the end the 70 ton vehicle did under perform when compared to the 74 ton



(a) 64 ton



(b) 70 ton



(c) 74 ton

Figure 38: Total pressure coefficient shown at a cut plane located 0.05 m above the ground, the vehicles was simulated at 5° yaw. A higher pressure zone can be observed between the truck and trailer for the 70 ton vehicle. There is also differences in the amount of flow entering between the truck and trailer.

vehicle. This vehicle can haul more timber and almost have the same aerodynamic performance. As was shown in the results this is due to the higher trailer on the 70 ton vehicle impacting the air that flows over the lower truck. If a 70 ton vehicle could be made longer instead of higher this option would be alot more attractive.

4.3 Baseline Vehicle

The baseline vehicle consists of the 74 ton truck trailer configuration as shown in section 3.1.1, which for the loaded case was equipped with timber stacks as described in section 4.1.4. This model was run both loaded and unloaded at different yaw conditions, 0° , 2.5° , 5° , and 10° , to evaluate its aerodynamic characteristics and performance.

For the working yaw angle of 5° the unloaded and loaded models perform similar, 771 and 780 counts of drag respectively. However, the total drag is highly dependent on the yaw condition, i.e., a higher yaw angle induces a higher drag. Comparing the loaded and unloaded cases, the unloaded vehicle has a higher drag at smaller yaw angles, $<5^\circ$, while the loaded case has a much higher drag at 10° yaw. Figure 39 shows the results of the baseline vehicle in terms of total drag; wind average drag is calculated in accordance to the SAE J1252 standard [12], wind average drag is 845 counts loaded and 806 counts unloaded which is closest to 5° yaw in both cases. Tabulated data of total drag is found in table D.1.

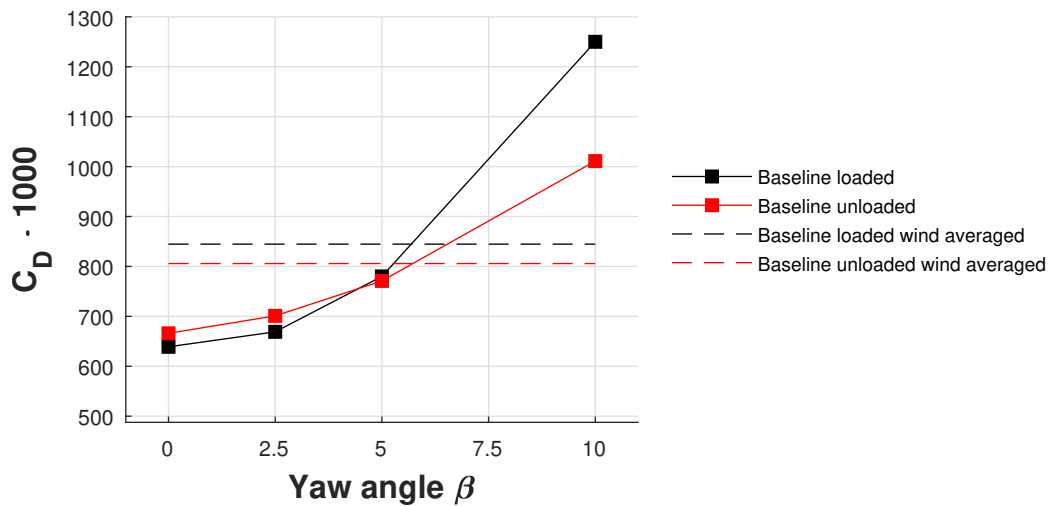


Figure 39: Total drag against yaw of baseline; drag is highly dependent on the yaw condition, a higher yaw angle induces a higher drag. The unloaded vehicle has a higher drag at smaller yaw angles, until 5° after which the loaded case had a much higher drag. Wind averaged drag was 845 counts loaded and 806 counts unloaded, the closest results from the yaw sweep is 5° yaw.

The drag increase due to yaw is exponential in character both loaded and unloaded, in the previous study the drag of the unloaded vehicle increased pretty much linearly with increased yaw [3]. However, the drag at medium yaw angles was probably over

predicted in the previous study due to using 1st-order discretization of the turbulent quantities.

Drag distribution along the vehicles as seen in figure 40 shows where the major contributions to drag are. These observations are done for loaded and unloaded at

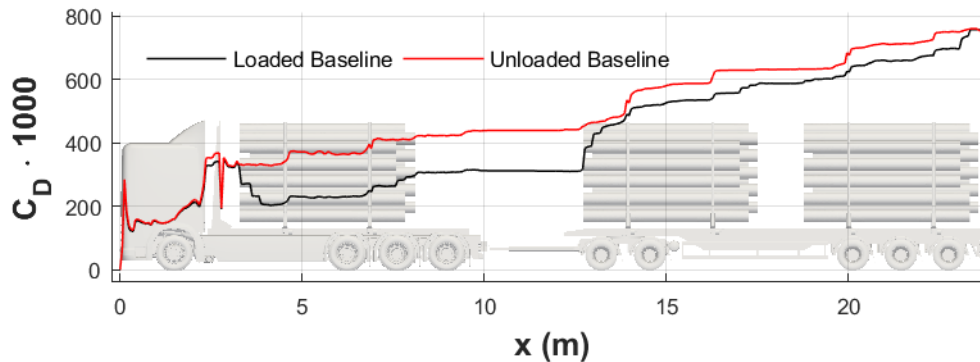


Figure 40: Accumulated drag on the baseline vehicle at 5° yaw for loaded and unloaded vehicle. The major contributions to drag is found at the cab front and end, the start of the trailer have also a large contribution. Over the truck the loaded vehicle is more efficient but have higher accumulation over the trailer.

5° yaw, however, it is later shown that these are similar in character for all yaw angles. It is observed that a significant portion of the drag originate from the high pressure stagnation on the frontal area of the truck cab, see figure 41a. Also, note the initial spike of approximately 280 count in drag that then settles after the cab radius on 160; the radii accelerates the flow and induce a low pressure effectively reducing drag. The cab as a whole contributes with approximately half of the total drag, in line with previous findings [4]. The drag accumulation is very similar between both cases until after the truck cab where it drops significantly for the loaded vehicle. Which is explained by the low pressure zone behind the cab which in itself induces a lot of drag, however, on the loaded truck this is virtually canceled out by the suction it creates on the first timber stack. This compared in figure 41b; it is also observed that the pressure on the stack backside is higher than on the back of the cab and bulkhead explaining the better net performance loaded if only the truck is considered. Only considering the truck the total drag is 313 counts loaded and 440 counts unloaded at 5° yaw.

Continuing downstream to the trailer, for the loaded case there is a rapid increase in drag due to the high pressure of the second stack front, approximately 200 counts, see figure 41c. Further downstream there are many smaller drag contributions that comes from banks, stakes, gap between stack two and three, and wake behind the vehicle mainly. In comparison the unloaded vehicle does not have the initial ramp in drag instead the effect from banks and stakes becomes much more prominent, as can be seen in figure 41c. Still, the total drag is very similar between cases at 5°.

Figure 42 depicts drag distribution along the vehicles at different yaw conditions. There are some differences between 0° and 2.5° solely on the trailer, although the difference is very minor on the loaded vehicle; the loaded case has less drag at these

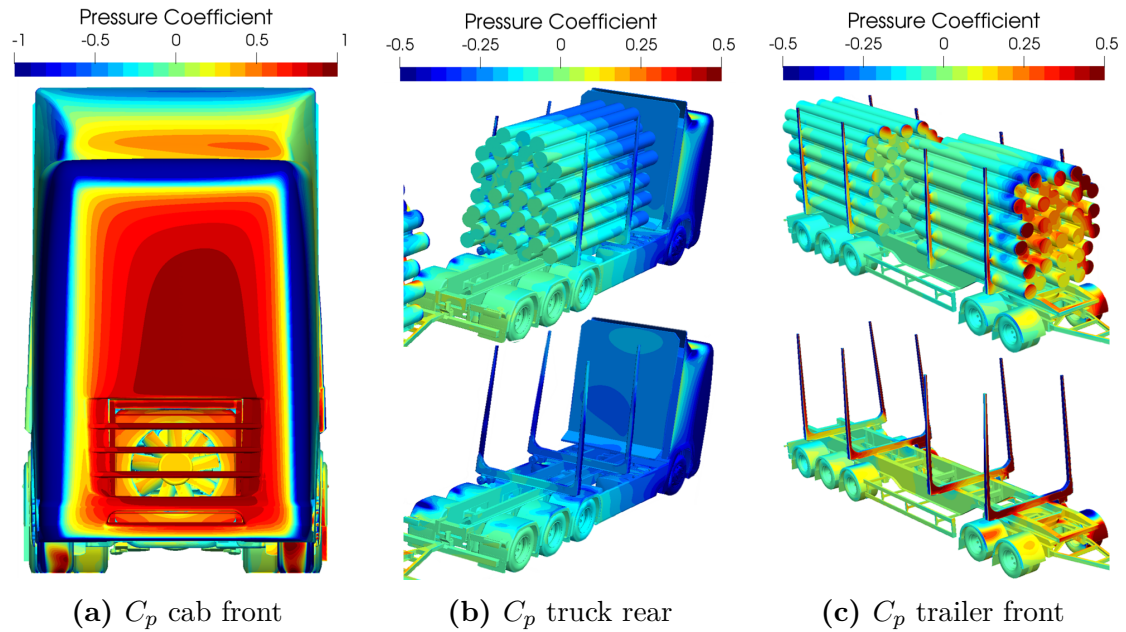


Figure 41: Pressure coefficient coefficient of pressure on baseline model at 5° yaw. a) Front base pressure cause a large portion of the drag, however, note the suction around cab radius reducing drag. b) Low pressure region rearward of the cab, the presence of timber reduce drag. c) The loaded trailer gets the main drag contribution from the front base pressure of second timber stack, while the unloaded trailer gets a larger contribution from banks and stakes.

yaw angles. Further, the increase of drag is more significant at 5° where most of the increase occurs on the trailer while only a small increase is seen behind the first timber stack on the truck. Recall that the total drag of the loaded vehicle surpass that of the unloaded vehicle at 5° yaw. Up to 5° most of the yaw induced drag occurs on the trailer while the truck is almost unaffected, this is not the case for 10° yaw where the drag increase substantially along the entire vehicle compared to the 5° case, both loaded and unloaded. This is due to flow separation occurring on the leeward side of the cab that is not present at the smaller yaw angles, see figure 43. For both the loaded and unloaded cases the difference between 5° and 10° yaw is about 130 counts starting on the cab, but at the end of the vehicle the difference grows to 240 counts unloaded and 470 counts loaded.

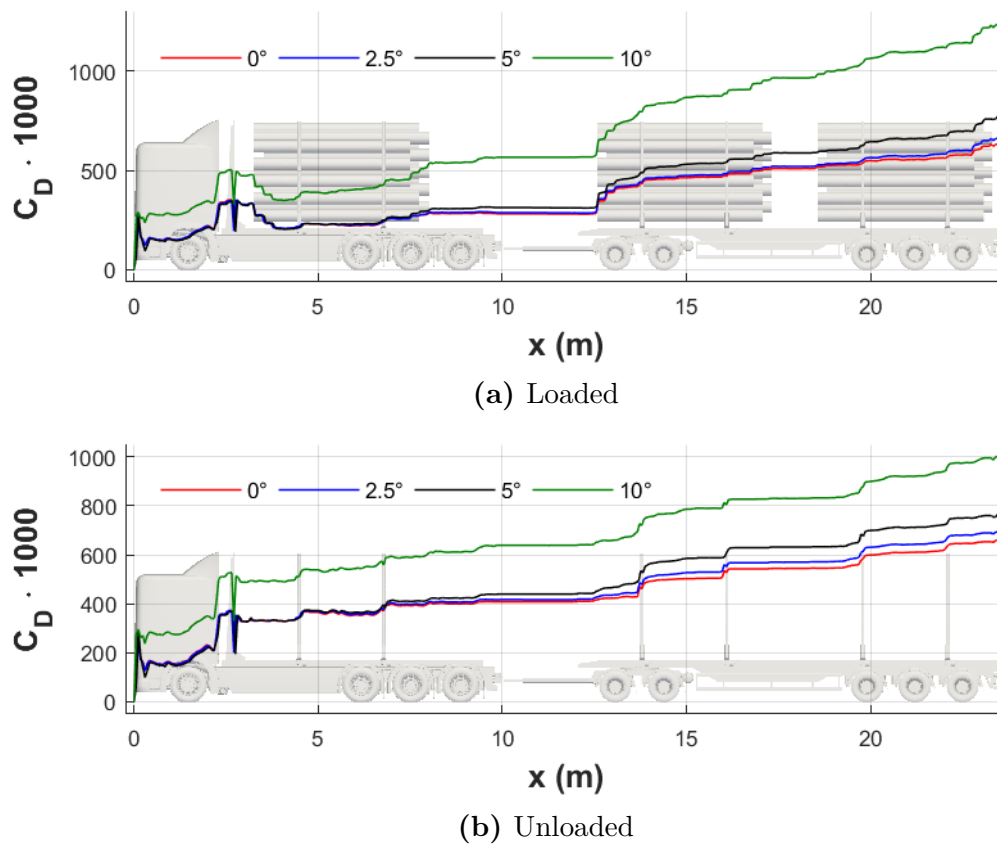


Figure 42: Accumulated drag loaded case for different yaw conditions. Minor differences between 0° and 2.5° , trailer is affected significantly at 5° , the whole vehicle is greatly affected at 10° due to flow separation on leeward side of the cab.

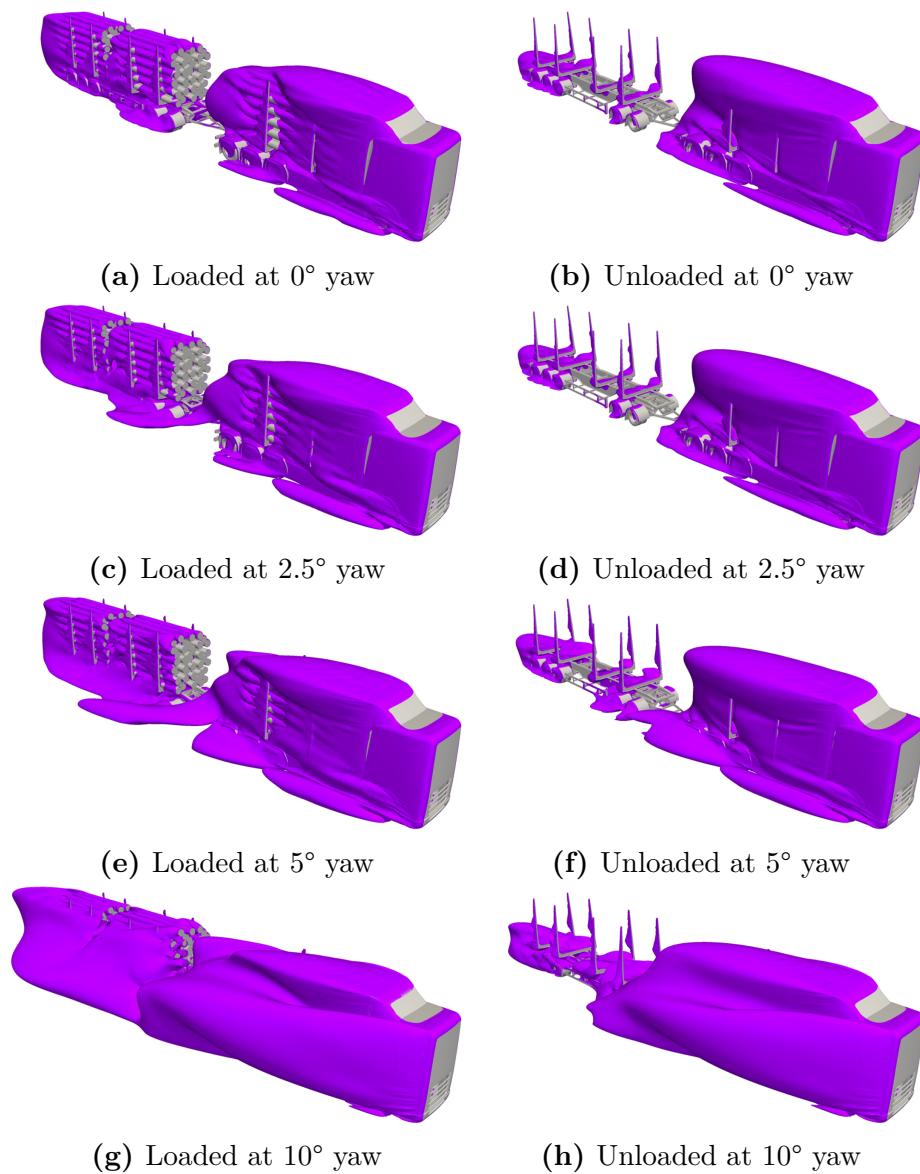


Figure 43: Contour of $C_{pt} = 0$ seen from leeward side, at 0° the only side wakes are essentially the tire wakes. 2.5° yaw produce a small leeward side wake along the trailer, the leeward side wake becomes significant at 5° most so on the loaded vehicle. Finally, at 10° flow separates at the leeward side cab radius; the leeward wake is similar on the truck regardless of the load, while the trailer wake is much larger when loaded.

While there are large differences in net drag between different yaw conditions the characteristics are still very similar in terms of where drag is generated and their magnitude relative to each other. In general it could be said that the slope of the accumulated drag essentially becomes steeper with increased yaw while maintaining the same characteristics, the exception is 10° where the curve is also virtually translated upwards.

Onwards to examining flow more carefully, again for the 5° case unless otherwise stated. Starting from the ground figure 44 show the total pressure field at 0.05 m above the ground, here it is observed that some high energy flow finds its way in

under the vehicle, understandably most at the front. Total pressure cut planes for all yaw cases loaded and unloaded are available in appendix D. However, a significant amount of high energy flow also slips in before the dolly and a little before the last three sets of wheels on the trailer. This is a source of drag because of the high pressure it cause on the internal chassis parts as seen in figure 46, not the most significant effect but not to be neglected. This effect is similar but larger on the unloaded vehicle.

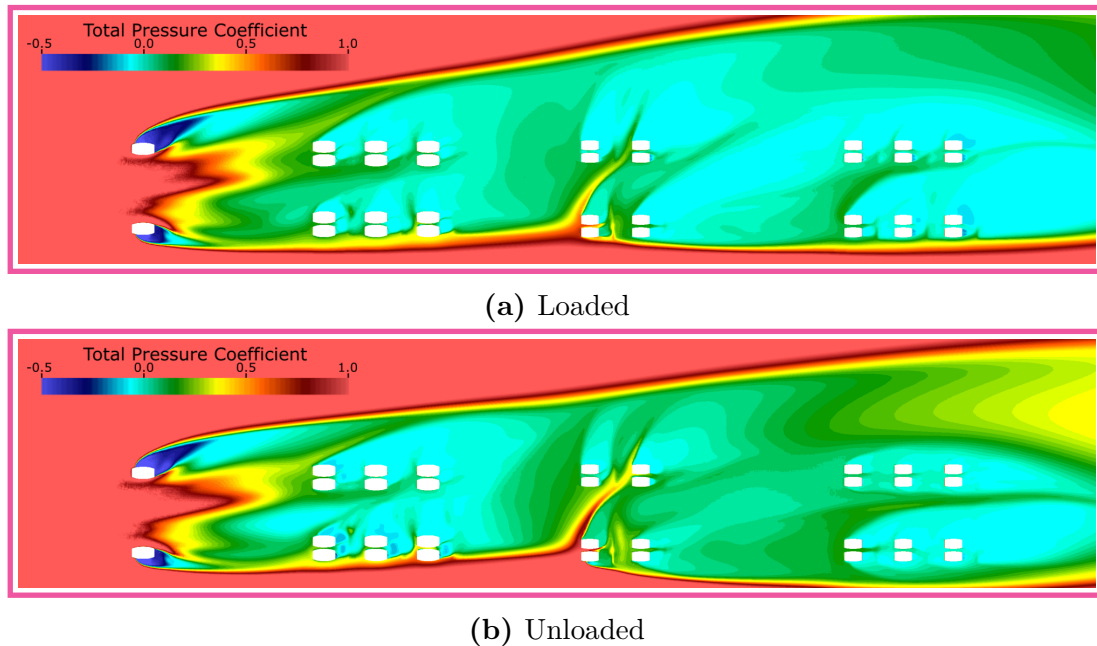


Figure 44: $C_{p,tot}$ shown at a cut plane located 0.05 m above the ground on the baseline vehicle at 5° yaw. Note the ingress of high energy flow under the chassis.

Further up, 0.6 m above the ground, similar problems can be seen; significant high pressure flow turns in before and hits the first left side dolly wheel assembly. Further downstream it is observed that the left side impact protection and chassis main beam are exposed to high pressure flow. The severity of these flow features were reversed compared to what was observed in the previous study, where the inflow was worse before the trailer triple axle [2, 3]. Also note the high pressure zone in front of the cooler which is a major contributor to drag. Most of the chassis is located in a lower pressure region which is favorable, the negative effect is, however, more severe on the unloaded vehicle. At this height there is a rather substantial leeward side wake on both the truck and trailer chassis, most serious when loaded, also seen in figure 43e and 43f.

Total pressure at the height of the banks as show in figure 47, 1.25 m above ground, show that the banks are highly affected by energized flow, especially in the unloaded case where the impacts on the banks are very obvious. The low pressure region downstream of the cab is also more detrimental on the unloaded vehicle, while the wake is somewhat smaller the intensity of the low pressure is much greater.

2.6 m above the ground, approximately in the middle of the loading volume vertically,

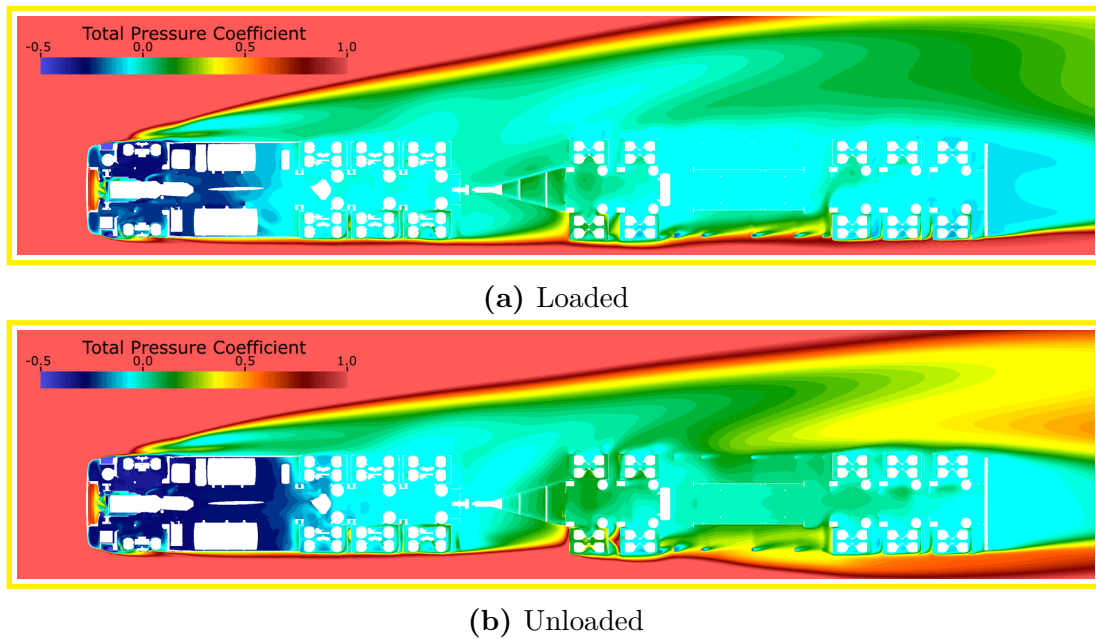


Figure 45: Total pressure coefficient shown at a cut plane located 0.6 m above the ground at 5° yaw for loaded and unloaded vehicle. The severe in flow of high energy flow can be noted in both cases.

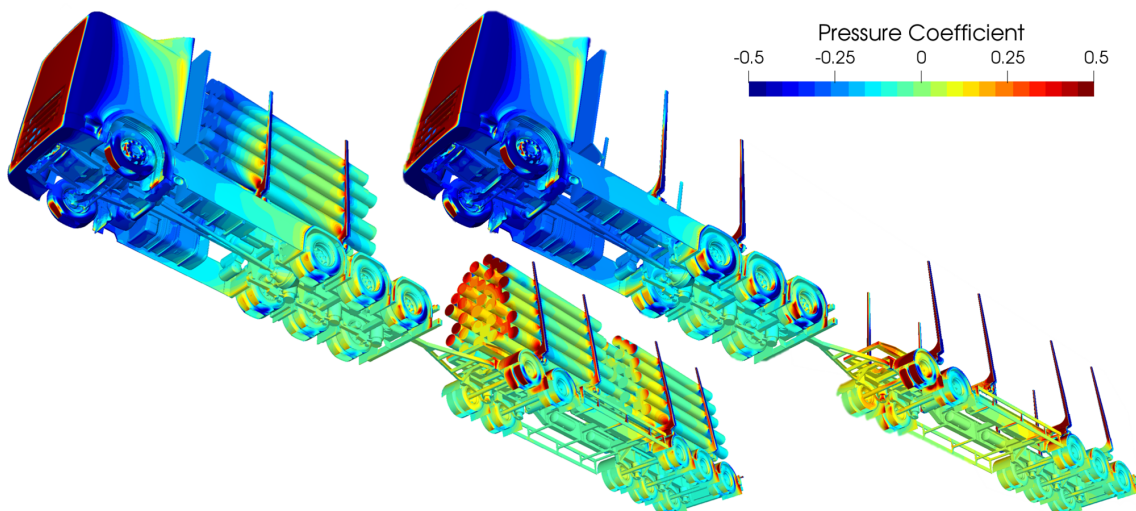


Figure 46: Pressure coefficient pressure coefficient on underside of loaded (left) and unloaded (right) baseline model at 5°.

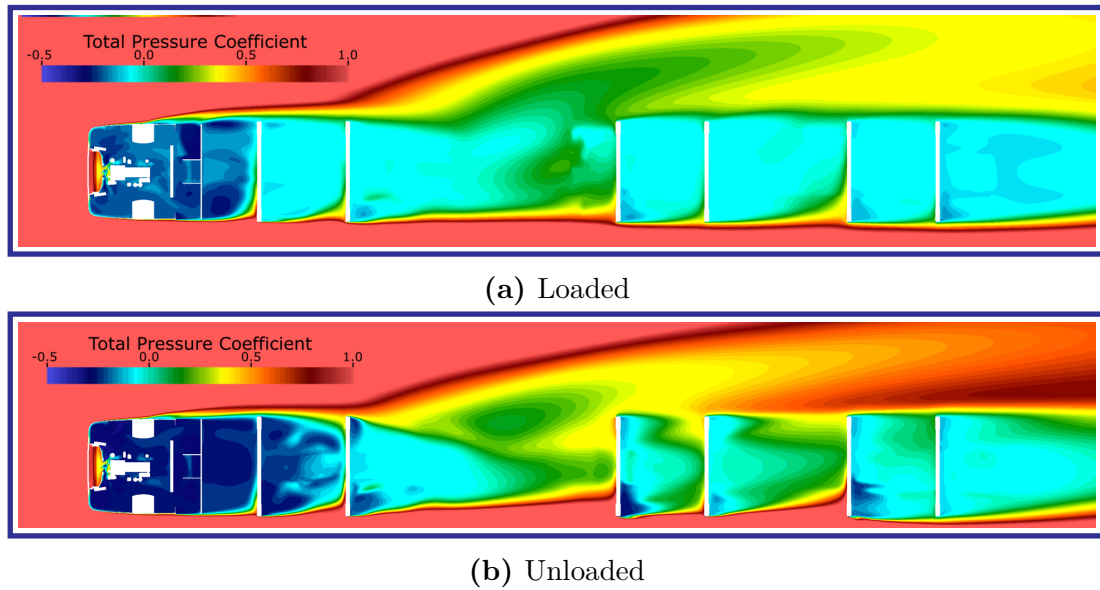


Figure 47: Total pressure coefficient shown at a cut plane located 1.25 metre above the ground at 5° yaw for loaded and unloaded vehicle. At this plane the high energy flow hitting the banks are shown. The problem is worse for an unloaded truck but is still very clear on a loaded truck.

there are obvious differences, as shown in figure 48. Again one can see the more intense low pressure zone behind the cab when unloaded. The wake of the loaded truck stretches almost to the second stack of timber and is wider, the second stack encounter a significant amount of high energy flow, a similar but much smaller effect is seen between stack 2 and 3. Recall the intense pressure drag on the stakes when unloaded, as seen earlier in figure 41c. All but the first windward side stake is exposed to freestream flow, stakes on the leeward side of the trailer are also much more exposed than on the loaded vehicle.

Viewing the total pressure field in plane $y = 0$ gives a good overview of the details discussed above. High energy flow affects the chassis more severely when unloaded, clearly visible is also the cab wake which when loaded gets less severe. It can also be seen that there are some flow through the timber stacks, especially on stack 2 where the pressure gradient between the front and back are large. Note the backwards flow through the first stack, this was also observed in the previous study of the simplified loaded vehicle [2].

In summary, the timber truck trailer vehicle like the one examined here have many aerodynamic problems and shortcomings. Comparing with swap body transport vehicles where first the external geometry does not depend on whether the vehicle is loaded or not in general, the geometry itself is also more problematic in the loading volume. Comparing the characteristics of the drag accumulation between timber vehicles [2] and wood chip vehicles [14], very similar to swap body vehicles, it can be concluded that drag contributions from stakes, banks, and spaces between stacks are much worse than for a smooth box shaped swap body.

On the other hand this means that there is much room for improvement, likely there

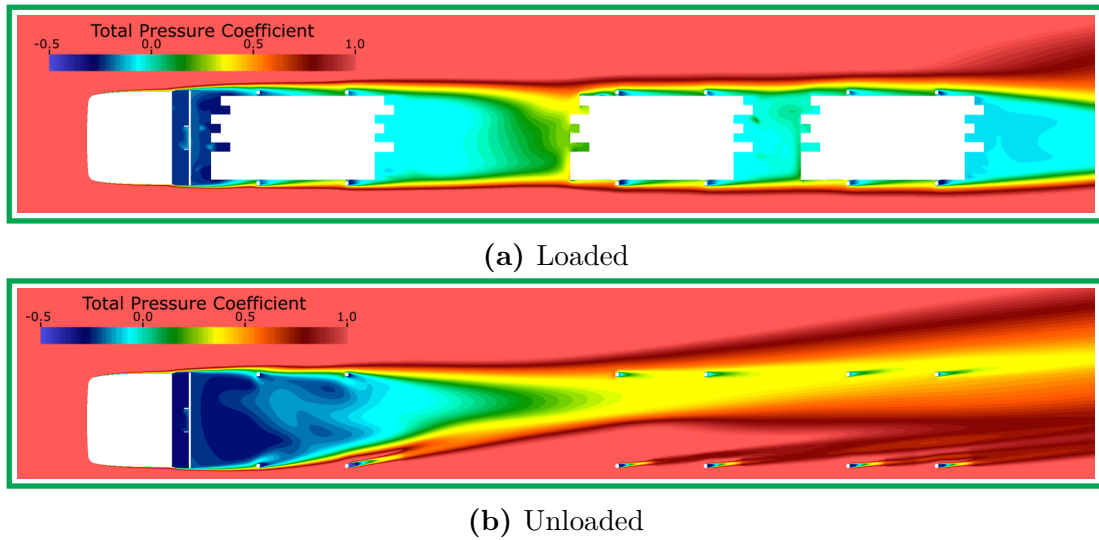


Figure 48: Total pressure coefficient shown at a cut plane located 2.6 metre above the ground at 5° yaw for loaded and unloaded vehicle. On the loaded truck the timber creates larger low pressure zones. For the unloaded truck the effects from the stakes are clearly shown.

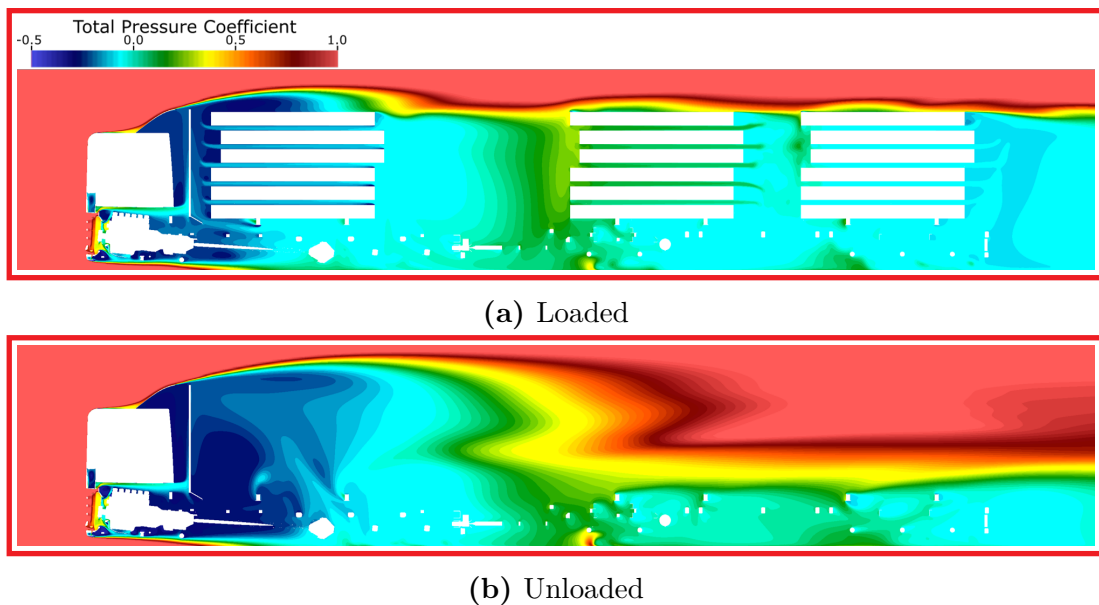


Figure 49: Total pressure coefficient shown at a cut plane $y = 0$ at 5° yaw for loaded and unloaded vehicle. The large truck wake is shown when the truck is unloaded. The pressure interaction between truck and trailer is shown for the loaded vehicle.

are some areas where drag can be reduced without interfering with the function of the vehicle. Table 13 lists the major contributors to drag in counts for the loaded and unloaded vehicle at 5° yaw. As previously stated the cab contributes with a large portion of the drag, however, making alterations to the cab does not lie within the scope of this work. Also, it is not expected that there is very much to gain by doing so compared with other major contributors on the timber vehicle.

For the loaded vehicle stacks of timber have a major impact on drag where stack 2 is the worst with 159 counts, stack 1 actually has a negative net contribution due to the low pressure zone behind the cab. Stack 3 gets most of its 74 counts of drag from the low pressure downstream of it. Other studies on truck trailer configurations have shown that the truck trailer gap has a major impact on drag [27]. Fenders add 100 counts of drag, majority of that comes from the trailer, 74 counts, these are parts that are exposed to the freestream. Wheel drag totals 56 counts, most on the truck where they are exposed the most to high energy flow. Finally, stakes and banks are responsible for 143 drag counts; the first set on the trailer is the least bad with 14 counts while the first set on the truck is the worst with 35 counts. The differences between loaded and unloaded is that an unloaded truck has higher drag per part. In particular the stakes and banks have considerably higher drag and stands for 29% of total vehicle drag.

Using as few banks and stakes as possible will have a significant positive impact on the drag both loaded and unloaded, many timber trucks do have more than two per timber stack since they can carry more types of wood in this way.

4.4 Drag Reduction Concepts

The implemented aerodynamic concepts are presented here and the results from the investigations are presented. All of the investigations were done using the baseline model presented in section 4.3. Some of the concepts are built upon other concepts.

4.4.1 Skirts

The concept that is the easiest to implement on a truck today would be the side skirts. In Sweden all vehicles that weigh more than 3500 kg need to have a side impact crash structure to prevent vehicles to end up under the vehicle in the event of a collision [28]. The skirt concept reduces the amount of high energy air that slips in under the vehicle. When the vehicle is under yaw conditions this becomes even more of a problem. The problem of in flow under the chassis was shown in section 4.3. Looking at the trailer that does not have any skirts the impact of high energy flow on the supports for the side impact structure can be seen. The same happens higher up when the banks and winches are located.

The concepts of side skirts were tested during earlier work on timber trucks with good results [2, 3]. When using skirts on a timber truck some considerations have

Table 13: Distribution of drag on loaded and unloaded baseline vehicle at 5° yaw, major contributors only, total drag is 780 counts and 771 for loaded and unloaded respectively. Note that the negative net drag on stack 1 is due to a low pressure zone interaction with cab rear effectively reducing drag from the cab. The drag per part increase for the unloaded vehicle.

Feature	Loaded		unloaded	
	$1000 \cdot C_D$	$\Sigma 1000 \cdot C_D$	$1000 \cdot C_D$	$\Sigma 1000 \cdot C_D$
Stack 1	-87	145	N/A	
Stack 2	159			
Stack 3	74			
Cab front	244	312	242	333
Cab rear	159		183	
Cab radius	-215		-221	
Grill & cooling	124		129	
Fenders truck	27	100	42	125
Fenders trailer	73		83	
Wheels truck	31	56	36	62
Wheels trailer	25		26	
Bank & stake 1	14	143	17	221
Bank & stake 2	25		34	
Bank & stake 3	35		58	
Bank & stake 4	19		39	
Bank & stake 5	29		46	
Bank & stake 6	21		27	

to be made. As timber trucks often have to drive on narrow small forest roads that have many hills the skirt can not extend to close to the ground to ensure ground clearance. The earlier mentioned problems regarding loading and unloading in 2.2.3 does also need consideration.

In this report three different types of skirts was investigated. One simple covering only between the first bogie and the last triple axle of the trailer. This would be the simplest concept to implement as the side impact crash structure could be used as a place to mount this skirt. The two other concepts have skirts extending forward and backwards to fully enclose the trailer chassis except the tires and the gap for the tow bar in the front. One of them ends shortly below the banks and clamping strap tighten winches while the other one enclosed them. Both of these concepts make use of so called boat tails that is supposed to reduce the wake size. A boat-tail is an extension of the vehicle that aims at directing the flow in behind the vehicle [24, 25]. All three concepts are shown in figure 50 with the modifications highlighted by red colour.

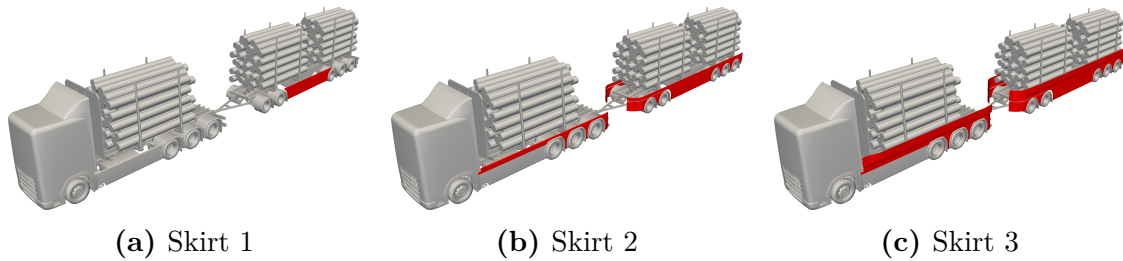


Figure 50: The different skirt concepts tested. The modifications are shown with a red colour. Skirt concept 1 uses a simple shield mounted on the side impact structure on the trailer. Skirts concept 2 and 3 have more complex shields on both the truck and trailer. They also extend higher than usual on tractor trailer vehicles.

The results from the skirts concepts is shown in table 14. Every concept did give and improvement in drag but in different amounts. The easiest to implement, skirt 1, did reduce the drag with 17 counts. The more complicated concepts that was investigated did drastically lower the drag with 75 and 99 counts for skirt 2 and skirt 3 respectively.

Table 14: Total vehicle drag for the different skirt concepts compared to the baseline model. All of the concepts give an improvement in drag. The simplest skirt shows a notable improvement while the more complex skirts shows very good potential.

Concept	$1000 \cdot C_D$	$\Delta 1000 \cdot C_D$	$\Delta\%$
Baseline	780	← Reference	
Skirt 1	763	-17	-2.20 %
Skirt 2	705	-75	-9.60 %
Skirt 3	681	-99	-12.7 %

The accumulated drag over the vehicle is shown in figure 51 for all of the skirt concepts and the baseline as a reference. It was found that the skirts did not have

a large impact on the accumulation of the drag on the truck. The truck did already have side skirts mounted on it when it was received from Scania. This is why there is no major difference between the baseline and the skirt concepts in this region of the vehicle. The skirt 3 concept do reduce the accumulation somewhat after the first bank and stake. On the trailer larger differences is observed, here the baseline and skirt 1 keep the same trend and skirt 2 and 3 have the same trend but a lower accumulation.

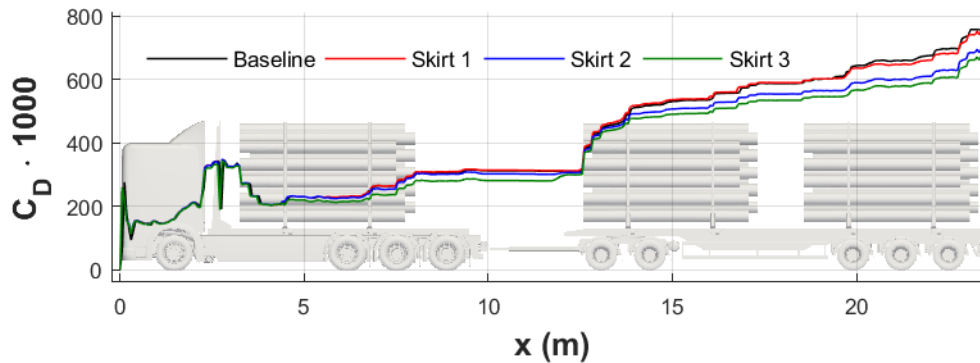
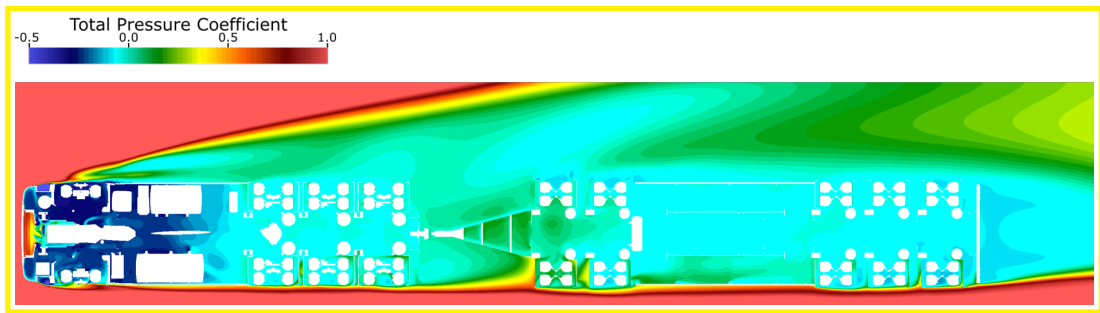


Figure 51: Accumulated drag for the different skirt concepts at 5° yaw. On the truck only skirt 3 shows a difference compared to the baseline model. On the trailer baseline and skirt 1 follow the same trend and skirt 2 and 3 follows a considerable lower trend.

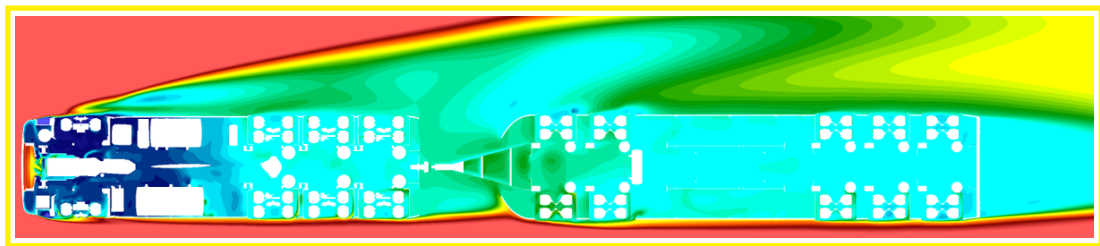
In section 4.3 the flow impact under the trailer was shown. In figure 52 total pressure coefficient in the same cut plane is shown for the concepts skirts 1 and 2. Here it is seen that skirts do have a good effect under the trailer. There is no longer any flow impacting the side crash structure and the flow is well aligned with the trailer. Differences between the skirts can be observed regarding how good they align the flow to the trailer. It is seen that the smaller skirt 1 does not align the flow as well as the full skirt 2. The skirt 1 concept does also have some high energy flow entering after the second wheel in the last triple boogie at this cut plane. This does not occur for skirt 2 as this region is closed off.

When the raised skirts (skirts 3) was tested in earlier work the reasoning behind the concept was to reduce the flow impact on the banks [2, 3]. A cut plane of total pressure coefficient through the banks is shown in figure 53 for skirt 2 and 3. There is clear differences in the pressure distribution when raising the skirts up and around the banks. The flow impact on the banks is reduced alot but not completely removed. Here it is shown that the reduction of drag accumulation on the truck is due to less high energy flow in the area for skirt 3. In these figures the reduction of wake size is also apparent where the pressure is higher on the leeward side of the vehicle. As mentioned both of these skirts was ended in a boat tail with the idea of reducing the wake behind the vehicle. There is a clear effect seen in the end of the truck that reduce the wake at this particular cut plane.

As mentioned above the skirts have an effect on the leeward side wake of the vehicle. The wake is illustrated in figure 54 with an iso contour of total pressure coefficient equals zero. The baseline and skirt 1 concept look alot alike but there is differences

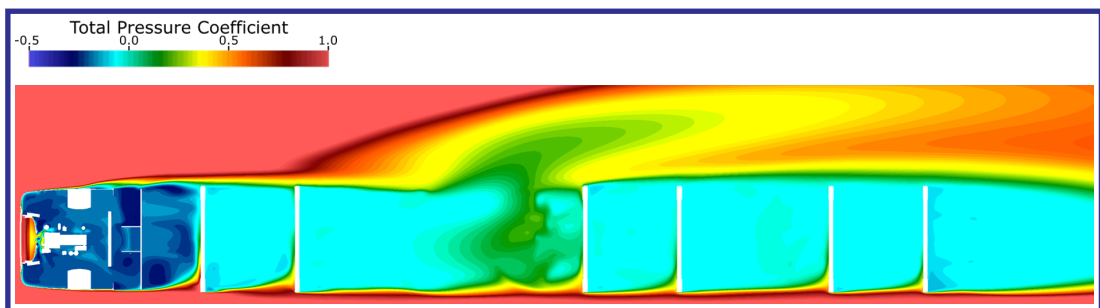


(a) Skirt 1

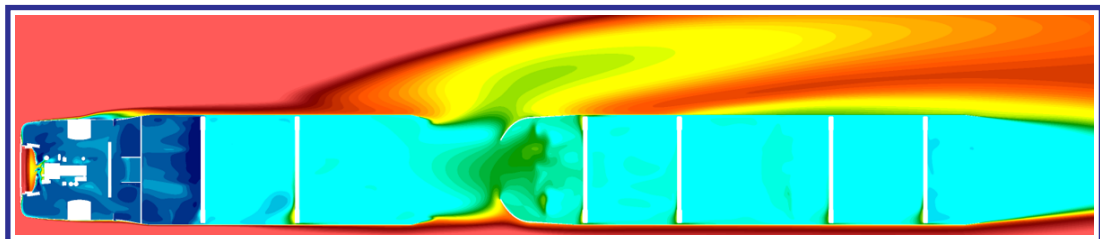


(b) Skirt 2

Figure 52: Total pressure coefficient shown in a cut plane located 0.6 m above the ground. With the skirts on there is almost no high energy flow under the trailer. The flow aligns better to the trailer when larger skirts are used and there is no high energy flow between the wheels that can be seen in the skirt 1 concept.



(a) Skirt 2



(b) Skirt 3

Figure 53: Total pressure coefficient shown in a cut plane located 1.25 m above the ground. The banks is clearly shown to hit alot of high energy flow when the skirts 2 concept is used. Skirts 3 does protect the banks and considerably reduce the flow impact on these components.

in both size and form. Note the small indentation in the wake close to the ground behind the vehicle, the wake on the leeward side is smaller even for the simple skirt 1. However, the effect of the skirts become more apparent on skirt concept 2 and 3. Here the wake close to the ground is completely removed along the trailer. The same observations can be seen in figure 53 regarding the boat tail ending of the skirts. In this figure the effected height can also be seen without flipping through the cut planes, this is at the vehicle end the same height as the boat tail but lowers the longer away from the vehicle.

The difference between the two types of skirts here becomes apparent. While the smaller skirt mostly reduce drag by preventing flow in under the vehicle the more covering skirt covers so much flow that the wake on the leeward side is removed. The skirts also provide a smooth surface along the truck that the air can attach to. This makes the larger skirts work with two areas to reduce the drag of the vehicle.

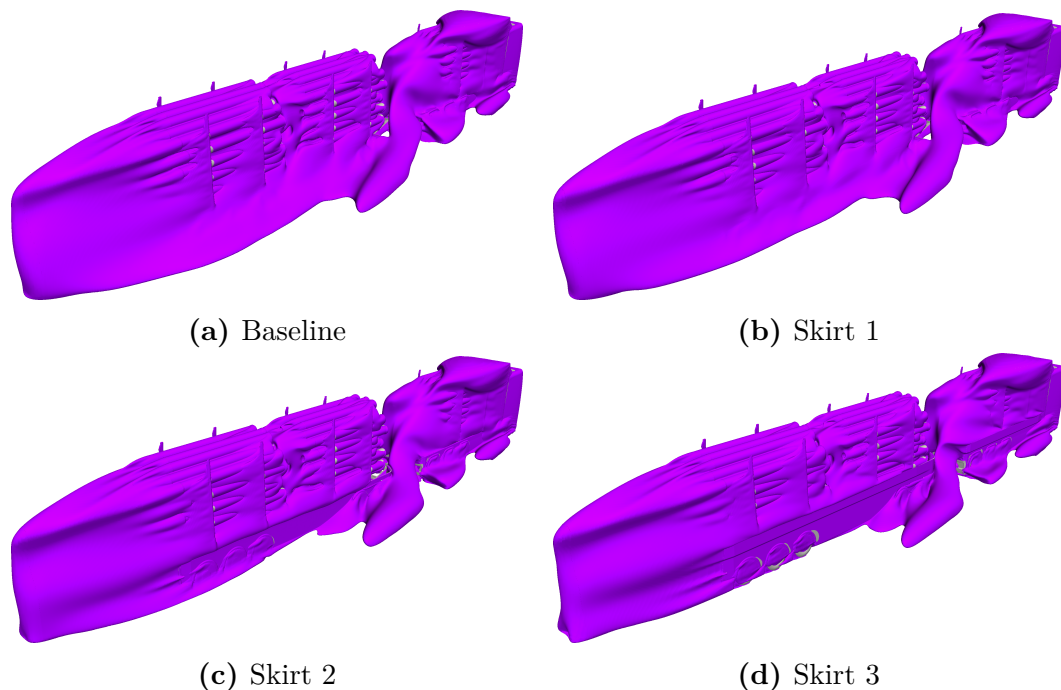


Figure 54: ISO contour of total pressure coefficient equals zero around the truck viewed from the rear windward side simulated with 5° yaw. The baseline and skirt 1 models have the same characteristics while the wake is somewhat smaller with skirt 1. Skirt 2 and 3 have a considerable and similar effect on the trailer windward side wake that is almost eliminated.

The effects from the boat tail on the skirts was noted above and the difference it made. There was also a boat tail on the end of the truck. In hindsight this does no good at this location, it rather worsen the drag accumulation as it forces more flow in between the truck and trailer. If this would be re done the ending of the truck skirt would be made flat or even with a small deflection out from the truck to reduce the flow impact on the lower parts of the trailer.

At the beginning of the trailer skirt there is a large radius towards the tow bar.

This was intended to catch the low pressure air and decrease the flow impact on the trailer. As the skirts is designed now it contributes alot to the drag in form of pressure drag. This can be seen in figure 55 where coefficient of pressure on the surface is shown for baseline and skirt 2. More effort could be put into designing this part of the skirt to better match the flow coming from the truck. If the design was to be remade the curved section would be ended earlier. This could increase the flow reaching in under the trailer so before drastic changes are made different types of concepts needs to be tested. One other idea is to make the radius sharper and bend it 180° degrees to line up at the inner part of the wheel cover. Thus giving the front of the wheel cover a more aerodynamic shape reducing drag. Once again the risk is that alot of high energy flow could be directed in under the trailer.

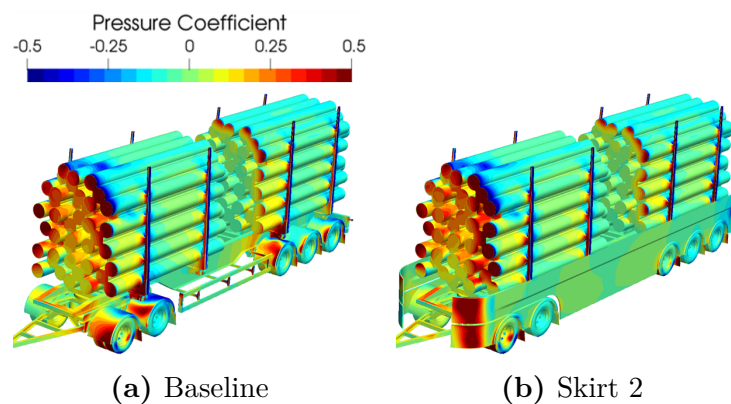


Figure 55: Pressure coefficient, pressure coefficient on the trailer for the baseline and skirt 3 model at 5° yaw. A large area of high pressure can be seen on the bend of the skirt.

The larger skirts have a huge impact on the total vehicle drag, but as mentioned earlier the loading and unloading of the timber truck requires access to both the top and sides of the stacks. The loading is expected to work quite well even with the higher skirts on. Problems could arise if the skirts do not have sufficient structural strength to allow for timber hitting the skirts. If one of the logs in the bottom layer would need to be moved the skirts could limit the possibility to reach these as the logs have been let go of the first time. But the largest problem would be to solve the unloading of the timber truck. To solve this the skirt would need to be maneuverable around and between the stakes. This could be done manually but would then take extra time for the driver or truck operator that is unloading the timber vehicle. The preferred way would be to find a solution that can be operated from within the cab of the timber truck. The the driver could simply lower the skirts when arriving to the plant and then raise them when leaving. Here the problem is to find a solution that can lift the skirts up and down and not weigh so much that the loss of timber transported eliminates the gain from the skirts. It is important that the concept is both improving the fuel economy but also the total revenue as this is a huge driving force for the industry to implement the concepts.

4.4.2 Bulkhead Shield

A shield around the bulkhead was tested in earlier work [2, 4] with a positive effect. This effect was mainly due to the reduction of base pressure on the bulkhead. When the A-pillar separation was present this was also reduced by this concept. As this have been shown to not be present when the method was corrected as described in the method chapter the effect from this concept is expected to be considerably lower. The aim of the concept is now to keep the flow closer to the vehicle and thus reducing the drag. As it have been shown this concept have a good effect on an unloaded truck but no trusted run have been done on a loaded truck it needs to be confirmed that it does not perform to bad on a loaded vehicle.

Two different concepts was tested, one only extending from the bulkhead forwards and one extending forward and all the way back to the first stake. The concepts are shown in figure 56 where the modifications is highlighted in red. No top panel was included in any of the concepts.

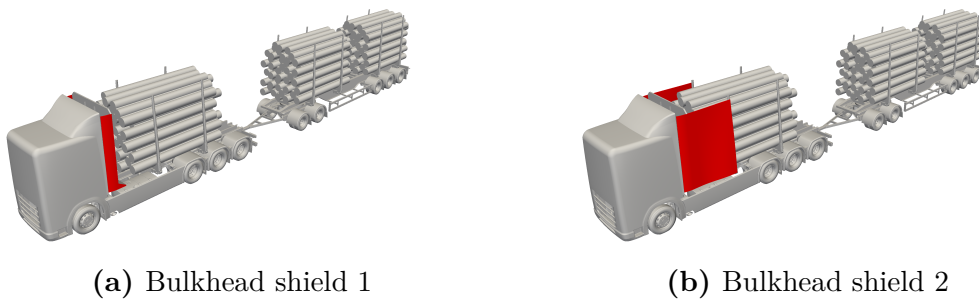


Figure 56: The two different bulkhead shield concepts that was tested, the modifications is highlighted by red colour.

The total vehicle drag is presented in table 15, there was no major differences in drag for any of the tested concepts. Bulkhead shield 1 have such a small difference in drag that it is within the error margin of the method. There is no significant changes in the flow field explaining the difference that can be seen. Bulkhead shield 2 does have an increase of drag that is small but still large enough to have an explanation in the flow field.

Table 15: Total vehicle drag for the bulkhead shield concepts compared to the baseline model results. The bulkhead shield does increase drag with a small amount.

Concept	$1000 \cdot C_D$	$\Delta 1000 \cdot C_D$	$\Delta\%$
Baseline	780	← Reference	
Bulkhead shield 1	787	+ 7	+0.9 %
Bulkhead shield 2	795	+15	+1.9 %

The accumulated drag over the vehicle shows that the difference in drag for bulkhead shield 2 starts at the shield. At this point the concept is actually performing better than the baseline model. It is where the second stack starts that the drag increase

and in the end the concept performs worse than the baseline model. No differences can be seen in the accumulated drag between the baseline and bulkhead shield 1.

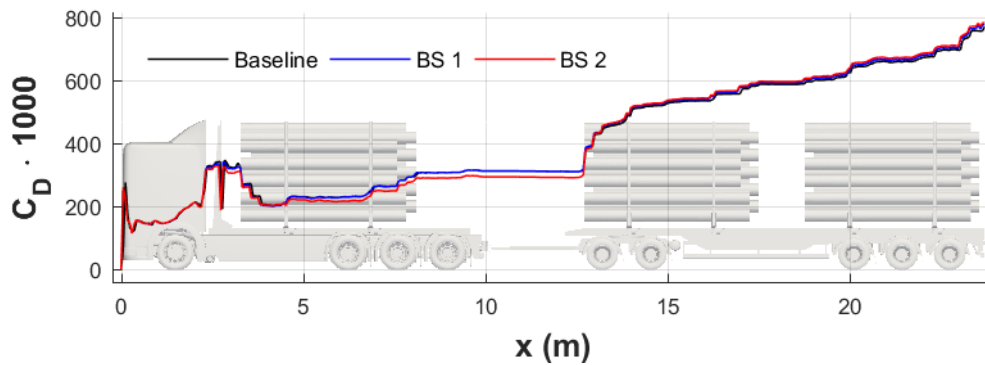


Figure 57: Accumulated drag along the vehicle comparing the bulkhead shield concepts with the base line model at 5° yaw. A reduction of drag accumulation can be seen for bulkhead shield 2 at the concept location. This improvement is lost at the trailer. No significant differences for bulkhead shield 1 can be seen in this graph. BS is short for bulkhead shield.

As the accumulated drag shows that something differs at the start of the second stack pressure coefficient on the truck is investigated and shown in figure 58 for the baseline and bulkhead shield 2. A considerable increase of pressure drag on the second stack front face can be seen. At this point all the gains on the truck are eliminated and the drag accumulation for bulkhead shield 2 is larger than baseline on the trailer.

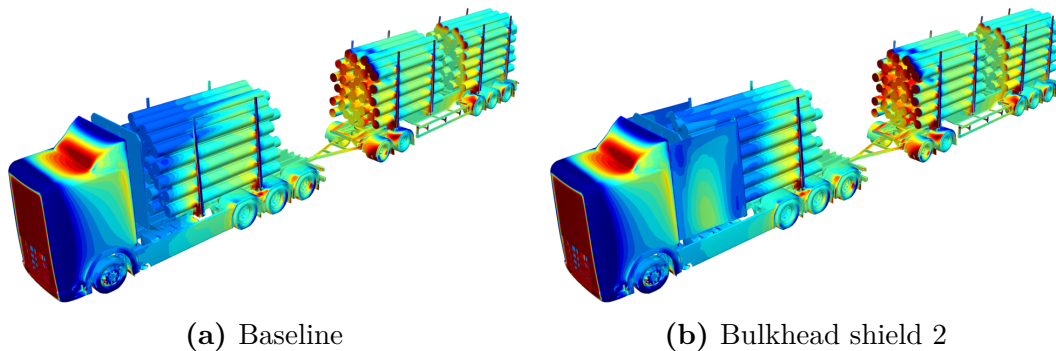


Figure 58: The baseline and bulkhead shield 2 model coloured by pressure coefficient from simulations done at 5° yaw. An increase of pressure can be noted on the front face of stack two.

The reason for the pressure drag increase is due to way the bulkhead shield deflects the air around the first stake. To visualize this a cut plane of total pressure coefficient at 2.6 m is used, this is shown in figure 59. It is found that the bulkhead shield does a good job of routing the flow around the first stake. This is what reduces the drag on the truck as seen in the accumulated drag. It does also mean that the flow impacts the second stake in a new way that changes the shape of the truck wake. A

region of higher pressure can be seen in front of the second stack due to this change in the flow field.

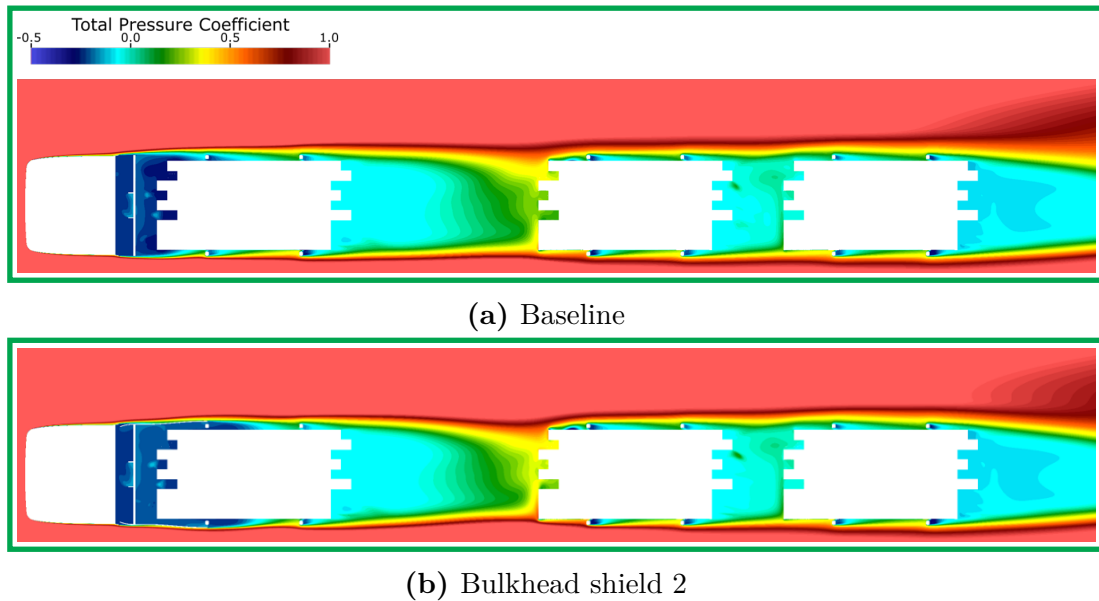


Figure 59: Cut planes located 2.6 m above the ground coloured by total pressure coefficient for the baseline and bulkhead shield 2 concept at 5° yaw. The flow is directed around the first stack by the bulkhead shield. This leads to a different impact on the second bank and stake which further increases the pressure in front of the second stack.

The bulkhead shield have been tested in earlier work using both scale resolving [4] and RANS methods [3]. Both of these works shows that the bulkhead shield concept lowers the base pressure on the bulkhead for an unloaded truck. The concept was also tested on a loaded timber truck in [2], here there was a reduction of drag that was even higher than the unloaded case. This was explained by a large reduction of the leeward side wake, this wake was shown to exist due to a methodology error. With the results from this work together with earlier results from unloaded timber trucks, especially the scale resolving simulation [4], shows that this concept have potential as the increase in drag was acceptable for the loaded timber truck.

All of the concepts mentioned above had some differences in geometry, for example the bulkhead shield in [3] was fitted with a top panel. This does definitely effect the results but the trends should still hold. For further work the design of this concept could be refined and the negative effects when the vehicle is loaded could probably be reduced.

This concept is located in the same area as the logs, this means that if this concept was to be built on a timber truck the construction would have to be strong enough to receive impacts from timber when the car is loaded and unloaded. The concept could be implemented without any moving parts due to the unloading of the timber trucks being done between the stakes on a stack and loaded from the top. A top panel on a bulkhead shield could probably lower the cab wake increasing performance on this part of the vehicle. This would probably increase the pressure drag on the second

stack as it would force more high energy air closer to the vehicle. It would also require some form of automated design for opening and closing the top panel when loading and unloading of the vehicle is performed.

4.4.3 Gap Spoiler and Boat Tail

Earlier work did some investigations of a gap spoiler and boat-tail concepts that showed good potential [2]. In this work both of these are combined with the third skirt concept. Both of these concepts are aimed at directing the flow in a way that are profitable for drag reduction. The gap spoiler is placed at the end of the truck and have a 12° outward angle. The idea is that the flow will be forced out and form a barrier for the high energy flow to not enter in between the truck and trailer. The profile used is called the Clark-Y profile [29], the reason that this profile was chosen will be described later as the boat-tail is introduced.

A boat tail could be fitted to the end of the trailer in a similar fashion as a gap spoiler. As the vehicle in this work is a timber truck some special considerations have to be made. The timber must be able to load and unload from the top of the truck and also different lengths and bent logs need to fit. The decision was therefore made to keep the inside of the boat-tail straight and only working with the outside profile. Thus the Clark-Y profile was chosen as it have a flat section. Boat-tails usually have a top part to that is not present in this design due to the loading requirements.

The gap spoiler have a chord length of 0.5 m and an angle of attack at 12° degrees. The boat tail's chord is 0.7 m long and have the flat bottom face parallel to the $y = 0$ plane. With the geometry of a Clark-Y profile this results in around 11° degrees of angle inwards. Both of the profiles is tilted as the stakes and does not have any parts within the imagined loading compartment of the truck.

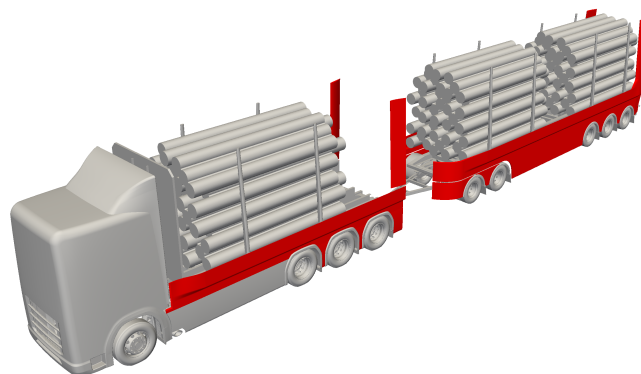


Figure 60: The gap spoiler & boat tail concept geometry shown with the modifications highlighted by red colour. This concept was based on the skirt 3 concept also included as a modification in this figure.

The gap spoiler and boat tail concept was based on the skirt 3 concept and is

compared with both baseline and skirt 3 in table 16. The total vehicle drag is reduced further by 40 counts when compared to skirt 3. The total reduction of drag from the baseline is 139 counts.

Table 16: The effect on total vehicle drag for the gap spoiler & boat tail concept, in this table named "GSBT". The concept is compared to both baseline and skirt 3 at 5° yaw.

Concept	$1000 \cdot C_D$	$\Delta 1000 \cdot C_D$	$\Delta\%$	$\Delta 1000 \cdot C_D$	$\Delta\%$
Baseline	780	← Reference			
Skirt 3	681	-99	-12.7 %	← Reference	
GSBT	641	-139	-17.8 %	-40	-5.9 %

Accumulated drag for the total vehicle is shown in figure 61, the compared runs is baseline, skirt 3 and gap spoiler & boat tail. The improvement on the truck from using skirts is eliminated by the gap spoilers, instead the drag accumulation is in good agreement with the baseline. At the start of the second stack the loss from the gap spoiler is gained back. Further down the trailer the gap spoiler & boat tail concept out performs skirt 3 concept. From the accumulated drag the boat tail at trailer does not seem to have such a big impact on the drag. A small jack in the curve can be noted where the gap spoiler is placed.

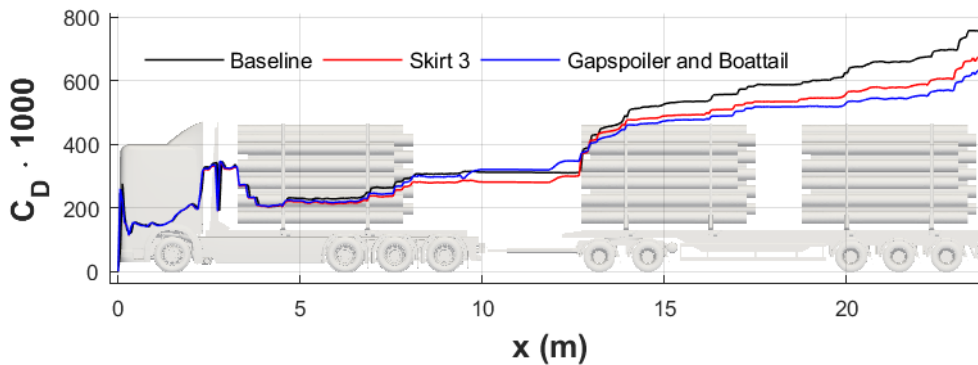


Figure 61: Accumulated drag over the vehicle for baseline, skirt 3 and gap spoiler & boat tail concept. The gap spoiler located on the rear of the truck have an effect on the accumulation of drag and is higher than skirt 3. On the trailer improvements can be seen for the gap spoiler & boat tail. This effect is present over the whole trailer. In the end of the trailer a small difference in drag accumulation between skirt 3 and gap spoiler & boat tail.

As the main drag reduction from this concept is located at the start of the second stack pressure coefficient on the trailer is shown in figure 62a. In this figure a large reduction of pressure drag can be found on the front face of the second stack. Benefits can be found also at the third stack front face, here the pressure drag is further reduced. There is also some reduction of high pressure on the trailer chassis.

To visualize the flow field cut planes showing total pressure coefficient at a height of 2.6 m is shown in figure 63. In this plane the effect of the gap spoiler is clearly

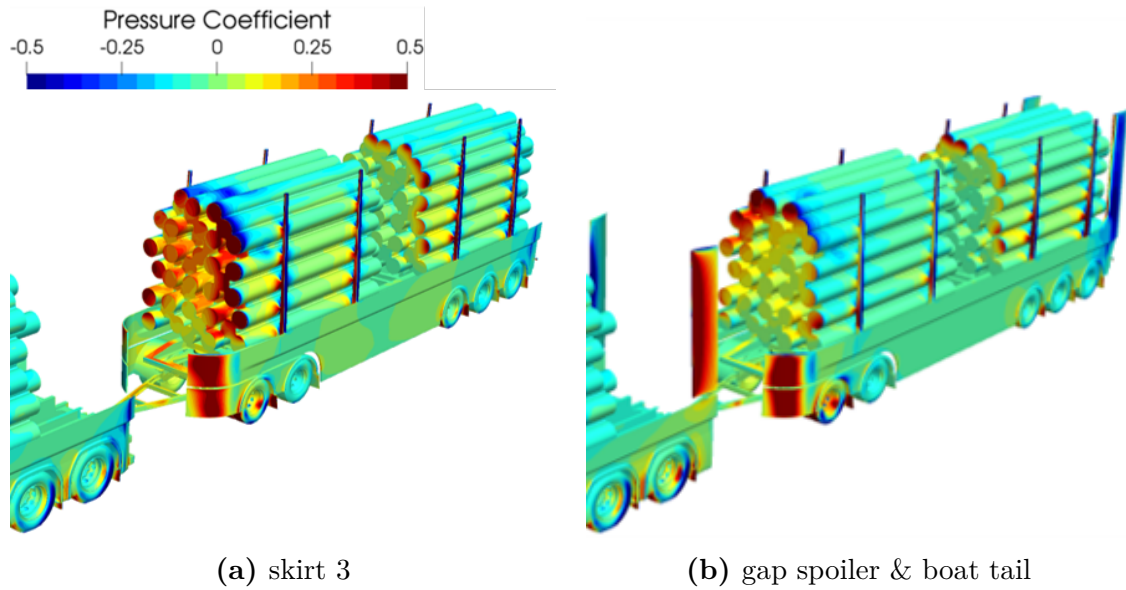
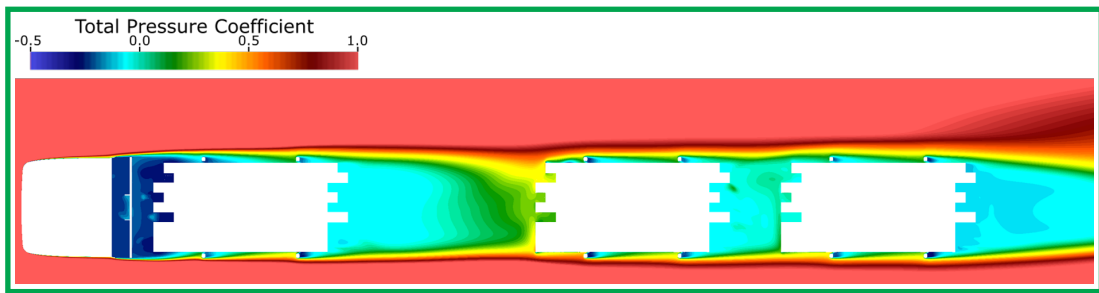


Figure 62: The baseline and gap spoiler & boat tail concept trailers coloured by pressure coefficient subjected to 5° yaw. A considerable reduction of pressure on the second stack front face can be noted. Improvements can also be seen at the third stack front face.

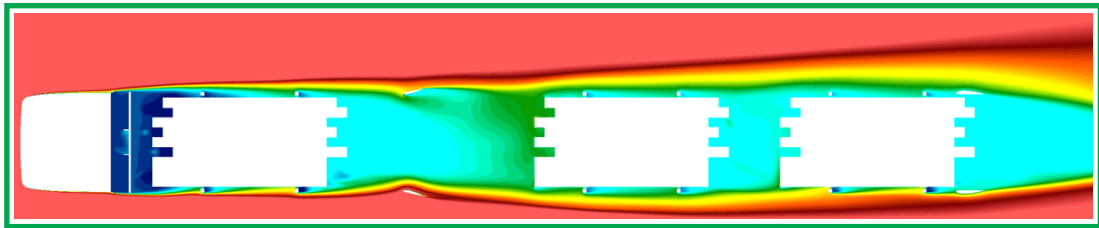
shown and a large out wash behind it can be seen. This out wash first attach shortly behind the start of the third stack. The reduction of high energy flow in front of stack 2 and 3 can be seen clearly and explains the reduction of pressure drag. At the end of the trailer the wake is reduced in size, but the boat tail is mostly inside the low pressure zone crated by the last bank and stakes.

The skirts was changed between this concept and skirt 3, the small boat tail on the truck was removed due to the bad design as earlier discussed. It was done as a test to see how much the boat tail effected the skirt on the trailer. Instead of reducing the pressure drag in this region the problem became worse. This is due to the gap spoiler reducing the pressure behind the truck, as intended. But the lower pressure will also increase the force that the high energy flow from the sides is pulled in with. This is illustrated in figure 64 where a cut plane of total pressure coefficient is shown at a height of 1.25 m. It can be seen that more high energy flow is forced in front of the skirts when the gap spoiler is mounted than when only skirts are used. At this height the gap spoiler is not effective and the flow leaks in underneath the flow barrier that the spoiler creates.

It was noted that the boat tail located on the rear of the trailer did not control the flow as good as it could. This was due to the location of the boat tail located within a low energy flow region. With the current regulations regarding vehicle width limiting the design to 2.6 metre [30]. it could not be moved further out. It could be moved further back on the trailer until the limit of 25.25 m. Another thing that could improve the effect would be to keep the flow attached better to the trailer. This can be done by enclosing the timber completely but this introduce many problems regarding loading and unloading. In the next section a compromise will be tested where the trailer is enclosed between the fourth and fifth bank and

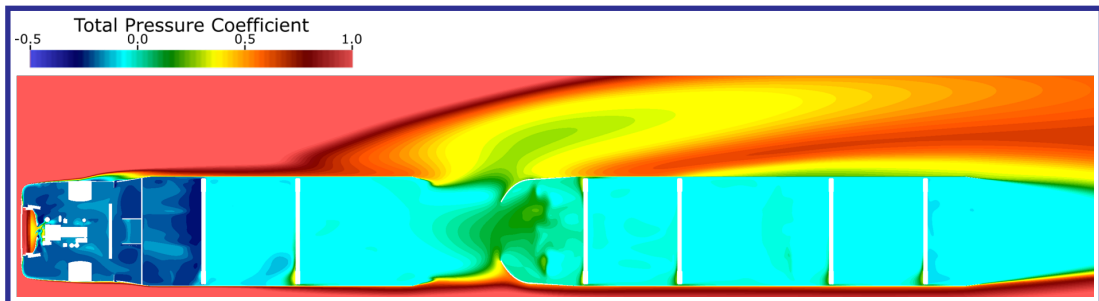


(a) skirt 3

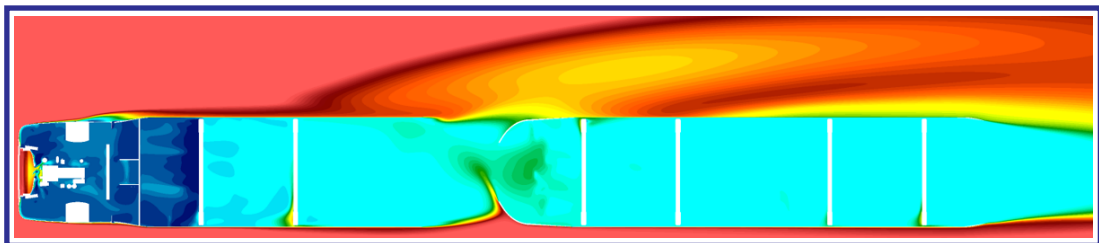


(b) gap spoiler & boat tail

Figure 63: A cut plane coloured by total pressure coefficient at a height of 2.6 m where the vehicle is at 5° yaw. The effect from the gap spoilers is clearly shown and the flow is forced out and around the second stack and reattaches at the beginning of the third stack. Lower pressures is observed both before the second and third stack.



(a) skirt 3



(b) Gap and tail

Figure 64: A cut plane coloured by total pressure coefficient at a height of 1.25 m where the vehicle is at 5° yaw. At this plane located below the gap spoiler and shows the inflow of high energy flow below the flow barrier that is created but the gap spoiler. Between the truck and trailer the pressure is considerably lower.

stake pair.

The angle of the spoilers is one thing that can be investigated further. Here it was shown that this particular angle of 12° degrees was good to use at 5° yaw. Investigations into if there exist a better angle is one thing to do but the most important before this concept is implemented on the road is to investigate the yaw sensitivity. There may be a requirement of the spoiler to be adjustable and adjusted during transport as the yaw angle changes.

4.4.4 Gap Seal

The gap seal concept tries to prevent the same thing as a gap spoiler does. By placing a vertical plate on the tow bar on the trailer the flow in to the gap should reduce as there is no way through the gap. This have been tested in the USA with mixed results on a tractor-semitrailer configuration [24, 25, 31].

This is combined with a plate covering the area between the fourth and fifth stake pair. This plate is also called a gap seal but two plates are used to seal the gap from both ends. This is done prevent flow to get in between the second and third stack and reduce pressure drag. But as discussed in the section above it will also hopefully reduce the wake size. The idea is to see if a boat tail could be placed in higher energy flow without moving it from the position used in the previous concept. In this concept the boat tail is not included but the distribution of pressure will be used to evaluate if the boat tail can be improved. A similar concept have been tested before in [2], here the gap between the stakes containing one stack was closed instead. An effect can be noted on the flow field where the flow became more attached on the windward side.

The geometry is shown in figure 65 where the modifications is highlighted in red. This concept was also based on skirts 3 with the boat tail on the truck skirt removed as in gap spoiler & boat tail. The gap seal is mounted on the tow bar and have a length of 1675 mm and height is in level with the timber stack.

The result is shown in table 17 and is compared to both baseline and skirt 3. From skirt 3 the gap seal further reduces drag by 24 counts and the total reduction from baseline become 123 counts.

Table 17: The effect on total vehicle drag for the gap seal concept. The concept is compared to both baseline and skirt 3.

Concept	$1000 \cdot C_D$	$\Delta 1000 \cdot C_D$	$\Delta\%$	$\Delta 1000 \cdot C_D$	$\Delta\%$
Baseline	780	← Reference			
Skirt 3	681	-99	-12.7 %	← Reference	
Gap seal	657	-123	-16.4 %	-24	-3.5 %

The accumulated drag is shown in figure 66, the compared cases is baseline, skirt 3 and gap seal. The accumulation have good agreement between skirt 3 and gap

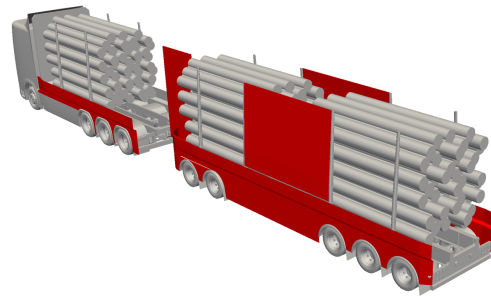


Figure 65: The gap seal concept geometry shown with the modifications highlighted by red colour. This concept was based on the skirt 3 concept also included as a modification in this figure.

seal until shortly before the trailer. Here the gap seal actually outperforms skirt 3, the bump in the curve observed before due to the bend in the skirt is not present for the gap seal concept. Further, moving down the trailer the concepts looks very close. It is at the start of the third stack that the curves starts to separate.

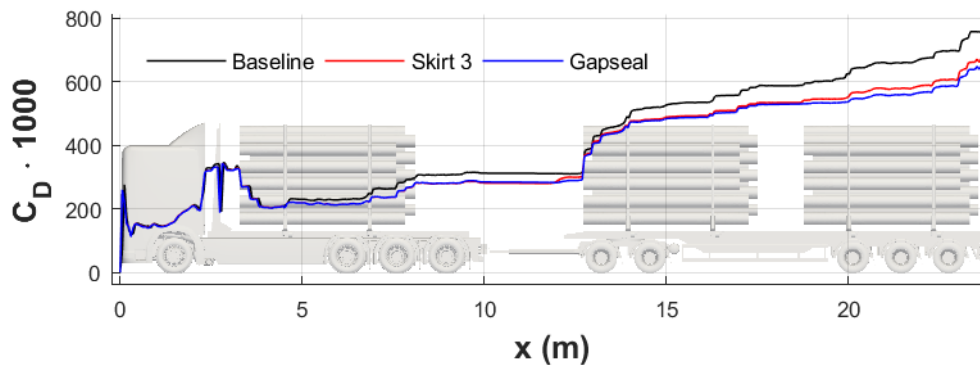


Figure 66: Accumulated drag over the vehicle for baseline, skirt 3 and gap seal concept at 5° yaw. The concepts are very close on the truck, no interesting observations are found before the trailer. A small reduction in drag accumulation can be found before the trailer when the gap seal is used. Over the second stack the accumulation continues to be very similar. It is at the start of stack three differences can be observed, here the gap seal reduces drag accumulation and the difference is kept to the end.

The pressure coefficient, coefficient of pressure on the vehicle is shown in figure 67. A reduction of pressure drag can be noted on the trailer skirt.

In figure 68 cut planes of total pressure coefficient at a height of 2.6 m is shown for skirt 3 and gap seal. Down the trailer the flow behaves different, most notable on the windward side where higher energy flow impacts the fourth stake. If one study the accumulated drag in figure 66 a small difference in drag can be noted here. The seal between the second and third stack does preform as expected and the high energy

in skirt 3 concept. Even though they come with an added complexity and requiring more detail design than a simpler skirt they have so more performance when it comes to aerodynamics that it is deemed worth the effort. The skirts will be combined with a combination of the gap spoilers and boat tail. Earlier the gap spoilers showed a very good performance increase for a vehicle in 5° yaw. The concepts efficiency can be effected alot by the yaw parameter in both lower and higher angles of yaw the benefits could be eliminated or reduced. The boat tail did not perform as good as it can do but is still kept for the final aero kit with the motivation that a gap seal between stake four and five is added. This is the last part of the aero kit and was added due to the reduction of pressure drag on the third stack and ability to keep the flow attached along the trailer. This will hopefully increase the performance from the boat tail. In figure 69 the loaded vehicle equipped with the aero kit is shown. Again the modifications is highlighted in red, the only difference between loaded and unloaded vehicle is the angle of attack on the gap spoiler. The required mechanical design to make this spoiler turn was deemed so easy as this can be done automatically without any complex designing or modification of existing trucks. The change in angle of attack is made due to the earlier suspicion that the angle of the spoiler lead to higher drag when the vehicle is traveling in low angles of yaw or unloaded. The gap spoiler was kept at the same constant angle of attack for all loaded yaw angles while for the unloaded cases the angle of attack was changed to 0° . The straight ends of the skirts on the truck that were tested on the previous two concepts were also kept.

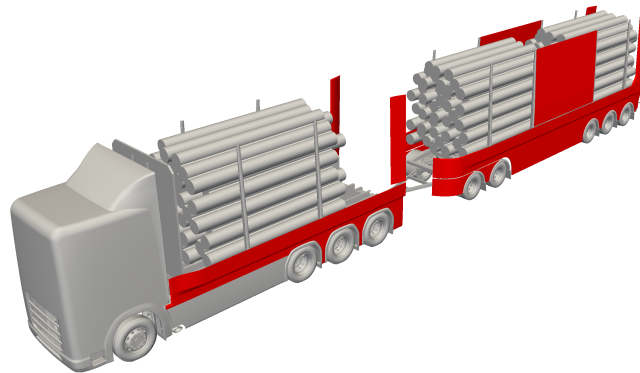


Figure 69: The final aero kit geometry shown with the modifications highlighted by red colour.

The total vehicle drag reduction at 5° yaw is shown in table 18 for the loaded configuration. A reduction of 151 counts down to 629 is achieved with the aero kit mounted, this is a further reduction of 12 counts from adding the gap seal. In total the whole vehicle drag is reduced by 19.3 % in this work.

The unloaded results for 5° yaw is shown in table 19 where the total vehicle drag is reduced to 599 counts with aero kit mounted, this is a reduction of 172 counts. This is a reduction of 22.3 %.

The new aero kit yaw sweep is shown and compared to baseline result in figure 70.

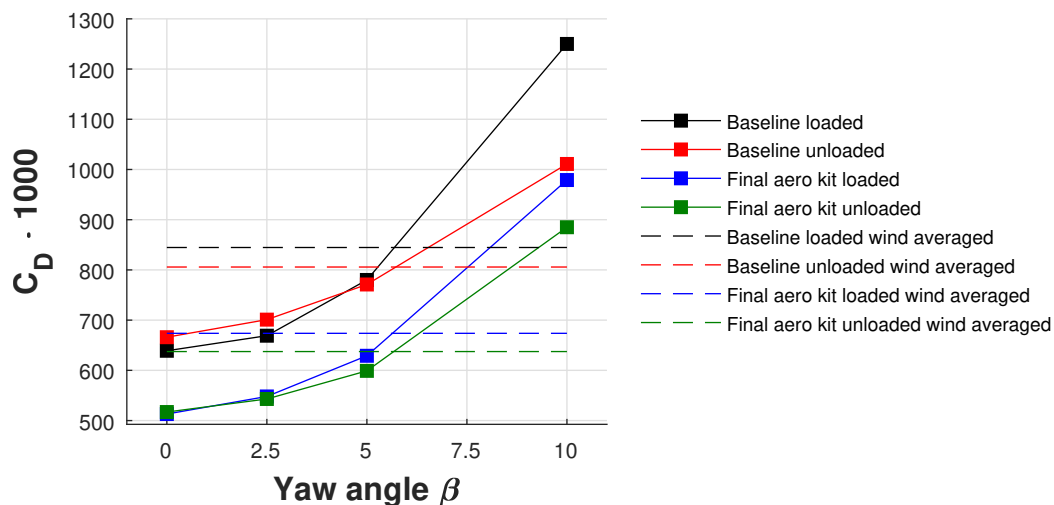
Table 18: Total vehicle drag compared between the baseline and final aero kit design on a loaded vehicle at 5° yaw

Concept	$1000 \cdot C_D$	$\Delta 1000 \cdot C_D$	$\Delta\%$
Baseline	780	← Reference	
Aero kit	629	-151	-19.3 %

Table 19: Total vehicle drag compared between the baseline and final aero kit design on a unloaded vehicle at 5° yaw.

Concept	$1000 \cdot C_D$	$\Delta 1000 \cdot C_D$	$\Delta\%$
Baseline	771	← Reference	
Aero kit	599	-172	-28.7 %

It can be found that the aero kit design lowers the drag over all angles and the kit does actually preform as good for loaded and unloaded when small yaw angles is used, yaw angle < 5 . Wind average drag was also calculated for the new aero kit again using the SAE J5212 method [12]. The wind averaged drag ended up shortly above the 5° yaw case as for the baseline model with values of 674 and 637 drag counts for loaded and unloaded respectively. The trends of drag over yaw angle did change alot for the loaded case where the increase between 5° and 10° was reduced by almost 100 counts with the aero kit.

**Figure 70:** Yaw sweep for baseline and aero kit both loaded and unloaded with the calculated wind averaged drag. Drag over yaw angle was reduced for all angles using the aero kit and the yaw sensitivity was improved for a loaded vehicle. The wind averaged drag became 674 and 637 for loaded and unloaded respectively.

Drag accumulation for the aero kit compared to baseline loaded and unloaded is shown in figure 71 for 5° yaw. The loaded vehicle does not see any large differences over the truck, no major jumps in drag can be found where the gap spoilers are placed. At the trailer effect of the aero kit starts to show and keeps growing all over the trailer. Accumulated drag for the unloaded vehicle does show larger differences

on the truck, also no major increase in drag around the gap spoilers can be found. On the trailer the effect of higher skirts is clearly shown at every bank and stake pair where the baseline model shows large increases of drag while the vehicle with a aero kit have a more linear increase of drag. Alone, the truck contribute with

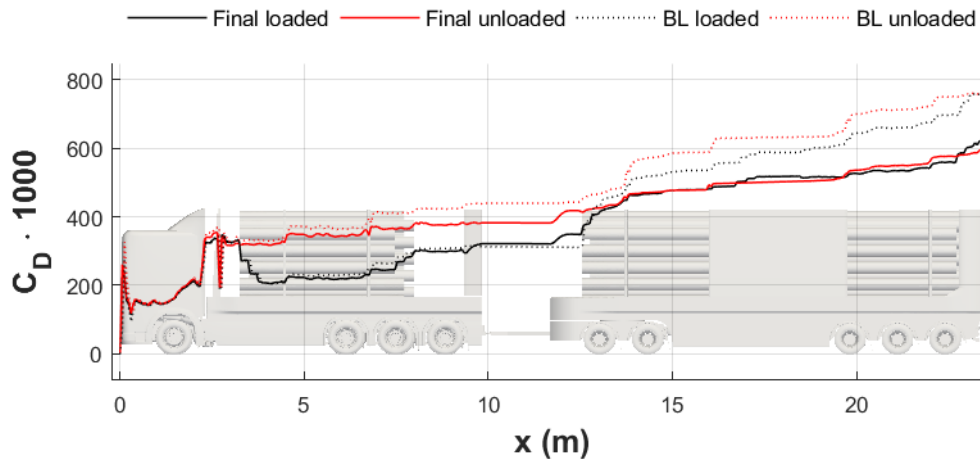


Figure 71: Drag accumulation for baseline (BL) and final aero kit vehicle both loaded and unloaded at 5° yaw. The loaded vehicle does not show much differences on the truck and all of the drag reduction is focused on the trailer. When unloaded drag accumulation is reduced from the first bank and stake pair all the way to the end with clear differences in characteristics over banks and stakes on the trailer.

321 and 382 counts of drag for the loaded and unloaded vehicle, respectively, at 5° yaw. Meaning that, for the truck isolated, the final aero kit increase the drag with 8 counts when loaded and reduced drag with 58 counts when unloaded.

As the differences between trends was noted above the difference in accumulated drag for different yaw angles is shown in figure 72. Still the difference between 10° yaw and the smaller angles is the major difference seen in both loaded and unloaded configuration. The 10° yaw case shows a soft bump in in drag accumulation between stack two and three. Besides becoming lower the accumulation of drag have not changed in any significant way. The bump in the accumulation is due to the pressure interaction between stack two and three. The spoilers did not have any large negative effect as was earlier feared during a yaw sweep.

The gap seal was combined with the gap spoilers with the idea that the flow would stay closer to the trailer allowing for the boat tail to have a larger effect. A cut plane at a height of 2.6 m is shown in figure 73 colored by total pressure coefficient, the aero kit is compared to the earlier gap spoiler concept. The difference in terms of geometry in this figure is the added gap seal between stake four and five. As was expected the flow did became some what more attached, this is clear when looking at the pressure around the boat tail profile. The performance from the boat tail can also be noted where the wake is reduced in area on both leeward and windward side. Off course the gap seal have an positive effect on the third stack as it does not allow for any high energy flow to enter in between stack two and three.

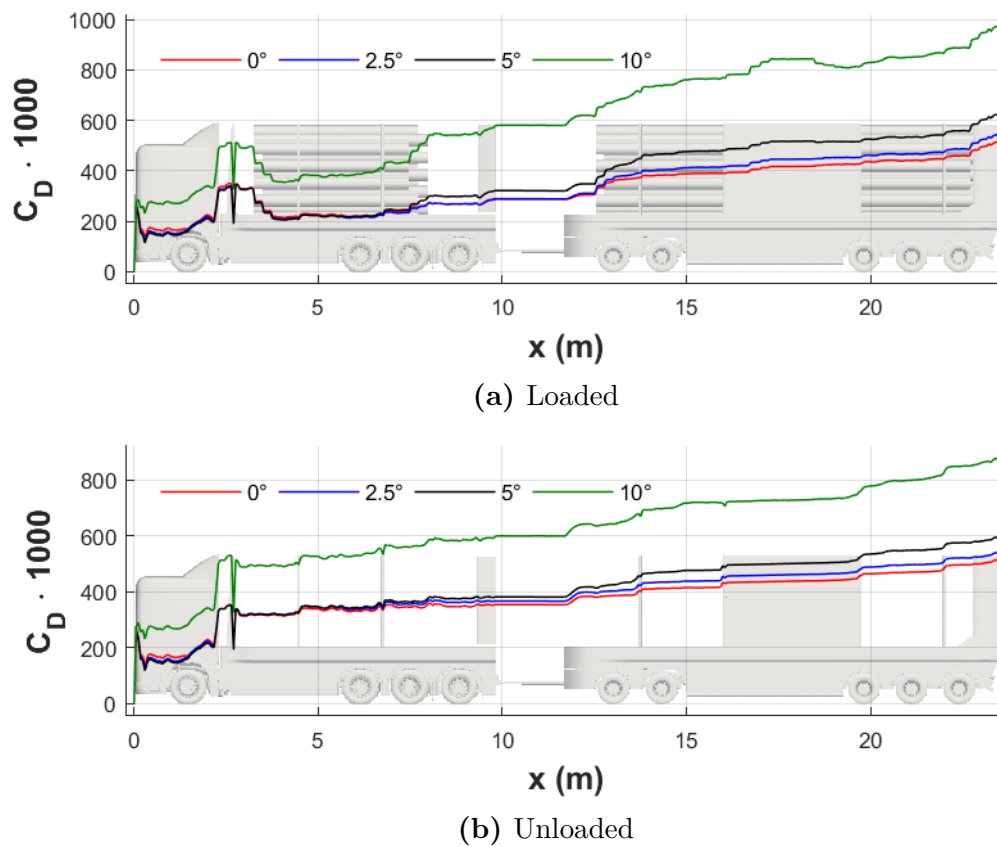


Figure 72: Drag accumulation for the aero kit vehicle in both loaded and unloaded configuration for all investigated yaw angles. In the loaded case small increases can be found at the gap spoiler and a smooth bump in the curve between stack 2 and 3.

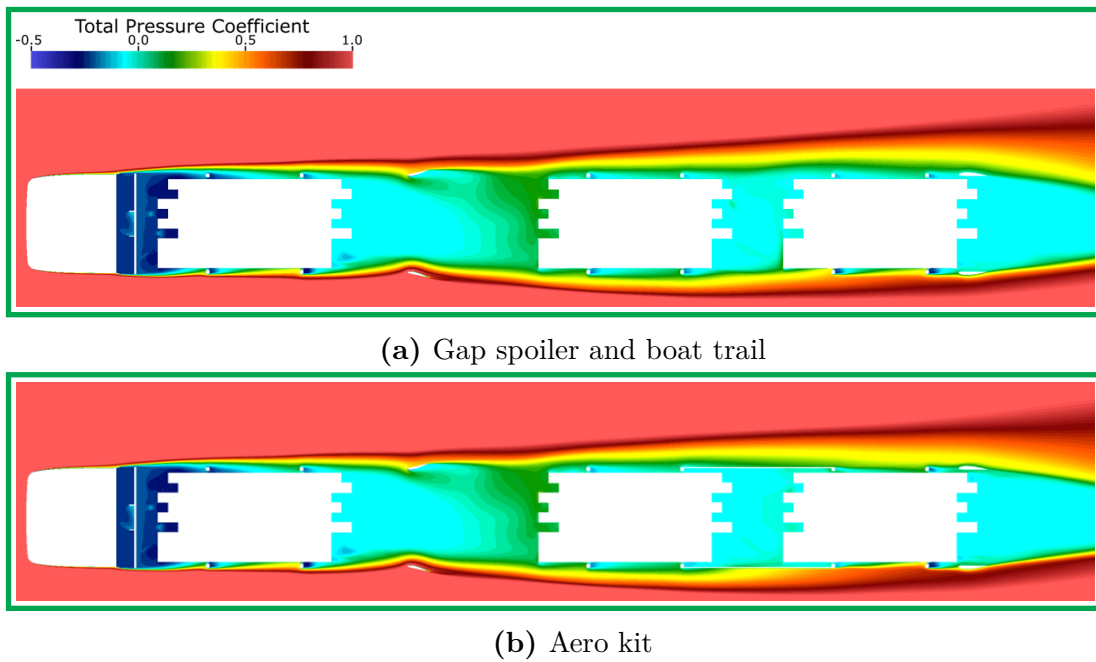


Figure 73: total pressure coefficient shown at a cut plane located 2.6 m above the ground at 5° yaw. The effect of the added gap seal between stack two and three is shown clearly as no high energy flow is present between the stacks. The boat tail at the trailer end is also improved.

In the accumulated drag the reduction of drag on the unloaded truck seems to come from the banks and stakes. This was investigated and a comparison of the drag contribution for these parts are shown in table 20 and compared between baseline and aero kit vehicle for 5° yaw. The majority of drag reduction was found at the banks and stakes, mainly drag on banks and winches was reduced. The total reduction of drag on these parts between the models was 132 counts, as the total reduction was 172 counts these parts stands for 87 % of the improvement on a unloaded vehicle. Out of the 89 counts of drag left on these parts the stakes stands for 70 of these counts.

Table 20: The difference in drag on banks and stakes for the unloaded baseline and aero kit vehicle. It was found that a reduction of 132 counts was made only on these parts

Feature	Baseline	Aero kit
Bank & stake 1	17	6
Bank & stake 2	34	8
Bank & stake 3	58	18
Bank & stake 4	39	17
Bank & stake 5	46	19
Bank & stake 6	27	20
Σ	221	89

In the end the reduced drag of the timber vehicle is estimated to reduce the fuel consumption with 5-10 % based on wind averaged drag. It is assumed that the 25

% of fuel is caused by aerodynamic drag when the vehicle is loaded and up to 50 % when it is unloaded.

4.6 Future concepts discussion

This section discuss some concepts found in literature and concepts that was thought of during the work. The concepts did not make it in to this work as both the time and computing resources were limited. Some of the concepts are based on the results seen in this report and combined with the concepts tested here. The focus in this work was on a loaded timber truck thus most of the concept that is mentioned here would be for a unloaded timber truck.

Folded stakes already exists from ExTe [32], this type of concept have been thought about in this work to. From the baseline model the total drag accumulated by the banks and stakes was responsible for 29 % of total vehicle drag. Using the higher skirts as in skirts 3 the effect from the banks is reduced alot, with folded stakes the effect of the stakes could also be reduced. Different ways of folding the stakes can be thought of, one of them as provided by ExTe. The stakes could also be folded in the longitudinal direction to eliminate the need for telescopic or stakes that fold on the middle once before being folded down. The design of the stakes from an aerodynamic standpoint should be so that the higher skirts that have been shown in this work can enclose them when folded. The case will always be that the lower the stakes get the better for the reduction of drag. Further studies needs to be done on the folded stakes concept to know for sure how these would behave with the higher skirts. Clearly the potential savings that can come from reducing the drag from banks and stakes are very large, 221 drag counts for the baseline vehicle and 89 counts with the aero kit, of which 70 is caused by the stakes. Folding the stakes in combination with the aero kit probably eliminate the majority of the 70 counts of drag caused by the stakes, as they would be covered by the high skirts.

Some times the timber vehicles does not travel fully loaded, this can depend on for example the timber density. Consider a case when a 74 ton vehicle is to transport logs with higher density. In this particular case the density happens to be so much higher that the truck can only be loaded to the same height as the 64 ton configuration. This results in a truck that have a higher deflector and bulkhead than necessary, i.e., an unnecessarily large cross section. It would in this case be beneficial to have an adjustable air deflector on the cab roof. There exists patents on solutions to this today [33], the thing that can not be found today is an adjustable bulkhead. The results show an considerable effect from having lower frontal area, if this adjustable bulkhead could be designed to be light enough it could save alot of fuel during timber transports. This concept could further be used when the timber truck is driving empty. Then there is no need for a bulkhead at all and it could be adjusted to fit within the wake of the cab. In turn the deflector could be lowered to its lowest position. An estimate of the gain that could come from this can be done from the loading configuration study where the 64 ton vehicle had 56 counts of drag less compared with the 74-ton vehicle. However, considering the different wheel

configurations where the wheel drag is 7 counts higher for the 74 ton vehicle, meaning that the potential gain from adjusting the height of the deflector and bulkhead is around 49 counts.

The gap between the truck and trailer was shown to have a negative impact on the total vehicle drag, if this gap could be reduced performance is to be gained. The reason for the long gap on the truck is so the axles and boogies is far enough for each other to be legal when the vehicle is fully loaded. For the largest roads in Sweden this minimum distance between the last truck axle and first trailer axle is 4 m for some smaller roads this is even 3 m [30]. The lengths depend on the weight of the vehicle, more specific the weight being carried by the axle/boogie. This combined with a maximum load on each axle or bogie forces these combinations for fully loaded truck trailer combination. When the vehicle is empty some of the axles could be lifted to allow for a shorter tow bar, this is already common practise. If the tow bar was adjustable this could save both tire ware and fuel due to less rolling resistance and aerodynamic drag.

The combination of truck and trailer does often leave a large gap between the truck and trailer as mentioned above. Even though the best solution would be to eliminate the gap some improvements could possibly be done. Today alot of research goes in to platooning on vehicles, especially trucks. When the trailer is following the truck this could be seen as similar case. Therefore, an aerodynamic concept could be constructed to improve the interaction between truck and trailer. Similar as the gap fairing tested earlier in [2], this concept showed good potential and could probably be designed to work even better in combination with the truck.

5 General Discussion

As mentioned in the method chapter it was found that 2nd order discretization of turbulent quantities was required for the result to be representative. During most of this work the earlier leeward side A-pillar separation was noted to be extremely large and earlier work showed that this separation behaved somewhat suspicious [2, 3]. During these earlier investigations the flow feature producing this wake was found, this together with the limited literature and physical test available lead to the conclusion that this was a plausible flow field of a timber vehicle. It was not until the concept phase in this work that this was identified as a an unphysical behaviour, it was during investigations of a bulkhead shield that no effect on the A-pillar separation was found that started the further investigations.

In hindsight there were clues that something was not right with the method, for example when the separation did occur on an unloaded truck at 5° yaw, also when the results were first introduced to Scania they were skeptical but did not dismiss it as implausible. It is suspected that k which is strongly related to EVR was the culprit by itself, however, EVR was evaluated as it was already being exported automatically from prior troubleshooting and in that way keeping computational cost down.

The discovery was made around one month before the end of this work prior to which many simulations had already been done in the first four months of work. This undoubtedly shows the strength and benefits of having an automated process, that it was possible to rerun the simulations in a rather simple way with regard to the circumstances. The change to new settings was done in a matter of minutes, the only concern was the wasted computational time and whether the remaining allocation would suffice. A couple of planned cases were abandoned, but in the end there were plenty of results, without automation it would have been unimaginable.

A direct comparison of the total drag scalar values between the results of this work and the previous study is not applicable except for comparison of trends due to the big discrepancy in total drag between 1st- and 2nd-order discretization of k and ε . However, as was show the distribution of drag was very similar.

A mesh density investigation was carried out before changing to 2nd-order k and ε , this was not rerun as its expected to have no or very little effect on the outcome, trends and drag distribution still shoved good agreement. On the other hand, solver relaxation strategy was also developed before the change of discretization, there is probably some more to gain, but as the performance only increased no further effort was put into this.

None of the vehicle models that were used was entirely symmetrical, mainly there

were parts within the truck chassis that were different between sides, such as air and fuel tanks, engine, and engine exhaust. All of the simulations that were done using only positive yaw angles, meaning that there are effects that occur only at negative yaw conditions that were not captured. However, considering the size and location of these parts it is not believed to have a significant impact on the result, the truck chassis was from the start mostly covered by skirts that were symmetric. Hence it was assumed that the results are symmetric when using the wind averaging method require positive and negative yaw angles.

The gap between the timber stacks was found to have a large effect on total vehicle drag, other studies on truck trailer configurations have shown that the gaps have a major impact on drag [27]. The European Modular System is a system of different type of vehicle components such as a tractor, dolly, link, and semi-trailer, only vehicles that adhere to this system are allowed to be as heavy and large as the ones in this study [5]. There are other combinations than truck trailer that have considerably shorter gaps between stacks, for example a vehicle with a tractor, link and semi-trailer could be used.

It is not uncommon that timber vehicles have an mounted crane that is used for loading, as previously stated this was not considered in this study due to mainly focusing on group vehicles where fuel efficiency per ton-km prioritized. The crane is often located at the end of the truck and the whole assembly consist of crane arm, operator cab and support legs, this is a large bunt object that is guaranteed to produce more drag. Expected is that the crane will have a large effect on the unloaded timber vehicle while its effects would be more limited on a loaded truck where it is behind the timber.

In the timber study the timber was always perfectly straight with no taper, also only uniform log diameter was examined. In reality timber stacks are most often composed of different diameter log and are tapered, but due to it being much more difficult to model and the fact that the taper by itself probably wont have a significant effect this was neglected. However, the perfectly straight longitudinal channels that constitute the voids in the timber stack are presumably an idealization compared to reality where the flow through most certainly is more evenly distributed and more restricted. Finally, one must remember that no timber stack will be the same as another and that things like badly delimited timber, branches and other debris can have an effect, there is for sure a reasonable amount of uncertainty to factor into the result.

6 Conclusion

In this work the geometry of a timber vehicle was constructed from parts gathered from many different sources. The model is suitable for the automated work flow process and have a surface mesh with good quality and properly named PID's.

During the work the CFD procedure was improved in many aspects, an improved automation framework was built where the user only have to supply a surface mesh. The process will mesh, solve and deliver images of the flow field and surface quantities. Data for convergence insurance is also exported together with data prepared to produce figures over accumulated drag.

During the work a problem with the methodology was found with regard to the discretization of turbulent quantities. It was found that much of the earlier work over predicted the total vehicle drag due to this. This does limit the amount of comparison that can be made between the results from this work and earlier work. It was found that the trends can be trusted but individual values of drag and flow features can not be compared.

Different types of timber geometry was tested, these geometrical changes was based on statistical data received from Biometria. Log size in terms of diameter and length, roughness and stack diversity was investigated. It was found that log length and stack diversity did show changes in the flow field around the vehicle while roughness and diameter showed effects on the drag but limited effect on the flow field.

This timber study was the base for a baseline model that represents a generic 74 ton timber vehicle. The model was investigated both loaded and unloaded for yaw angles of 0° , 2.5° , 5° and 10° . The wind averaged drag for the baseline model became 845 and 805 drag counts for a loaded and unloaded vehicle respectively. These results was used to study the specific flow features was evaluated and investigated thoroughly.

Selected aerodynamic concepts found in the previous work or other literature was tested on the loaded baseline model. The concepts that showed good potential was combined in to a final aerodynamic concept that was studied both loaded and unloaded for the yaw angles of 0° , 2.5° , 5° and 10° . The aerodynamic kit vehicle have a wind averaged total vehicle drag of 674 and 637 drag counts for loaded and unloaded vehicle respectively. This is a reduction of 171 and 168 drag counts, or 20.2 % and 20.9 %, for loaded and unloaded vehicle respectively, which equates to an estimated fuel saving between 5-10 %.

7 Outlook

The scope of this study has been relatively large ranging from evaluating the aerodynamics of timber diversity, vehicle configurations, current vehicles, and drag reduction devices. Even though the significant amount drag reduction that was achieved by the concepts constructed the time spent on designing these devices was limited and designs were not revised. There is with all certainty more potential in these concepts than was extracted in this study, e.g., optimizing gap spoiler angle of attack or shape of skirt wheel faring on the trailer. Also, expand on these concepts and evaluate the concepts discussed in section 4.6.

The automated procedure covered most of the workflow, although it would have been convenient to add the Matlab part with convergence report and drag accumulation plots being produced as a part of it and only need to do manually in special cases. To make the method more flexible an automatic convergence check based on the force report history could be implemented, in that way computational cost could be saved in faster converging cases and eliminate the need to manually continue a simulation that is harder to converge. The largest part of the total turnaround time, 11-14 hours, was the meshing that took 5-7 hours meshing depending on geometry, this is mainly due to the meshing method that was used does not allow for parallel processing at the time of the study. Thus there could be relatively much time to be saved by switching to a meshing method that allows for parallel construction of the volume mesh. Also, there were some instances where mesh quality was poor automatic detection of this would reduce the risk of problems and needing to check the quality report manually.

The economic aspect of the concepts were not considered when evaluating concepts, of course this is a major factor to whether they are profitable; even if there is a massive drag reduction as a result of a concept that also takes a long time to set up when loading and unloading it won't get used due to cost. Such an assessment economical has been done previously on the subject of timber vehicle drag reduction at LiU, where an investment calculation software for timber trucks developed by Skogforsk was used [34]. The same approach could be applied to the results of this report to evaluate the economical aspects.

8 Perspectives

The work have a positive impact on the environment as the whole work builds on the goal to reduce fuel consumption. This reduces negative effects on the the environment when less fuel is burned and produced. The work also have a positive effect on the economics of both the forest companies individual drivers. Lower fuel consumption lowers the costs of hauling timber and increasing the margins in this business. This leads to a lower price due to an open market. It will also create more work opportunities as someone have to design and also produce and assemble these devices that are presented in this work. As the fuel consumption lowers the society will gain in fewer citizens suffering from for example climate change in the future. Also the air quality is improved for citizens living close to roads with heavy timber vehicle traffic. The only ethical aspect that can be discussed here is the ones above mentioned, producing this work and making use of it is for the benefit of everyone.

Bibliography

- [1] Ekman P. *ETTaero2 – Aerodynamisk utformning av tunga timmer- och flisfordon*. Oct. 2017. URL: <https://www.energimyndigheten.se/contentassets/8e9d250e9d534d848e37d637a99d2073/session-12/3-ettaero2-aerodynamisk-utformning-av-tunga-timmer-och-flisfordon.pdf>. accessed may 2019.
- [2] Fernández del Río Á. “CFD Investigation of Aerodynamic Drag Reduction for a Fully Loaded Timber Truck”. ISRN: LIU-IEI-TEK-A-18/03233-SE, 2018.
- [3] Colombi R. “CFD Investigation of Aerodynamic Drag Reduction for an Unloaded Timber Truck”. ISRN: LIU-IEI-TEK-A-18/03231-SE, 2018.
- [4] Ekman P., Gårdhagen R., Virdung T., and Karlsson M. “Aerodynamics of an Unloaded Timber Truck - A CFD Investigation”. SAE Technical Paper 2016-01-8022, 2016. DOI: 10.4271/2016-01-8022.
- [5] von Hofsten H. *Skogsbrukets transport- och arbetsfordon*. Tech. rep. ARBETSRAPPORT 1003-2019. Skogforsk, 2019.
- [6] ANSA v18.1.4, Pre-processing Software, BETA CAE Systems SA. S.A. Thessaloniki, Greece, 2018.
- [7] ANSYS Fluent r19.0, CFD Software, ANSYS Inc. Canonsburg, PA, USA, 2018.
- [8] ParaView 5.4.1, Post-processing Software, Kitware Inc. Albuquerque, NM, USA, 2017.
- [9] MATLAB R2017b, Data analyzing software, The MathWorks Inc. Natick, MA, USA, 2017.
- [10] National Supercomputer Centre at Linköping University, Sweden. URL: www.nsc.liu.se. accessed may 2019.
- [11] Versteeg H.K. and Malalasekera W. *An introduction to computational fluid dynamics*. 2nd ed. Pearson Education Limited, 2007. ISBN: 9780131274983.
- [12] SAE International. *SAE Wind Tunnel Test Procedure for Trucks and Buses*. SAE Standard J2966. July 2012.
- [13] Hucho W.-H. *Aerodynamics of Road Vehicles*. 4th ed. Society of Automotive Engineers, Inc, 1998. ISBN: 0-7680-0029-7.
- [14] Fuentes X.L. “CFD Investigation of Aerodynamic Drag Reduction for a Wood Chip Truck”. ISRN: LIU-IEI-TEK-A18/03234-SE, 2018.
- [15] Karlsson M., Gårdhagen R., Ekman P., D. Söderblom, et al. “Aerodynamics of Timber Trucks - a Wind Tunnel Investigation”. SAE Technical Paper 2015-01-1562, 2015. DOI: 10.4271/2015-01-1562..
- [16] SAE International. *Guidelines for Aerodynamic Assessment of Medium and Heavy Commercial Ground Vehicles Using Computational Fluid Dynamics*. SAE Standard J2966. Sept. 2013.

- [17] Wood R. “Reynolds number impact on Commercial Vehicle Aerodynamics and Performance”. SAE Technical Paper 2015-01-2859, 2015. DOI: 10.4271/2015-01-2859.
- [18] *ANSYS Fluent User’s Guide*. 19.0. ANSYS Inc. Canonsburg, PA, USA, 2018.
- [19] Ekman P., Gårdhagen R., Virdung T., and Karlsson M. “Aerodynamic Drag Reduction - from Conceptual Design on a Simplified Generic Model to Full-Scale Road Tests”. SAE Technical Paper 2015-01-1543, 2015. DOI: 10.4271/2015-01-1543.
- [20] Anbarci K., Acikgoz B., Aslan R., Arslan O., and et al. “Development of an Aerodynamic Analysis Methodology for Tractor-Trailer Class Heavy Commercial Vehicles”. SAE Technical Paper 2013-01-2413, 2013. DOI: 10.4271/2013-01-2413.
- [21] *ANSYS Fluent Meshing User’s Guide*. 19.0. ANSYS Inc. Canonsburg, PA, USA, 2018.
- [22] *ANSYS Fluent Theory Guide*. 19.0. ANSYS Inc. Canonsburg, PA, USA, 2018.
- [23] Slurm, workload manager software, SchedMD LLC. Lehi, UT, USA. URL: www.schedmd.com.
- [24] Cooper K.R. “Commercial vehicle aerodynamic drag reduction: historical perspective as a guide”. *The Aerodynamics of Heavy Vehicles: Trucks, Buses, and Trains*. Springer, 2004, pp. 9–28.
- [25] Cooper K.R. and Leuschen J. “Model and Full-Scale Wind Tunnel Tests of Second-Generation Aerodynamic Fuel Saving Devices for Tractor-Trailers.”, 2005.
- [26] Marius-Dorin Surcel, Yves Provencher, and Jan Michaelson. “Fuel consumption track tests for tractor-trailer fuel saving technologies”. *SAE International Journal of Commercial Vehicles* 2.2009-01-2891, 2009, pp. 191–202.
- [27] Martini H., Bergqvist B., Hjelm .L, and Löfdahl L. “Influence of Different Truck and Trailer Combinations on the Aerodynamic Drag”. SAE Technical Paper 2011-01-0179, 2011. DOI: 10.4271/2011-01-0179.
- [28] Transportstyrelsens föreskrifter och allmänna råd om bilar och släpvagnar som dras av bilar.
- [29] CLARK Y airfoil, UIUC Applied Aerodynamics Group. URL: <https://m-selig.ae.illinois.edu/ads/coord/clarky.dat>. accessed may 2019.
- [30] Lasta lagligt. URL: https://www.transportstyrelsen.se/globalassets/global/publikationer/vag/yrkestrafik/lasta_lagligt_web_2014.pdf.
- [31] Ron Schoon and Fongloon Peter Pan. “Practical devices for heavy truck aerodynamic drag reduction”, 2007.
- [32] ExTe. *Bankar med fällbara stakar*. URL: <https://www.exte.se/produkter/bakar-med-fallbara-stakar>. accessed June 2019.
- [33] W Jason Spence, Michael C Sorrells, Lennart Höglin, et al. *Adjustable roof extension for reducing vehicle wind resistance*. US Patent 6,991,281. Jan. 2006.
- [34] Johannes E., Ekman P., Hüge-Brodin M., and Karlsson M. “Influence of Different Truck and Trailer Combinations on the Aerodynamic Drag”. SAE Technical Paper 2011-01-0179, 2011. DOI: 10.4271/2011-01-0179.

- [35] Tsan-Hsing S., Liou W.W., Shabbir A., Yang Z., and Zhu J. “A new $k-\varepsilon$ eddy viscosity model for high reynolds number turbulent flows.” *Computers and Fluids* 24.3, 1995, pp. 227–238. ISSN: 0045-7930.

A Realizable k- ε model

The realizable k- ε model was introduced in 1995 and is a development on the standard k- ε model introduced in 1972 [35]. The two transport equations shown used by the k- ε model are shown in equation 23 for the transport of k and 24 for transport of ε .

$$\frac{\partial(\rho k)}{\partial t} + \frac{\partial(\rho k u_j)}{\partial x_j} = \frac{\partial}{\partial x_j} \left[\left(\mu + \frac{\mu_t}{\sigma_k} \right) \frac{\partial k}{\partial x_j} \right] + G_k + G_b - \rho \varepsilon - Y_M + S_k \quad (23)$$

$$\begin{aligned} \frac{\partial(\rho \varepsilon)}{\partial t} + \frac{\partial(\rho \varepsilon u_j)}{\partial x_j} = \frac{\partial}{\partial x_j} \left[\left(\mu + \frac{\mu_t}{\sigma_\varepsilon} \right) \frac{\partial \varepsilon}{\partial x_j} \right] + \rho C_1 S \varepsilon \\ - \rho C_2 \frac{\varepsilon^2}{k + \sqrt{\nu \varepsilon}} + C_{1\varepsilon} \frac{\varepsilon}{k} C_{3\varepsilon} G_b + S_\varepsilon \end{aligned} \quad (24)$$

In these equations a number of model constants are used. These are most often left to what they have been tuned to be during early development of the turbulence models. ANSYS Fluent uses the following values for the constants and no changes to them have been made in this thesis $C_{1\varepsilon} = 1.44$, $C_2 = 1.9$, $\sigma_k = 1.0$, $\sigma_\varepsilon = 1.2$ [22]. The coefficient C_1 is calculated as shown in equation 25. Other variables in the equation is ρ the density, t the time, velocities in index notation as u_j and coordinates as x_j . The dynamic viscosity μ , kinematic viscosity ν and turbulent viscosity μ_t . In the equations the terms G_k and G_b appear and these represent the generation of turbulent kinetic energy due to the mean velocity gradients and buoyancy respectively. These terms are then calculated as shown in equations 26 and 27. Definitions for the other variables can be found in [22].

$$C_1 = \max \left[0.43, \frac{\eta}{\eta + 5} \right], \eta = S \frac{k}{\varepsilon}, S = \sqrt{2S_{ij}S_{ij}} \quad (25)$$

$$G_k = -\rho \overline{u'_i u'_j} \frac{\partial u_j}{\partial x_i} \quad (26)$$

$$G_b = \beta g_i \frac{\mu_t}{Pr_t} \frac{\partial T}{\partial x_i} \quad \text{where } \beta = -\frac{1}{\rho} \left(\frac{\partial \rho}{\partial T} \right)_p \quad (27)$$

In the Realizable k- ε model the turbulent eddy viscosity is modelled as shown in 28.

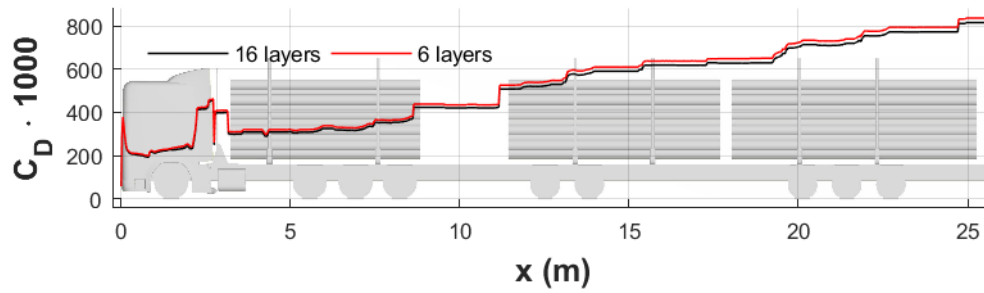
$$\mu_t = \rho C_\mu \frac{k^2}{\varepsilon} \quad (28)$$

The variable C_μ is in the realizable k- ε model no longer a constant as in the standard k - ε model. Instead it is calculated as in equation 29.

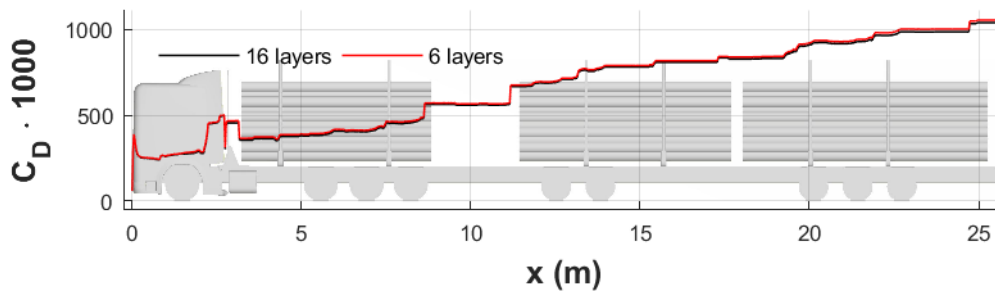
$$\frac{1}{A_0 + A_s \frac{kU^*}{\varepsilon}} \quad (29)$$

The constants A_0 and A_s together with the definition of U^* can be found in the paper deriving the model [35].

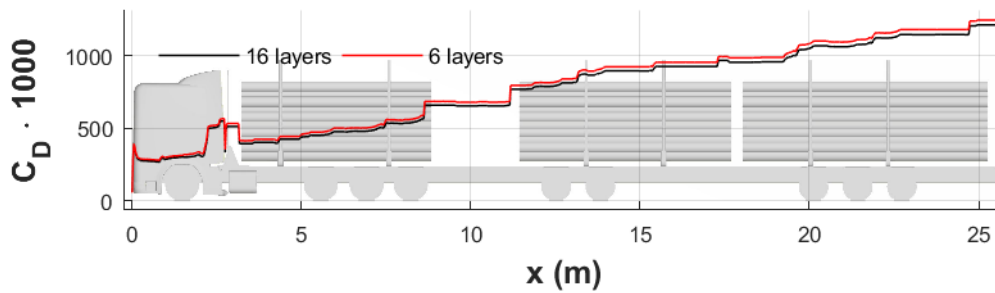
B Inflation Study



(a) 5° yaw



(b) 10° yaw



(c) 15° yaw

Figure B.2: Comparison of drag accumulation between inflation and surface mesh strategies on the previous model, trends show very good agreement

Table B.2: Drag coefficient inflation study on 2018 model for yaw angles 0° - 15° , averaged over the last 1000 iterations

Yaw	Layers	$1000 \cdot C_D$	$1000 \cdot SD$	Δ	%
0	16	547	0.05	+8	+1.4
	6	555	8.15		
5	16	884	0.13	+6	+0.7
	6	891	0.04		
10	16	1125	1.29	-4	-0.4
	6	1121	1.63		
15	16	1316	0.48	+13	+1.0
	6	1329	0.42		

C Method Problem data

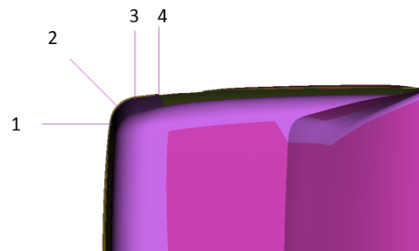


Figure C.2: Viewed from above, the leeward side of the cab radius with the lines used to create velocity and EVR profiles. The lines was placed 2030 mm above the ground plane and extending 0.5 m normal from the cab wall

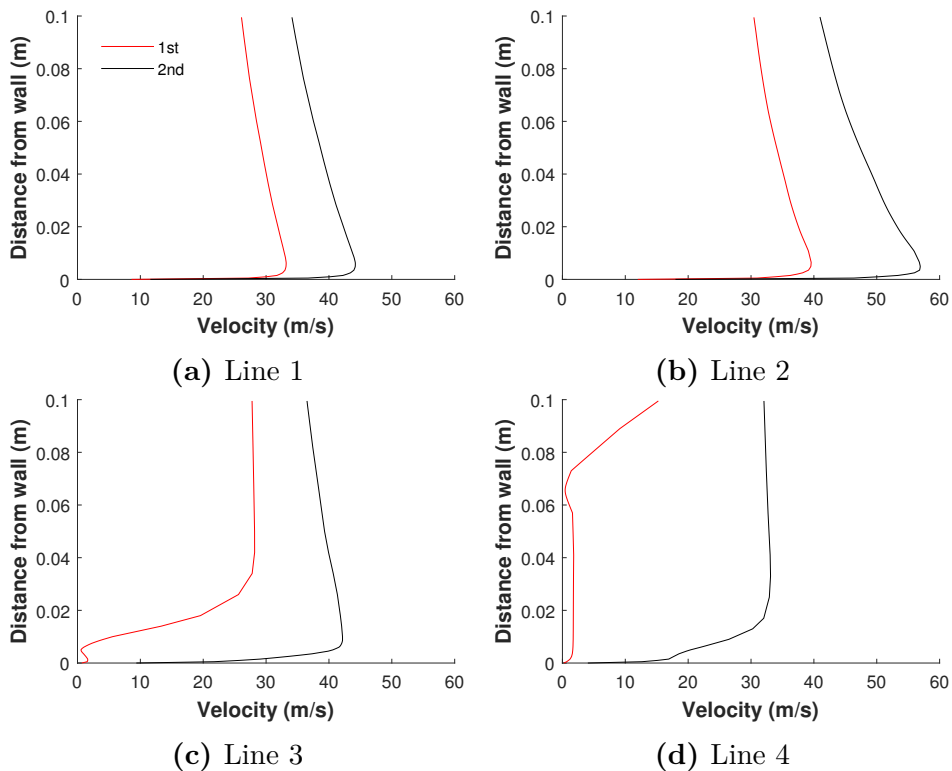


Figure C.3: Velocity profiles comparing 1st- and 2nd-order discretization of k and ε clearly showing the under prediction of velocity around the radius when using 1st- order discretization of k and ε

D Results Baseline Vehicle

Table D.1: Drag coefficient in counts for the baseline vehicle, loaded and unloaded at yaw 0° - 10°

$1000 \cdot C_D$	0°	2.5°	5°	10°	Wind average
Loaded	639	669	780	1250	845
Unloaded	666	701	771	1011	806

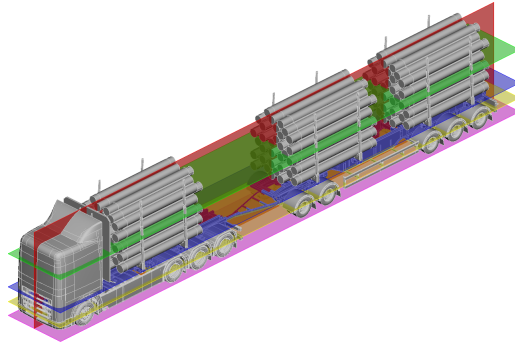


Figure D.2: Positioning of standard cut-planes. Planes in the z -direction: pink is just above the ground at ≈ 0.05 m, yellow is in height with the chassis at 0.6 m, blue is at 1.25 m through the banks, and green approximately the middle of the stacks at 2.6 m. The red plane, normal in y , is placed in the middle of the vehicle. This color coding is used to distinguish standard cut-planes by a colored frame